THE HONG KONG
POLYTECHNIC UNIVERSITY
香港理工大學
Pao Yue-kong Library
包玉剛圖書館

Copyright Undertaking

This thesis is protected by copyright, with all rights reserved.

By reading and using the thesis, the reader understands and agrees to the following terms:

1. The reader will abide by the rules and legal ordinances governing copyright regarding the use of the thesis.
2. The reader will use the thesis for the purpose of research or private study only and not for distribution or further reproduction or any other purpose.
3. The reader agrees to indemnify and hold the University harmless from and against any loss, damage, cost, liability or expenses arising from copyright infringement or unauthorized usage.

IMPORTANT

If you have reasons to believe that any materials in this thesis are deemed not suitable to be distributed in this form, or a copyright owner having difficulty with the material being included in our database, please contact lbsys@polyu.edu.hk providing details. The Library will look into your claim and consider taking remedial action upon receipt of the written requests.

Pao Yue-kong Library, The Hong Kong Polytechnic University, Hung Hom, Kowloon, Hong Kong

http://www.lib.polyu.edu.hk

This thesis in electronic version is provided to the Library by the author. In the case where its contents is different from the printed version, the printed version shall prevail.

ADAPTIVE RADIATION THERAPY OF NASOPHARYNGEAL CARCINOMA USING MEGAVOLTAGE COMPUTED TOMOGRAPHY IN HELICAL TOMOTHERAPY

FUNG WING KI

M.Phil

The Hong Kong Polytechnic University

2013

The Hong Kong Polytechnic University

Department of Health Technology and Informatics

ADAPTIVE RADIATION THERAPY OF NASOPHARYNGEAL CARCINOMA USING MEGAVOLTAGE COMPUTED TOMOGRAPHY IN HELICAL TOMOTHERAPY

FUNG WING KI

A thesis submitted in partial fulfillment of the requirements for the degree of Master of Philosophy

April 2012

CERTIFICATE OF ORIGINALITY

I hereby declare that this thesis is my own work and that, to the best of my knowledge and belief, it reproduces no material previously published or written, nor material that has been accepted for the award of any other degree or diploma, except where due acknowledgement has been made in the text.

Signed _____

FUNG WING KI

(Candidate)

Signed _____

DR. WU WING CHEUNG VINCENT

(Chief supervisor)

Signed _____

DR. YING TIN CHEUNG MICHAEL

(Co-supervisor)

ABSTRACT

Adaptive radiotherapy (ART) has been introduced in treating head and neck cancer recently. It refers to the restoration of the planned dose distribution by modifying the treatment plan according to the radiation-induced anatomic changes during a treatment course. ART in interval basis is feasible in head and neck cases because the organ changes in this region are shown to follow a progressive trend rather than in a random manner. Nevertheless, few studies have been carried out specifically on nasopharyngeal carcinoma (NPC), and the issue of when and how often the ART should be performed is still controversial. This study evaluated the potential dosimetric benefits of applying a three-phase adaptive radiotherapy protocol in NPC patients treated with helical tomotherapy. Comparison was made between the three-phase protocol and the non-adaptive single phase treatment protocol. Using daily megavoltage computed tomographic (MVCT) images provided by the tomotherapy system, this study also quantified and characterized the volumetric and geometric changes of tumors and organs at risk (OARs). An optimum ART strategy for NPC was therefore established by defining various thresholds that indicated significant anatomic changes during the treatment course and hence the needs for replanning.

A retrospective study involving 30 NPC patients who had a total of 37-38 fractions of radiotherapy was conducted. Among them, 24 patients that followed the routine three-phase radiotherapy protocol were included in the first part of the study. Two new plans, denoted as PII-ART and PIII-ART, were generated based on the up-to-date CT images and contours and were used for treatment in

phase two (PII; after 25th fraction) and phase three (PIII; after 35th fraction) respectively. To simulate the situation of no replanning, two hybrid plans denoted as PII-NART and PIII-NART were generated using the original contours pasted on the PII- and PIII-CT sets by CT-CT fusion. Dosimetric comparisons were made between the NART plans and the corresponding ART plans. For all 30 patients on their alternate day MVCT images, the posterolateral wall of nasopharynx (P-NP) which represented the nasopharyngeal gross tumor, neck volume covering the whole cervical spine level, bilateral parotid glands and vertebral canals at the level of 3 cm (VC3), 6 cm (VC6) and 9 cm (VC9) inferior to the base of skull were manually contoured. Pattern of their anatomic changes throughout the treatment course were being assessed. Statistical analysis was applied to each recorded parameter to define threshold(s), which indicated a significant change that replanning was suggested at any time point of the treatment course.

This study showed that due to the radiation-induced tumor shrinkage took place within the initial planned high-dose region, the dose homogeneity to the targets was better even if no replanning was applied. Nevertheless, the significantly low degree of dose conformity of all target volumes without replanning revealed that there were many abutting normal tissues being unnecessarily irradiated with high dose due to the tumor shrinkage. In particular, some patients would have their brainstem, spinal cord and optic chiasm dose exceeding tolerance, inducing disastrous complications and hence degrading their quality of life after treatment. The present study demonstrated that replannings in between the treatment course restored the target dose conformity, hence allowed significantly better sparing of

the surrounding OARs. In addition, ART strategy with multiple replannings was deem necessary to account the continuous anatomic changes over the radiotherapy course.

The study also showed that the volumes of the P-NP, the parotid glands and the neck region demonstrated a progressive regression trend over time. For parotid glands, they tended to displace towards the medial and superior directions throughout the treatment course. Due to the decreased neck volume, the cervical cord was displaced backwardly during the treatment course, leading to the significant posterior shifting of the VC6 and VC9 in this study. Based on the found characteristic trends and the threshold occurrences in targets and OARs, an optimum ART strategy specifically for NPC cases was established. Three replans at 9^{th}, 19^{th} and 29^{th} treatment fractions were proposed as most of the thresholds appeared in these time points of the treatment course.

The present study emphasized the importance of implementing ART strategy in NPC cases by quantifying the dosimetric benefits of applying the three-phase adaptive radiotherapy protocol. The benefits mainly lied on limiting the dose to OARs than keeping the tumor coverage. This study also emphasized the necessity of multiple replanning strategy, in which an optimum ART strategy for NPC cases involving three replans was proposed. This proposed strategy can accommodate the dosimetric consequences due to anatomic deviation over the treatment course. It also enables prompt reaction to the regressed tumor by conforming the target dose, hence allowing safe target dose escalation without risking the surrounding OARs. This proposed strategy is clinical feasible with

justified increase of departmental workload and should be promoted especially in centres where adaptive planning system is not yet available.

PUBLICATIONS ARISING FROM THE THESIS

Conference Presentation and Proceeding

Fung, W. W. K., & Wu, V. W. C. (2011). Dosimetric evaluation of a three-phase adaptive radiotherapy for nasopharyngeal cancer using helical tomotherapy. 11th Biennial European Society for Radiotherapy & Oncology Conference on Physics and Radiation Technology for Clinical Radiotherapy, London, United Kingdom, 7th May –12th May 2011. *Radiother Oncol, 99*(1), S73.

Fung, W. W. K., & Wu, V. W. C. (2011). Dosimetric evaluation of a three-phase adaptive radiotherapy for nasopharyngeal cancer using helical tomotherapy. 3rd Annual Scientific Meeting of The Hong Kong College of Radiographers and Radiation Therapists, Hong Kong, 8th October 2011.

Fung, W. W. K., & Wu, V. W. C. (2012). Optimum adaptive radiation therapy strategy for nasopharyngeal carcinoma. European Society for Radiotherapy & Oncology 31, Barcelona, Spain, 9th May –13th May 2012.

Fung, W. W. K., & Wu, V. W. C. (2012). Optimum adaptive radiation therapy strategy for nasopharyngeal carcinoma. Annual Scientific Meeting in Radiotherapy 2012, Hong Kong, 23rd September 2012.

Publication

Fung, W. W. K., Wu, V. W. C., & Teo, P. M. L. (2012). Dosimetric evaluation of a three-phase adaptive radiotherapy for nasopharyngeal cancer using helical tomotherapy. *Med Dosim, 37*(1), 92–97.

ACKNOWLEDGEMENTS

First of all, I would like to thank my chief supervisor, Dr. Vincent Wu, for his continuous guidance and support throughout the research period. Without his valuable advice and encouragement, I would never have finished my study. I would also thank my co-supervisor, Dr. Michael Ying for his kind participation in my study. I must also thank Dr. Peter Teo for his clinical advice and devotion of time to perform the tumor delineation for my study, and Dr. Daniel Chow for his professional advice on statistical aspect. Thanks also go to the patients who involved in the present study for providing such valuable clinical data.

I would like to extend my gratitude to Mr. George Chiu, the Head of the Department of Radiotherapy in the Hong Kong Sanatorium & Hospital where I am working, for his indefinite support in providing time and resources for me to complete my study. Thanks also go to my colleagues and friends, especially Ms. Szeming Wong, Mr. Franky Cheng, Ms. Jocelyn Chan, Ms. Lenis Lee and Ms. Eunice Wong for keeping me company and creating laughter for me whenever I came across difficulties and frustration. In particular, I want to thank Mr. Alan Mui for his professional opinion on the study settings and Ms. Kitty Leung for helping me during data collection.

Most importantly, I would like to thank my parents for their unconditional love and taking good care of me during the study period.

TABLE OF CONTENTS

LIST OF ABBREVIATIONS

Adaptive radiotherapy (ART)

Adrenocorticotropic hormone (ACTH)

American Joint Committee on Cancer (AJCC)

Analysis of variance (ANOVA)

Base of skull (BOS)

Centre of mass (COM)

Clinical target volume (CTV)

Clinical target volume of lymph nodes (LN-CTV)

Clinical target volume of nasopharynx (NP-CTV)

Computed tomography (CT)

Cobalt gray equivalent (CGE)

Conformation number (CN)

Dice similarity index (DSI)

Dose to *x* % of organ volume (D_x)

Dose volume histogram (DVH)

Epstein-Barr virus (EBV)

Equivalent uniform dose (EUD)

^{18}F-fluoro-2-deoxy-D-glucose (^{18}F-FDG)

First cervical vertebra of the spine (C1)

Follicle stimulating hormone (FSH)

Fourth cervical vertebra of the spine (C4)

Fraction (fr)

Gross tumor volume (GTV)

Gross tumor volume of lymph nodes (LN-GTV)

Gross tumor volume of nasopharynx (NP-GTV)

Growth hormone (GH)

Homogeneity index (HI)

Image guided radiotherapy (IGRT)

Intensity modulated radiotherapy (IMRT)

International Commission on Radiation Units (ICRU)

International Union Against Cancer (UICC)

Kilovoltage cone-beam computed tomography (kVCBCT)

Linear accelerator (LINAC)

Luteinizing hormone (LH)

Magnetic resonance imaging (MRI)

Maximum dose (D_{max})

Mean dose (D_{mean})

Megavoltage (MV)

Megavoltage computed tomography (MVCT)

Minimum dose (D_{min})

Multileaf collimator (MLC)

Nasopharyngeal carcinoma (NPC)

Normal tissue complication probability (NTCP)

Organ at risk (OAR)

Organ volume receiving *x* Gy (V_x)

Phase one (PI)

Phase two (PII)

Phase three (PIII)

Planning target volume (PTV)

Planning target volume of lymph nodes (LN -PTV)

Planning target volume of nasopharynx (NP-PTV)

Positron emission tomography (PET)

Posterolateral wall of nasopharynx (P-NP)

Prolactin (PRL)

Quality of life (QOL)

Radiation-induced optic neuropathy (RION)

Second cervical vertebra of the spine (C2)

Second thoracic vertebra of the spine (T2)

Squamous cell carcinoma (SCC)

Standard deviation (SD)

Third cervical vertebra of the spine (C3)

Three-dimensional conformal radiotherapy (3D-CRT)

Thyroid stimulating hormone (TSH)

Tumor control probability (TCP)

Tumor Node Metastasis staging (TNM staging)

Two-dimensional radiotherapy (2D-RT)

Vertebral canal at the level of 3 cm inferior to the base of skull (VC3)

Vertebral canal at the level of 6 cm inferior to the base of skull (VC6)

Vertebral canal at the level of 9 cm inferior to the base of skull (VC9)

World Health Organization (WHO)

LIST OF FIGURES

LIST OF TABLES

CHAPTER ONE

INTRODUCTION

Nasopharyngeal carcinoma (NPC) is prevalent in Southern China including Hong Kong. It was the sixth most common cancer in men and the twelfth in women in 2009 in Hong Kong (Hong Kong Cancer Registry, 2009). Radiotherapy is the treatment of choice for NPC owing to its deep-seated anatomic location and relatively high radiosensitivity. The complex anatomic relationship between the nasopharyngeal region and surrounding critical organs such as the brainstem, spinal cord and optic chiasm poses challenges to radiotherapy. Overdosing these critical organs can lead to severe complications like central nervous system injury, myelopathy and optic neuropathy. All these significantly degrade the patient's quality of life and some of them can be life threatening. Since the prognosis of NPC patients after treatment is promising, more effort is put in minimizing the radiation-induced side effects while delivering adequate doses to the target volumes. Intensity modulated radiotherapy (IMRT) is commonly used nowadays in treating NPC because of its ability in shaping the dose distribution, which provides highly conformal treatment with steep dose fall off outside the targets. This allows target dose escalation with sufficient sparing of the surrounding critical structures, thus improving the therapeutic gains. One of the prerequisites to successfully implement IMRT is to achieve a high level of treatment precision.

Recently, image guided radiotherapy (IGRT) has been introduced for the correction of setup uncertainties during a treatment course. In-room imaging techniques using computed tomography (CT) such as kilovoltage cone-beam CT from conventional linear accelerator and megavoltage (MV) CT from tomotherapy system provide volumetric images with reasonably good soft tissue visualization for treatment verification. Daily image guidance aids in precise setup errors correction prior to each fraction of NPC treatment, thus increasing the accuracy of dose delivery to the intended target volumes. Moreover, the daily image data set allows monitoring of anatomic changes throughout the treatment course. NPC patients usually suffer from weight loss and radiation-induced tumor/lymph nodes or parotid glands shrinkage and displacement in progressive trend. These non-rigid deformations, if not properly dealt with, can lead to violation of the original treatment plan and consequently result in underdosing of the tumors and/or overdosing of adjacent critical organs.

Adaptive radiotherapy (ART) for NPC is the interest of the present study. ART is a potential solution to overcome the dosimetric defect due to the non-rigid anatomic changes during a course of radiotherapy. Plan modification is done based on the tumor volume changes as well as organ deformations to restore the original planned dose distribution. ART in interval basis i.e. replanning in specific fraction(s) of a treatment course has demonstrated dosimetric benefits in head and neck cancer patients. However, few studies have reported its effect specifically on NPC cases. Besides, the issue of when and how often the replanning should be conducted is still controversial. Reports on defining ART strategy are lacking. In the Department of Radiotherapy of the Hong Kong

Sanatorium & Hospital, a three-phase radiotherapy protocol i.e. two replannings in between the treatment course for NPC treated with helical tomotherapy has been adopted since 2005. In the present study, the potential benefits of applying ART in NPC cases were quantified by comparing the dosimetric results between the currently adopted three-phase protocol to the single phase treatment protocol. With the use of daily MVCT image set, the present study also quantified and characterized the volumetric and geometric changes of tumors and organs at risk during a treatment course. An optimum ART strategy for NPC was established by evaluating any significant deviation that signaled the need for replanning.

The present study is of great significance to reveal the progression trends of various anatomic changes over the NPC treatment course. The findings of this study will also provide a novel insight of the potential advantages and clinical feasibility of implementing ART in interval basis for NPC. The optimum ART strategy suggested in the present study can effectively accommodate the dosimetric consequences due to anatomic deviation with acceptable increase of departmental workload. The proposed strategy is believed to give a positive impact to the current clinical settings and should be promoted especially in centres where adaptive planning system is not yet available.

This thesis consists of eight chapters. Chapter one gives a brief introduction of the background, objectives and significance of the present study. Chapter two describes the general features of NPC, including its anatomy, epidemiology, pathology, tumor spread and clinical features, investigations, staging, treatment modalities and prognosis. Chapter three gives an extensive literature review on

this disease in radiotherapy aspect. Practical issues in treatment planning, radiation complications and treatment uncertainties are discussed followed by an introduction of various radiotherapy techniques commonly used nowadays. The basis, objectives and clinical values of this thesis are also defined in chapter four. Chapter five describes the materials and methods used in the present study. Chapter six presents the findings of the study and chapter seven gives a comprehensive discussion on the study results and limitations. Recommendations for future research and development are also included. A summary as well as the conclusion of the thesis are given in chapter eight.

CHAPTER TWO

NASOPHARYNGEAL CARCINOMA

2.1 Anatomy of nasopharynx

Nasopharyngeal carcinoma (NPC) is the malignant neoplasm in the epithelial lining of the nasopharynx, which anatomically lies between the nasal cavity and the oropharynx. Anteriorly it is bounded by the posterior choanae, superiorly by the body of sphenoid bone which slopes backward and downward to merge with the posterior wall that formed by the first and upper portion of second vertebrae. The nasopharynx itself follows the curve and continues itself with the posterior pharyngeal wall, which is ridged by the prevertebral muscle of longus capitis. Its floor is the upper surface of the soft palate (Figure 2.1). The lateral wall on both sides includes the opening of the eustachian tube, the torus tubarius and the fossa of Rosenmuller. Figure 2.2 shows the anatomic relationship of these structures in transverse and coronal view using computed tomography (CT). The torus tubarius is a comma-shaped elevation shielding the eustachian tube opening in superior and posterior aspects, and the fossa of Rosenmuller is a pharyngeal recess situated supero-posterior to the torus tubarius. There is an extensive lymphatic plexus includes the posterior cervical nodes, Rouviere's node, the subdigastric, upper and mid deep cervical nodes existing in the nasopharyngeal region. Close to the nasopharyngeal region, the third to sixth cranial nerves are situated immediately above the foramen lacerum in the base of skull on each side.

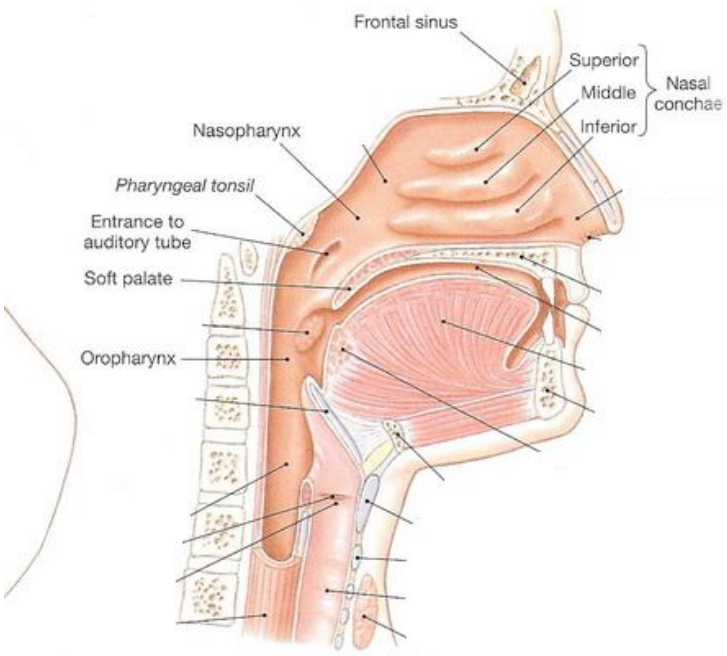

Figure 2.1: Graphical diagram of the anatomy of nasopharynx (Martini et al., 2001).

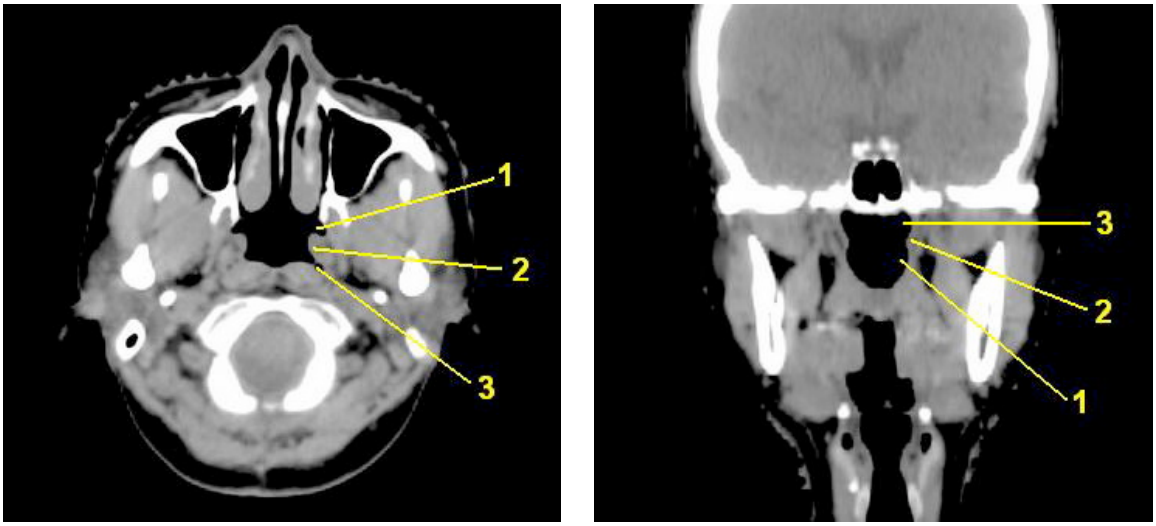

Figure 2.2: CT images of the nasopharynx showing the opening of the eustachian tube (1), the torus tubarius (2) and the fossa of Rosenmuller (3) (left, transverse view; right, coronal view).

2.2 Epidemiology

NPC is a complex disease caused by the interaction between the environmental, viral and genetic factors. NPC is prevalent in Southern China especially in the Cantonese-speaking region but not in most Western countries like Europe and North America. In general, the age-standardized incidence rate for both sexes approximately ranges from 5–30/100 000 for Chinese populations but < 1/100 000 for North American places (Parkin et al., 2002). This suggests that there are environmental factors governing the incidence of this disease. Studies of Chinese populations showed that the consumption of salted fish and other preserved food products, mainly during weaning period and childhood, was strongly associated with increased risk of NPC (Yuan et al., 2000; Zheng et al., 1994).

The association between NPC and Epstein-Barr virus (EBV) is well established, although the exact mechanism of pathogenesis remains unclear (Tabuchi et al., 2011). The influence of environmental and/or genetic factors is believed to trigger the EBV to infect the B lymphocytes (primary target of EBV), followed by replication and later development of several malignancies including NPC (Chang & Adami, 2006; Zhou et al., 2007). Studies demonstrated an increase in the titers of EBV-associated antigens and the presence of EBV genome in the tumor cells of almost all NPC cases (Dickens et al., 1992; Zhou et al., 2007), suggesting EBV plays a important role in the cause of the disease.

It is showed that the genetic factor also contributes to the development of NPC. Studies on familial aggregation of NPC showed that there is a significant higher risk of NPC in people whose family member already suffered from it (Jia et al., 2004). For first degree relatives, the relative risk of NPC is 8.0 (Friborg et al., 2005). This hereditary feature is most likely the result of shared genetic susceptibility and/or shared environmental factors (Chang & Adami, 2006).

According to the Hong Kong Cancer Registry (2009), NPC was the sixth most common cancer in men and twelfth in women in 2009. Overall it contributed 3.5 % of all cancer new cases. The age group with highest incidence and mortality rate was 45–64 years old and > 65 years old respectively. Both rates showed downward trends over the past two decades. These findings reflect the change of local diet habit with reduced consumption of preserved food, the rapid advancement of diagnostic tools which enable early detection of the disease, as well as the advance in treatment techniques and protocols have improved the therapeutic rate in the modern era.

2.3 Pathology

In 1991, World Health Organization (WHO) categorized NPC into two histological groups: keratinizing squamous cell carcinoma (SCC) and nonkeratinizing carcinoma. The latter group is further subdivided into differentiated and undifferentiated carcinoma (Shanmugaratnam & Sobin, 1991; Wei & Sham, 2005). It is found that the keratinizing SCC is predominant in low-incidence compared with high-incidence region, which accounts for 25 % of

all cases in North America but only 2 % in Southern China. In contrast, undifferentiated carcinoma is responsible for 95 % of all cases in Southern China but about 63 % in North America (Chan et al., 2005; Wei & Sham, 2005).

2.4 Tumor spread and clinical features

NPC frequently arises from the lateral wall, especially the fossa of Rosenmuller and the eustachian tube cushions, and the superoposterior wall of nasopharynx (Chan et al., 2005; Spano et al., 2003; Wei et al., 1991; Zhou et al., 2007; Figure 2.3). It is a highly malignant tumor which prone to extensive loco-regional infiltration, lymphatic spread and sometimes distant metastasis. According to the pattern of spread, Wei and Sham (2005) grouped the symptoms presented by NPC patients into four categories: (1) epistaxis, nasal obstruction and discharge, due to the presence of tumor mass in nasopharyngeal region which may also invade the soft palate and oropharynx; (2) tinnitus and deafness, due to the dysfunction of the eustachian tube by the posterolateral extension of tumor; (3) headache, diplopia, facial pain and numbness, due to skull base erosion and palsy of the cranial nerves by the superior extension of tumor through the foramen lacerum; and (4) neck masses, due to the lymphatic spread of tumor. Patients with NPC can be asymptomatic or suffer from multiple symptoms. A retrospective study of 4768 NPC patients summarized the incidence of various symptoms. The three most common presenting symptoms are the painless enlargement of upper neck nodes (76 %), followed by the nasal (73 %) and aura (62 %) symptoms (Lee et al., 1997).

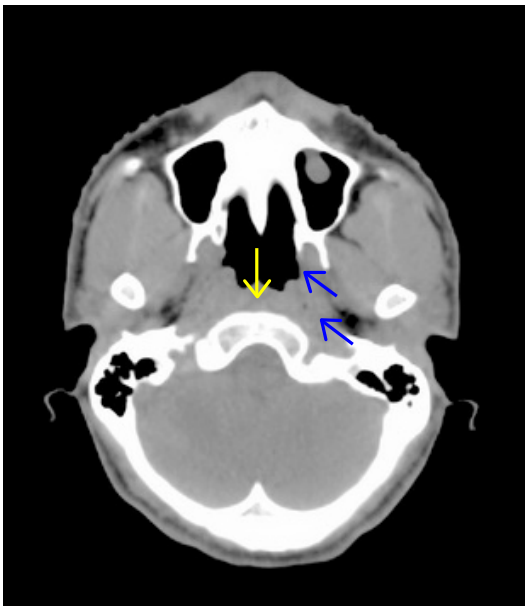

Figure 2.3: Transverse CT image of the nasopharynx demonstrating the nasopharyngeal tumor filled up the fossa of Rosenmuller and the eustachian tube opening in both sides (blue arrows). Thickening of the posterior wall of nasopharynx can be seen (yellow arrow).

The extensive lymphatic network in the nasopharyngeal region freely communicates with those in the parapharyngeal space and upper neck region. This explains the high incidence of neck node metastasis in NPC patients. In addition, the fact that the anatomic position of nasopharynx is posterior to the nasal space inherently makes clinical examination difficult. In most cases, the diseases are diagnosed only when an observable neck mass being noticed, which indicates the disease has already spread to the neck region (Lee et al., 1997; Leong, Fong, & Low, 1999; Wei & Sham, 2005). The incidence of distant metastasis is also correlated strongly with the degree of neck node involvement. Once the lower neck nodes that drain into the blood vessels are involved, tumor cells may gain access to other part of the body through the vessels. The common metastatic sites of NPC are bone, lung, liver and distant lymph nodes, which is presented as corresponding bone pain and organ dysfunction. (Chan et al., 2005; Teo et al., 1996b).

2.5 Investigations

The preliminary investigations for patient who is suspicious of NPC include physical examinations, such as neck node palpation and cranial nerve examination, and nasopharyngeal endoscopy. An EBV-related serological test can be performed for detection of raised antibodies against EBV (King et al., 2011; Wei & Sham, 2005). A definitive histological diagnosis is confirmed by performing endoscopic biopsy of the primary tumor site (Chan & Felip, 2009; Wei et al., 1991; Wei & Sham, 2005). Since the physical and endoscopic examinations cannot easily ascertain deep extension, skull base erosion or intracranial spread, multiple imaging tests are used to determine the extent of disease including the degree of nodal involvement and distant metastasis. Among all, commonly used imaging techniques of CT and magnetic resonance imaging (MRI), as well as recently used positron emission tomography with CT (PET-CT) are discussed below.

CT and MRI are regarded as routine cross-sectional examinations for NPC staging. Both of them allow soft tissue visualization and in turn provide exquisite anatomic picture in the nasopharynx especially the fossa of Rosenmuller (common site of NPC origin). They also allow detection of any infiltration outside the nasopharynx and enlargement of neck nodes. CT is better in detecting bone erosion. However, its detection of primary tumor mainly depends on the displacement or erosion of normal anatomy as the CT density of malignant tissues is similar to that of normal tissues (Spano et al., 2003). MRI allows multiplanar images and has a better contrast on soft tissues with higher

spatial resolution, which gives a more sensitive assessment of both superficial and deep nasopharyngeal tissues (Wei & Sham, 2005). The superb soft tissue discrimination allows radiologists to distinguish tumor from normal tissues, to precisely identify the tumor location and extension, and to detect specific tumor appearances. MRI helps in defining nasopharyngeal lesions involving the parapharyngeal space, base of skull, brain and oropharynx. It also visualizes the intracranial extension, cranial nerve infiltration and bone marrow involvement (Chung et al., 2004; Emami, Sethi, & Petruzzelli, 2003; Ng et al., 1997; Spano et al., 2003; Wei & Sham, 2005). All these lead to a more accurate diagnosis when used in combination with CT.

Recently, PET using ^{18}F-fluoro-2-deoxy-D-glucose (^{18}F-FDG) has been suggested in NPC diagnosis by assessing the metabolic status of the tumor. This functional tumor information is linked with anatomic details by integrating PET with CT. However, the benefit of this modality is not ascertained. King et al. (2008) demonstrated that PET-CT had underestimated the extent of primary tumor in 15 % of patients when compared to MRI, suggesting it has the potential to miss small volume tumors. Nevertheless, it helps in detecting neck nodes involvement as well as distant metastasis which may be missed by other imaging modalities (Chang et al., 2005). Nowadays, PET-CT is sometimes performed in addition to routine examinations to increase staging accuracy especially in patients with high risk of distant metastasis.

2.6 Staging

The clinical stage of NPC is usually classified according to a TNM staging system established by the International Union Against Cancer (UICC) and American Joint Committee on Cancer (AJCC). In general, T (**T**umor) describes the tumor size and their extent of locoregional spread; N (lymph **N**odes) describes the regional involvement of the lymph nodes; whereas M (**M**etastasis) shows if there is distant metastasis of the disease. The stage grouping is a combination of the above 3 aspects to describe the disease progression from earliest to most advanced stage. Table 2.1 shows the TNM staging system published in 1997 (Fleming et al., 1997) for the sake of this thesis. The most updated version was published in 2010 with minor amendment (Edge et al., 2010).

Table 2.1: The UICC/AJCC staging system for NPC (Fleming et al., 1997).

Nasopharynx (T)

Tis	Carcinoma *in situ*
T1	Tumor confined to nasopharynx
T2	Tumor extends to soft tissues
T2a	Tumor extends to oropharyngx and/or nasal cavity extension without parapharyngeal extension
T2b	Tumor with parapharyngeal extension
T3	Tumor invades bony structures and/or paranasal sinuses
T4	Tumor with intracranial extension and/or involvement of cranial nerves, infratemporal fossa, hypopharynx, orbit or masticator space

Regional lymph node (N)

N0	No regional lymph nodes metastasis
N1	Unilateral metastasis in lymph node(s), 6 cm or less in greatest dimension, above supraclavicular fossa
N2	Bilateral metastasis in lymph nodes, 6 cm or less in greatest dimension, above supraclavicular fossa
N3	Metastasis in lymph node(s), > 6 cm in dimension (N3a) or in the supraclavicular fossa (N3b)

Distant metastasis (M)

M0	No distant metastasis
M1	Distant metastasis

Stage grouping

Stage 0	Tis	N0	M0
Stage I	T1	N0	M0
Stage IIA	T2a	N0	M0
Stage IIB	T2b	N0	M0
	T1/T2a/T2b	N1	M0
Stage III	T3	N0/N1	M0
	T1/T2/T3	N2	M0
Stage IVA	T4	N0/N1/N2	M0
Stage IVB	Any T	N3	M0
Stage IVC	Any T	Any N	M1

2.7 Treatment modalities

Surgery is not a primary option for treating NPC, because the deep-seated anatomic location of nasopharynx limits the margin of resection and the removal of widespread lymphatic permeation is not effective. Besides, NPC is relatively radiosensitive. Thus radiotherapy becomes the mainstay of treatment for almost all NPC patients. Nevertheless, radiotherapy for NPC is challenging as the primary site is anatomically surrounded by various critical normal structures such as brainstem, spinal cord, optic chiasm, pituitary gland and parotid glands. Moreover, the treatment volume is frequently irregular in order to cover both the primary tumor and the high risk subclinical lymph nodes. The goal of radiotherapy is to deliver adequate radiation dose to the tumor site without risking the surrounding normal structures with unwanted side effects.

Chemotherapy is used in combination with radiotherapy to improve treatment outcome of advanced NPC patients who bare a higher risk of local recurrence and disease metastasis. Some common drugs used in NPC cases are cisplatin, bleomycin, doxorubicin and 5-fluorouracil. The application of chemotherapy can be through three different approaches. Neoadjuvant chemotherapy is used in order to shrink the tumor before radiotherapy and reduce sub-clinical spread, so as to improve the local control and relapse-free survival (Spano et al., 2003). Adjuvant chemotherapy is given after radiotherapy to reduce the risk of distant metastasis (Spano et al., 2003). Other than these two approaches, concurrent chemo-radiotherapy is the one which is mostly used for the treatment of NPC to increase the local control and decrease the risk of distant spread at the same time

(Spano et al., 2003).

The selection of appropriate treatment regimen is generally stage dependent. Radiotherapy alone is used for primary treatment of early staged NPC. For advanced local disease, concurrent chemo-radiotherapy is used to improve the local control. An addition of systemic chemotherapy to the treatment program may be used for advanced nodal disease (Chua et al., 2001). Moreover, different combination of radiotherapy techniques and protocols can be applied according to the extent of disease progression (Chan et al., 2005; Chua et al., 2001).

2.8 Prognosis

Lee et al. (2005) retrospectively analyzed 2687 NPC patients who treated in Hong Kong in 1996–2000. The 5-year progression-free, overall and cancer-specific survival rates were 63 %, 75 % and 80 % respectively. For NPC, the extent of disease i.e. the presenting stage is the key prognostic factor (Cheng et al., 2001; Chua et al., 2001; Lee et al., 2005; Teo et al., 1996a). A decrease of the overall survival rate from 90 % for Stage I disease to 58 % for Stage IV disease was observed (Lee et al., 2005). The WHO classification for NPC was also shown to have a prognostic value (Cheng et al., 2001; Reddy et al., 1995). In particular, Reddy et al. (1995) showed the undifferentiated carcinoma has a significantly higher primary tumor and nodal control rates with treatment but a higher chance of distant metastasis when compared to keratinizing SCC. Other adverse prognostic factors include increasing age and male gender (Teo et al., 1996a), rising titers of EBV-associated antigens and EBV DNA in serum (Zhou

et al., 2007). The use of imaging techniques for staging and the duration of symptoms before diagnosis are those considered as indirect factors that influence the staging accuracy and in turn prognosis (Lee et al., 1997; Lee et al., 2005). These prognostic groupings provide important implications for failure patterns and help determining appropriate treatment strategies for better therapeutic results.

CHAPTER THREE

LITERATURE REVIEW ON RADIOTHERAPY OF NASOPHARYNGEAL CARCINOMA

3.1 Practical aspects in radiotherapy treatment planning

The treatment planning process for radiotherapy of NPC involves several steps: patient immobilization and CT simulation, target and critical structures delineation as well as target dose prescription and computer planning. Patient immobilization during treatment is crucial in NPC cases because of the proximity of target to many vital organs such as spinal cord, brainstem and optic chiasm. An effective immobilization system can increase setup reproducibility and accuracy thus minimizing potential target misses and critical organs injuries. A thermoplastic mask is made for each patient to stabilize the head and neck region during CT simulation and is used in every fraction of treatment to maintain the treatment position. CT images covering the whole head and neck region are acquired during simulation, which provides anatomic details for oncologist to contour the tumor volumes and organs at risk (OARs). The CT images also provide electron density data that is essential for dose calculation in the treatment planning process.

Target volume delineation is based on the definition described in International Commission on Radiation Units (ICRU) report 50 (ICRU, 1993) and supplement report 62 (ICRU, 1999). In brief, the gross tumor volume (GTV) should include the primary tumor and any involved lymph nodes based on clinical information and various imaging results. The clinical target volume (CTV) encompasses the GTV plus areas suspected to contain potential microscopic disease. Finally, the planning target volume (PTV) is yielded by adding a margin to the CTV to enable the prescribed dose is fully delivered to the CTV taken into account of day-to-day organ motions and setup uncertainties. Precise delineation of the target volumes and OARs is mandatory to generate optimal treatment plans. As stated, MR images provide superb soft tissue contrast which may be more sensitive than CT in defining the primary tumor extension (Chung et al., 2004). It usually fuses to the planning CT as a complementary information for target and OARs delineation.

Recently, the use of FDG-PET for gross tumor delineation has been widely studied, in which the GTV is derived from biologic basis. Daisne et al. (2004) compared the GTVs defined by various imaging modalities with the true tumor volume from laryngeal surgical specimen in pharyngo-laryngeal SCC patients. The results showed 29 %, 65 % and 89 % overestimation of tumor extent in FDG-PET, CT, and MRI respectively. They concluded that the GTV defined by FDG-PET was the closest match of the true tumor. Paulino et al. (2005) assessed the GTV defined by PET and CT in head and neck patients. Majority of the PET-GTV (75 %) was smaller than but not necessarily encompassed by the corresponding CT-GTV, indicating there could be a miss when using CT for

tumor delineation. They therefore adopted to use the composite CT- and PET-GTV as the final target for treatment planning. Improvement in local control with the use of composite target remained to be seen. It should be noted that the gross tumor delineation by FDG-PET is highly dependent on how one interprets the PET signals on the images. Schinagl et al. (2007) evaluated five methods for FDG-PET based tumor delineation in head and neck cancer patients and showed that the choice of contouring tools heavily influenced both the volume and shape of the resulting GTV. Furthermore, uptake of FDG by inflammatory tissues could lead to false-positive signals on the images. In the mean time, FDG-PET may be used as a supplementary data for gross tumor delineation. Validation and standardization should be established before safely implementing this delineation tools in routine clinically practice.

After outlining the target volumes and OARs in the planning CT, treatment planning computer is used to design the radiation field coverage, beam arrangement and perform dose calculation. Customized field is created for irregular target by using multileaf collimator (MLC), which consists of multiple leaves that project into the primary beam to shield away the normal tissue volume in the vicinity. Radiotherapy techniques for NPC have been evolved rapidly. The application of conventional two-dimensional (2D-RT) and three-dimensional conformal radiotherapy (3D-CRT) has been recently replaced by the more advanced intensity modulated technique. Regardless of the techniques used, the goal of treatment planning remains unchanged, which is to generate the best dose distribution to the target volumes based on oncologist's prescription with OAR doses as low as possible. Generally, the dose scheme for

NPC cases is about 66–70 Gy in 33–35 fractions with conventional techniques (Ang & Garden, 2006; Chan, Teo, & Johnson, 2002). Higher doses of about 70–76 Gy may be prescribed to the targets in 35–38 fractions with intensity modulated technique (Lee et al., 2002).

3.2 Dose-volume effects and radiation-induced complications

As stated, nasopharyngeal tumor is surrounded by numerous critical organs, which are inevitably included in the irradiated volume during radiotherapy. Various complications may arise depending on the dose received by the organ and its volume being irradiated. The prognosis for NPC patients after radiotherapy with/without chemotherapy is promising, thus patient's quality of life (QOL) after treatment becomes a big concern. In the following, the radiation dose-volume effects and radiation-induced complications in the brainstem, spinal cord, optic chiasm, pituitary gland and parotid glands are discussed in details. For simplicity, the presented clinical results below were of conventional fractionated dose (2.0 Gy/fraction) to eliminate the fractional size effect on dose response.

1.1.1 Brainstem

Brainstem is situated posterior to the nasopharyngeal region inside the skull. It includes the midbrain that connects superiorly to the cerebrum, the pons in the middle and the medulla oblongata that connects inferiorly to the spinal cord. The brainstem contains many important processing centres as well as motor and

sensory nuclei that link to various cranial nerves, therefore relay information between the brain and the rest of the body. It also contains centres that regulate autonomic cardiovascular, respiratory and digestive function and help maintain consciousness. The brainstem is very close to the nasopharynx. In fact, the PTV contoured during NPC treatment planning usually right in front of the brainstem with only 2–3 mm margin. Significant radiation dose may be contributed to this unaffected organ. Radiation damage to brainstem usually manifests months and years after treatment as necrosis, infarction and/or neurological deficits (Debus et al., 1997; Mayo, Yorke, & Merchant, 2010). In mild case, it leads to motor weakness and/or sensory loss with little interference to normal activities. However, severe injury can cause body numbness, paralysis and even death (Debus et al., 1997; Mayo, Yorke, & Merchant, 2010).

Studies on radiation-induced brainstem injury are scarce because of its low incidence and short survivals of suffered patients (Debus et al., 1997; Mayo, Yorke, & Merchant, 2010). Uy et al. (2002) presented the treatment outcome of 40 meningioma patients. One patient died of brainstem necrosis in around 41 months after radiotherapy. The maximum brainstem dose of this patient was 55.6 Gy and the volume that received > 54 Gy (V_{54}) was 4.7 mL. Debus et al. (1997) conducted a more detailed study investigating the long-term incidence of brainstem toxicity in patients with skull base tumors treated with combined photon and proton radiotherapy. Doses reported in this paper were stated in cobalt gray equivalent (CGE), which took into account that the relative biological effectiveness of proton was 10 % greater than that of photon. In their study, 17 out of 347 patients developed radiation-induced brainstem toxicity in a

mean onset time of 17 months (4.5–92 months). Three patients died 4–5 months after the onset of symptoms. The severity of symptoms varied greatly among patients with no common pattern. For these patients, the average maximum brainstem dose and V_{55} were 64.3 CGE (60.0–70.0 CGE) and 5.6 mL (2.7–9.6 mL) respectively. Using univariate analysis, several dosimetric predictors of brainstem toxicity were defined, they were the maximum dose > 64 CGE, $V_{50} \geq$ 5.9 mL, $V_{55} \geq 2.7$ mL and $V_{60} \geq 0.9$ mL. Although data is limited in defining a complete dose-response relationship, a maximum brainstem dose of 54 Gy or dose to 1 % of brainstem volume (D_1) ≤ 54 Gy is a common dose constraint in clinical practice nowadays, believing this will cause minimal risk of severe or permanent injury (Daly et al., 2007; Kam et al., 2004; Wu et al., 2009). Small volume of 1–10 mL may be irradiated up to 59 Gy. However, the risk appears to increase substantially when the dose > 64 Gy (Mayo, Yorke, & Merchant, 2010).

Some studies suggested linkage between brainstem dose and acute nausea and vomiting during head and neck radiotherapy due to the irradiation of the specific emetic-associated nuclei in the area postrema and dorsal vagal complex in the brainstem. Rosenthal et al. (2008) and Ciura et al. (2011) reported these symptoms were associated with mean brainstem dose > 36 Gy and 15–25 Gy respectively. Another study using univariate analysis found that patients with grade 1–2 acute nausea had a significant higher median dose to the dorsal vagal complex (26.9 Gy) than those with no symptom (6.5 Gy) (Monroe et al., 2008). Nevertheless, the role of low-integral dose to brainstem in acute nausea and vomiting is still unclear without conclusive recommendation on dose threshold. Moreover, these radiation-induced symptoms are relatively mild and tend to

abate rapidly (Ciura et al., 2011). These findings therefore may serve as an optional consideration during radiotherapy treatment planning.

1.1.2 Spinal cord

Spinal cord, which encased by the spinal canal, is the continuation of the brainstem. It extends from the skull base down to the lumbar region. Similar to brainstem, it consists of bundles of sensory and motor tracts that transfer information to and from the brain to the rest of the body. With similar parenchyma, the complications in brainstem and spinal cord due to radiation are alike. Myelopathy i.e. radiation-induced spinal cord injury often first presents as a Brown-Sequard syndrome with pain, paresthesia and sensory and/or motor deficits. It may progress to paralysis over weeks or months (Keime-Guibert, Napoltano, & Delattre, 1998; Schultheiss et al., 1995). The symptoms usually occur between 6–36 months after radiotherapy (Kirkpatrick, van der Kogel, & Schultheiss, 2010). In particular, the cervical cord that frequently involves in the neck field during NPC radiotherapy innervates the shoulder girdles and upper limbs, thus radiation damage to this portion may eliminate sensation and motor control of the upper limbs (Martini et al., 2001).

Dose response relationship for radiation-induced myelopathy had been analyzed by some studies. It has been suggested that the incidence of myelopathy are 0.2 %, 5 % and 50 % for the total spinal cord dose of 45–50 Gy, 57–61 Gy and 68–73 Gy respectively (Kirkpatrick, van der Kogel, & Schultheiss, 2010; Schultheiss et al., 1995). Another study (Marucci et al., 2004) evaluated the

cervical cord dose of 85 patients with cervical vertebral tumors treated with proton-photon irradiation. The maximum equivalent uniform dose (EUD) for the cord was 59.4 CGE in 1.5 CGE/fraction. In this study, 13 patients experienced grade 1–2 spinal cord toxicity and 4 patients with grade 3 toxicity. The median onset time was 6 months (3–49 months). The authors therefore concluded that a maximum EUD of 60 Gy with 1.5 Gy/fraction, which corresponded to 52.5 Gy with 2 Gy/fraction to the cervical spinal cord, was considered safe. Recently, Schultheiss (2008) analyzed several published reports to establish the dose response model on radiation-induced myelopathy. For cervical cord, the estimated median tolerance dose was 69.4 Gy, and the incidence of myelopathy was estimated as 0.2 % and 0.03 % if the cord dose reached 50 Gy and 45 Gy respectively.

There is a common belief that the dose to the spinal cord should be decreased if the irradiated length is long. Nevertheless, papers on spinal cord injury mostly described a dose threshold, indicating insufficient data to support the existence of a volume effect (Schultheiss et al., 1995; Schultheiss, 2008). The dose tolerance of 45 Gy to spinal cord or $D_1 \leq 45$ Gy is commonly set during treatment planning (Hoppe et al., 2007; Kam et al., 2004; Wu et al., 2009). According to stated studies, this limit may be too conservative. Moreover, there are clinical reports demonstrated the possibility of recovery in months to years after radiotherapy (Nieder et al., 2005; Ryu et al., 2000). It is therefore suggested the dose limit to the spinal cord can be relaxed, say 50 Gy, whenever higher tumoricidal dose is necessary for curative purpose (Schultheiss et al., 1995).

1.1.3 Optic chiasm

Optic chiasm is an "X" shaped junction where the left and right optic nerves from retina of each eye converge. At the chiasm, the medial portion of two optic nerve fibers crosses over to the opposite side of the brain. Anatomically it is superior to the sella turcica and just below the hypothalamus. Compared to other critical organs, optic chiasm is relatively distant from the nasopharyngeal region with a lower chance of receiving high dose during radiotherapy. However, it is not uncommon that the chiasm gets close to the high dose zone due to the superior progression of the disease. Radiation damage to the optic chiasm can result in radiation-induced optic neuropathy (RION), which is a traumatic late complication that usually presents as sudden profound irreversible vision loss. Depending on the lesion site inside the chiasm, the visual impairment can be unilateral or bilateral, temporary or permanent (Danesh-Meyer, 2008; Mayo et al., 2010). In worst case, acute bilateral blindness may result from injury to the entire chiasm (Mayo et al., 2010). The onset of RION can be within 3 months or as long as 8 years after radiotherapy. The treatment to RION is limited (Danesh-Meyer, 2008; Mayo et al., 2010).

Complication data for RION had been presented in several papers. Two studies evaluated the treatment outcome of paranasal sinus and nasal cavity radiotherapy and showed a maximum dose of ~52 Gy could be delivered to the chiasm without RION (Daly et al., 2007; Hoppe et al., 2007). Another study on radiotherapy for pituitary adenoma showed that 1 out of 34 patients developed bilateral RION with a chiasm dose of 56.1 Gy. The interval between treatment

and onset of symptoms was 8 months (Mackley et al., 2007). Martel et al. (1997) tried to correlate the dose and chiasm volume for RION. They showed that 1 out of 20 patients had suffered from bilateral temporal vision loss due to chiasm damage 4 years after radiotherapy. The maximum dose to the chiasm was 59.5 Gy. For the rest of patients with no symptoms of RION, the average maximum dose was 53.7 Gy (28.0–70.0 Gy), in which 5 patients in this group had their maximum dose exceeded 60 Gy and the V_{60} was 10 % in 3 patients. These inconsistent results suggested that the incidence of RION might be probabilistic. Although the dose response relationship for RION has not yet been clearly defined, it is generally believed that the onset of RION starts at a dose of 50–55 Gy but the chance is minimal (Danesh-Meyer, 2008; Mayo et al., 2010). The risk increases to 3–7 % when the dose reaches 55–60 Gy and can be as high as 7–20 % when the dose is beyond 60 Gy (Mayo et al., 2010). The common radiotherapy planning constraint for optic chiasm is 45–60 Gy, depending on the tumor site and prescribed doses to the targets (Daly et al., 2007; Hoppe et al., 2007; Kam et al., 2004; Mackley et al., 2007; Martel et al., 1997).

1.1.4 Pituitary gland

Pituitary gland, together with the hypothalamus above, belongs to the neuroendocrine system. It is anatomically situated in the sella turcica at the base of the brain and behind the nasopharynx. The pituitary gland monitors and regulates daily body functions by secreting various hormones to different organs and glands. It also plays an important role in growth, development and reproduction. The pituitary composes of two lobes. The anterior lobe accounts

for about 80 % of the gland and produces adrenocorticotropic hormone (ACTH), growth hormone (GH), gonadotropins of luteinizing hormone (LH) and follicle stimulating hormone (FSH), prolactin (PRL) and thyroid stimulating hormone (TSH) according to the signals from hypothalamus. The posterior lobe is linked to the hypothalamus via the pituitary stalk and stores vasopressin and oxytocin produced by the neurons in hypothalamus for later release. Pituitary gland usually receives high dose during radiotherapy of NPC because the primary tumor frequently arises from the superoposterior wall of nasopharynx. Moreover, the tight dose constraint to the optic chiasm also leads to scarification of underlying pituitary gland. Radiation damage to the pituitary gland may result in hypopituitarism i.e. deficiency in pituitary hormone production, which may manifest over several years after radiotherapy. Hormone deficiency can be single or multiple, and panhypopituitarism usually describes the loss of all ACTH, gonadotropins, GH and TSH (Toogood, & Stewart, 2008). Table 3.1 gives the functional descriptions on these anterior pituitary hormones and the clinical presentation due to their deficiencies (Fernandez et al., 2009; Pai et al., 2001; Toogood, & Stewart, 2008). In brief, patients may suffer from fatigue, changes in body composition, infertility, sexual dysfunction, abnormal thyroid function and inability to lactate etc depending on specific hormone deficits (Toogood, & Stewart, 2008). All these symptoms are presented across lifespan that significantly decrease patient's QOL after radiotherapy. Adequate monitoring and lifelong hormone replacement therapy to the target organs are essential (Fernandez et al., 2009; Pai et al., 2001).

The incidence of radiation-induced hypopituitarism was dose- and time-dependent. A study (Pai et al., 2001) on 107 patients treated with proton-photon radiotherapy to base of skull tumor showed that 61 % patients developed various degree of endocrine dysfunction in a median follow-up time of 5.5 years. This study identified two pituitary dose thresholds: the minimum dose of 50 CGE and maximum dose of 70 CGE, both of them were associated with a significant higher incidence of hypopituitarism. The severity of hypopituitarism also tended to increase with radiation dose. The percentages of patients suffered from two or more endocrinopathies were 7 %, 24 %, 29 %, and 40 % with the minimum doses of ≤ 50 CGE, 50–60 CGE, 60–70 CGE, and ≥ 70 CGE respectively. The incidence of endocrine dysfunction was shown to increase with longer length of follow-up. The respective 5-year and 10-year actuarial rates of endocrinopathy were 72 % and 84 % for hyperlactinemia, 30 % and 63 % for hypothyroidism, 29 % and 36 % for hypogonadism, and 19 % and 28 % for hypoadrenalism. Consistent finding was seen in another study (Agha et al., 2005) when the dose-time response of hypothalamic-pituitary function of 56 patients with primary non-pituitary tumor after radiotherapy was assessed. In this study, 41 % patients suffered from single to multiple hypopituitarism. The incidence of GH deficiency, hyperlactinemia, hypogonadism, hypoadrenalism and hypothyroidism were 32 %, 32 %, 27 %, 21 %, and 9 % respectively. The risk of radiation-induced hypopituitarism was significantly associated with greater biological equivalent dose (median: 71 Gy vs 43 Gy; p = 0.012) and longer time interval after radiotherapy (median: 6.5 years vs 2.3 years; p = 0.02). Darzy and Shalet (2009) summarized the incidence of various pituitary hormone deficiencies following radiotherapy in different pituitary dose ranges. The

incidence in the dose range of 50–70 Gy, which is commonly received by the pituitary during radiotherapy of NPC, is restated here for reference (Table 3.2). The above studies provide suggestion to the dose constraint for pituitary gland during radiotherapy treatment planning and emphasize the necessity of lifelong endocrine surveillance after radiotherapy in order to detect progressive hypopituitarism.

Table 3.1: Functional descriptions of anterior pituitary hormones and clinical presentations of their deficiencies.

Anterior pituitary hormones	**Target organs & hormone functions**	**Hormone deficiencies & clinical presentations**
ACTH	Adrenal glands – Stimuate cortisol produciton	-Secondary hypoadrenalism i.e. insufficient cortisol, causing anoresia, , intolerance to stress, lethargy, fatigue, weight loss and nonspecific abdominal pain, severe hyponatremia and hypovolemic shock may develop and are fatal.
GH	Bones, muscle & fat – Regulate growth & body composition	-Tiredness, lack of energy -Abnormalities of protein, fat and carbohydrate metabolism contributed to abnormal body composition -Decreased bone mineral density, increased risk of fracture -Abnormalities of cholesterol, increased risk of heart disease

Gonadotropin (LH & FSH)	Ovaries & testes – Regulate reproduction & sexual function	-Hypogonadism -Men: atrophy of seminiferous tubules due to FSH deficiency, slow bread growth, decrease in sperm counts, libido, inability to achieve and maintain an erection -Women: oligomenorrhea or amenorhea, vaginal dryness, dyspareunia, hot flashes, breast atrophy
PRL	Breast – Stimulate milk production	-Hypolactinemia due to damage of pituitary gland, causing failure of lactation -Hyperlactinema due to disruption of the pituitary stalk, where inhibit hormone of dopamine from hypothalamus cannot release to the pituitary
TSH	Throid gland – Stimulate thyroid hormones production	-Central hypothyroidism i.e. insufficient thyroid hormones, causing fatigue, cold intolerance, weight gain, constipation, dry skin

Table 3.2: Summary of anterior pituitary hormones abnormalities following radiotherapy, extracted from Darzy and Shalet (2009) study.

Radiation dose	**Hormonal abnormalities**
50–70 Gy Nasopharyngeal carcinoma & tumors of the skull base	-GH deficiency (almost in all patients after 5 years) -Gonadotrophin deficiency (variable severity in 20–50 % long-term) -TSH deficiency (up to 60 % long-term) -ACTH deficiency (27–35 % long-term) -Hyperprolactinemia (early complication in 20–50 %, mostly in women)

1.1.5 Parotid glands

Parotid glands mainly produce stimulated salivary and accounts for 60–65 % of total salivary volume (Cooper et al., 1995). They are anatomically located in juxtaposition to the nasopharynx and are lateral to the parapharyngeal space and level II neck nodes on both sides. Xerostomia i.e. inadequate salivary function is a common toxicity for NPC patients due to irradiation of the parotid glands (Cooper et al., 1995; Hsiung et al., 2006; Lee et al., 2002). Parotid glands are parallel organs i.e. they can continue to function until a critical number of functional subunits are damaged (Eisbruch et al., 1999). Therefore the planning strategy for NPC cases usually focuses on sparing other more critical organs such as brainstem and optic chiasm. This eventually may lead to higher doses to the parotid glands and thus higher incidence of xerostomia. Although xerostomia is not life threatening, suffered patients experience changes in speech and taste, difficulties in mastication and swallowing which lead to nutritional compromise, and chronic changes in oral flora which increase the risk of fissures, ulceration, dental caries and infection. All these dramatically decrease patient's QOL after treatment (Blanco et al., 2005; Cooper et al., 1995; Li et al., 2007b).

A reduction in parotid gland function usually begins in early course of radiotherapy and persists till treatment ends. Recovery after treatment is possible if the radiation damage is not severe. Many studies correlated the mean parotid gland dose with salivary output after treatment. In general, mild saliva reduction occurs at a mean dose of < 10–20 Gy (Eisbruch et al., 2001; Li et al., 2007b), with a gradual increase of reduction at mean dose of 20–30 Gy (Blanco et al.,

2005; Eisbruch et al., 2001; Li et al., 2007b). Largest saliva reduction occurs in 1–3 months after radiotherapy followed by gradual recovery, with a return to pre-treatment salivary level in 6–24 months (Blanco et al., 2005; Eisbruch et al., 2001; Eisbruch et al., 1999; Hsiung et al., 2006; Li et al., 2007b). Modest yet incomplete recovery can be seen at dose range of 30–40 Gy. However, mean dose of > 40 Gy will lead to strong saliva reduction which may lead to permanent damage (Cooper et al., 1995; Eisbruch et al., 2001; Li et al., 2007b). In particular, several studies indicated the risk of xerostomia was significantly decreased if the parotid gland mean dose was kept < 26 Gy (Blanco et al., 2005; Eisbruch et al., 2001; Eisbruch et al., 1999; Li et al., 2007b). Blanco et al. (2005) further showed that greater sparing of late salivary function could be achieved by even lower mean dose and every Gy increase in parotid mean dose could lead to an exponential loss of 5 % in salivary function. Eisbruch et al. (1999) on the other hand found the partial volume constraints, in which 67 %, 45 % and 24 % parotid volumes received less than 15 Gy, 30 Gy and 45 Gy respectively, were recommended during treatment planning for salivary preservation. Another report showed a compensatory overproduction of saliva by the contralateral gland in unilateral neck irradiation, emphasizing the importance of sparing at least one parotid gland in order to retain patient's QOL after radiotherapy (Eisbruch et al., 2001).

3.3 Treatment uncertainties

The success of radiotherapy greatly depends on the accuracy of delivering the doses to target volumes as planned while sparing the normal tissues in every single fraction of a treatment course. However, this is not easily achievable due to the presence of treatment uncertainties. The daily setup variation as well as geometric and volumetric changes in internal organs may lead to discrepancies in dose distribution between treatment and planning. As the initial image set acquired before the start of treatment for planning no longer reflects the true appearance of the targets and OARs, the treatment plan is no longer valid. The potential consequences will be insufficient dose coverage to tumors and/or overdose to adjacent OARs, which ultimately decreases the therapeutic ratio.

For head and neck cases, internal organ motion is not an issue, and the daily setup uncertainties are relatively small. However, most patients experience tumor, involved lymph nodes or parotid glands shrinkage and displacement throughout the prolonged radiotherapy course (about 6–8 weeks). Moreover, they also suffer from weight loss, which can lead to unfit of the immobilization mask. The factors contributing to treatment uncertainties during head and neck radiotherapy are discussed below.

3.3.1 Setup errors

The interfractional setup errors consist of systematic component, which repeats in every fraction of treatment, and random component, which varies from day to day throughout a radiotherapy course (Li et al., 2007a). The systematic errors can be the result of various machine-specific mechanical effects such as inconsistency of setup laser position between the treatment machine and the CT simulator or treatment couch sag (Burnet et al., 2010; Han et al., 2008; Mechalakos et al., 2007; Schubert et al., 2009). The random errors may be resulted from patient mis-positioning. Basically, setup errors are estimated by assessing the geometric deviation between the treatment verification images and the planning images. The error measurement is institution-dependent, in which the staff anatomic knowledges and interpretation on the images as well as the imaging devices and strategies used for detecting errors will affect the outcome (Schubert et al., 2009).

Table 3.3 summarizes the reports documenting the interfractional setup errors of head and neck cancer patients undergoing radiotherapy. In all studies, thermoplastic mask was used and was shown to be an effective immobilizing device to limit patient motion during treatment (Li et al., 2007a; Mechalakos et al., 2007). Together with the rigid anatomy of the head and neck region, the setup errors were relatively small compared to those in other body regions e.g. abdomen and pelvis (Burnet et al., 2010; Li et al., 2007a; Schubert et al., 2009). The mean translational errors were ranged from 0 to 10.5 mm and the mean rotational errors are $< 1.4°$ in these studies. In particular, Schubert et al. (2009)

showed majority of treatment fractions (85 %) were shifted ≥ 2 mm in 3D vector distance but only 54.7 % required ≥ 4 mm shift. In terms of roll correction, only 29.6 % treatment fractions required a shift of ≥ 1°.

Although the setup errors are small, leaving it without correction will lead to dosimetric consequences. Hong et al. (2005) demonstrated a decrease of 3–21 % in the EUD to the defined tumor volumes as well as an increase of ≤ 3 Gy for parotid mean dose when the geometric offsets were applied in the treatment plan. Without setup corrections, Han et al. (2008) showed the maximum dose to the spinal cord was significantly increased by 7.6 % (3.3–15.5 %) when compared to those with setup corrections. As mentioned, A CTV-PTV margin is added to the tumor to account for these interfractional deviations. However, these errors can be patient-specific and in random basis with different degree and combination, thus accurate radiation dose still cannot be guaranteed. Currently, rotational setup correction is somehow hindered by the inability of the treatment couch. Depending on the treatment system used, these rotational adjustments especially the pitch can only be corrected by manually moving the patient, which is difficult to apply with accuracy (Kaiser et al., 2006; Schubert et al., 2009; Zhang et al., 2006). Therefore, careful initial patient positioning remains important to prevent any unpleasant errors that require patient manipulation before proceeding to treatment.

Table 3.3: Selected reports documenting the interfractional setup errors of head and neck cancer patients undergoing radiotherapy.

Investigators	No. of patients	Imaging techniques /Frequency		Mean translational errors (SD)/mm			Mean rotational errors (SD)/°		
				Lateral	Longitudinal	Vertical	Roll	Pitch	Yaw
Burnet et al., 2010	37	MVCT/Daily		1.7	2.3	2.8	na	na	na
			Σ	1.8	2.1	1.7			
			σ	1.4	1.6	1.4			
Han et al., 2008	5 (all NPC)	MVCT/Daily		10.5* (3.4)	0.1 (2.5)	1.0 (2.4)	0.1 (1.1)	na	na
Hong et al., 2005	10	Optical guided patient localization system/Daily		0.8 (4.4)	0.4 (3.4)	2.1 (5.1)	1.4 (3.2)	0.5 (2.3)	0.5 (1.6)
Li et al., 2007a	37	MVCT/Daily		0.3 (1.1)	0.1 (2.2)	0.2 (1.3)	0.3 (0.7)	na	na
Mechalakos et al., 2007	7	kV orthogonal /~3 times weekly		0 (2)	2 (3)	1 (3)	na	1.1 (1.7)	0.5 (0.9)
			Σ	1	3	2			
			σ_{RMS}	2	2	2			
Schubert et al., 2009	30	MVCT/Daily	Σ	2.3	1.9	1.6	0.8	na	na
			σ_{RMS}	1.8	1.9	1.9	1.2	na	na

-Only magnitudes are given for comparison purposes, numbers are rounded to nearest 0.1 mm (except Mechalakos et al., 2007) and 0.1 °.

-Standard deviations (SD) are quoted if they appeared in the original paper.

-Σ: Standard deviation of the systematic errors; σ (σ_{RMS}): Standard deviation (root mean square) of the random errors.

-MVCT: Megavoltage computed tomography.

-*A known systematic lateral shift of about 10 mm between the home position of the treatment couch and that of the CT simulation couch was contributed to the data.

3.3.2 Anatomic changes in tumor volumes

Many studies have proved there was a radiation-induced shrinkage of primary tumors as well as lymph nodes during head and neck radiotherapy (Barker et al., 2004; Fang et al., 2001; Geets et al., 2007; Kodaira et al., 2009; Loo et al., 2011; Vasquez Osorio et al., 2008; Wu et al., 2009). Vasquez Osorio et al. (2008) assessed the degree and pattern of tumor volume loss in 10 oropharyngeal cancer patients 2 weeks after external beam radiotherapy, in which 46 Gy in 23 fractions was delivered. The primary tumor showed a significant volume reduction of 25 % when compared to its original volume. The shrinkage was asymmetric with more pronounced reduction on the posterior aspect but least effect on the right sub-region of the tumor. Another study evaluated the tumor and nodal regression rates for 101 NPC cases after 45 Gy of radiotherapy (Fang et al., 2001). The mean volume losses were 70 % and 81 % for primary tumor and lymph nodes respectively. In particular, the regression rates of primary tumor and lymph nodes were considered rapid (> 75 % loss) in most patients (48 % and 66 % respectively), with 32 % and 24 % patients showed moderate regression (50–70 % loss), and 21 % and 10 % showed slow regression (< 50 % loss), respectively. In Barker et al. (2004) study, CT scans of 3 times weekly were done to monitor the volumetric and geometric changes of the GTVs in 14 head and neck cancer patients throughout the radiotherapy course. Progressive volume loss was noted in both primary tumor and involved lymph nodes, at a median rate of 1.7 % and 1.8 % of their initial volumes/day respectively. At the end of the treatment course, a median total reduction of 69.5 % of the initial GTV volume was observed. The shrinkage pattern was again showed to be

asymmetric, as the centre of tumor mass changed in location with time.

Radiation-induced tumor shrinkage could lead to violation of the planned dose distribution. One study on 5 head and neck cancer patients calculated the actual delivered doses to the CTVs according to their volumetric changes during the radiotherapy course (Loo et al., 2011). The mean volume losses of the low-, intermediate- and high-risk CTVs were 10.7 %, 7.1 % and 5.8 % respectively. Though modest, these volume reductions led to the respective calculated delivered doses of 1.9 %, 2.4 % and 1.3 % higher from their planned doses. Another study evaluated the dosimetric changes caused by tumor shrinkage at mid-course of NPC treatment (Kodaira et al., 2009). In 14 out of 20 patients, there was an increase in PTV receiving ≥ 110 % of the prescribed dose compared with the initial plan, though the exact effect was not quantified.

3.3.3 Anatomic changes in parotid glands

Several factors attribute to the volumetric and geometric changes in parotid glands during radiotherapy. Other than radiation-induced shrinkage, the position of the parotid glands can also be displaced due to tumor especially the adjacent lymph nodes regression and body weight loss (Kodaira et al., 2009; Kuo et al., 2006; Loo et al., 2011). The progressive volume shrinkage and medial shifting of the parotid glands during head and neck radiotherapy have been extensively documented. Both Barker et al. (2004) and Lee et al. (2008a) showed similar median rates of relative parotid volume loss, which were 0.6 %/day and 0.7 %/day respectively. These corresponded to a respective median volume

reduction of 28.1 % and 21.3 % at the end of the treatment course. The median medial shifts of the parotid glands were 0.31 cm and 0.26 cm respectively in these two studies. Lee et al. (2008a) additionally suggested that the parotid glands tended to lose volume faster in earlier stage of a treatment course. This was supported by Wang et al. (2009) study, who reported a volume reduction of 20.01 % in the first 3 weeks of radiotherapy compared to 8.57 % in the last 3 weeks of treatment. The total volume loss at the end of treatment was 26.93 %. Wang et al. also found that there was a significant correlation between the planned mean dose and volume loss during the treatment course, in which the parotid glands with higher planned mean doses (> 30 Gy) suffered a larger volume loss than those with lower planned mean doses (< 30 Gy). Vasquez Osorio et al. (2008) gave similar finding that the mean volume reduction was only 5% in the spared gland with lower planned mean dose of 6.97 Gy but reaching 17 % in the irradiated gland with higher planned mean dose of 25.15 Gy. The medial shifting of the irradiated gland was also significantly larger than those in the spared one. All these suggested the anatomic changes of parotid glands were dose-dependent.

The parotid glands that experience shrinkage and medial displacement may consequently translate into the high dose region and receive higher actual doses than expected in the original treatment plan. Robar et al. (2007) assessed the parotid anatomic changes and their subsequent dosimetric effects in 15 head and neck patients during radiotherapy. They demonstrated an increase of 2.6 % in mean doses and 3.5 % in the V_{26} of the parotid glands from the initial plan. In their study, the glands had shrunk by 4.9 %/week and shifted medially by 0.85

mm/week. Another study (Loo et al., 2011) showed a significant volume reduction in the contralateral and ipsilateral glands, with a mean percentage loss of 17.5 % and 30.2 % respectively. This in turn led to a corresponding increase of 19.3 % and 8.9 % in the mean percentage dose/fraction. Lee et al. (2008b) studied the trend of parotid dose increase resulting from anatomic changes over a radiotherapy course in 10 head and neck cases. They found that the increase in parotid gland dose was highly correlated with their medial displacement towards the high dose region. As the treatment course progressed, the parotid glands shifted more and more to the medial aspect and led to a gradual increase in the parotid dose. At the end of the treatment course, the mean parotid dose and V_{26} were increased by 11 % and 31.3 % compared to the planned one respectively. Another trial (Han et al., 2008) performed on 5 NPC patients also provided similar results. While the parotid volume dropped 40.2 % at the end of treatment, the median fraction dose to the parotid increased by 77 % compared to the planned one.

3.3.4 Body weight loss and spinal cord displacement

It is common that head and neck cancer patients lose weight throughout the radiotherapy course. Radiation to the mouth, oral cavity, pharynx and salivary glands can lead to complications like xerostomia, oral mucositis and dysphagia (Fua et al., 2007; Kodaira et al., 2009). Patients often lose appetite and hence decrease nutritional intake. Body weight loss can also due to tumor, involved lymph nodes and parotid shrinkages during radiotherapy. It usually manifests as alterations in body habitus especially in the neck region. Some studies monitored

the patient weight changes during head and neck radiotherapy. The median weight loss was reported as 7.1 %, 3.3 % and 7.3 % in three studies (Barker et al., 2004; Lee et al., 2008b; Robar et al., 2007) respectively. In particular, Barker et al. (2004) showed the body weight change was highly correlated with the external skin contours at levels of C2 vertebral body and base of skull. The weight change was also closely related to the medial displacement of the parotid glands to the high dose region (Barker et al., 2004) and the parotid mean dose (Lee et al., 2008b). It was thus suggested that significant weight loss could act as an indicator of large parotid shift to medial aspect with increasing dose.

Continuous weight loss during radiotherapy increases the chance of patient motion. Due to the decrease in neck volume, the immobilization mask becomes loosen. Patients are therefore prone to spinal cord displacement and in turn setup uncertainties. Zhang et al. (2006) showed that the mid-lower neck region was the least stable region compared to the central part of the head and neck area during radiotherapy. Robar et al. (2007) assessed the spatial displacement along the craniospinal axis during radiotherapy and found that the mean displacement had increased systematically from 2.9 mm at the level of superior brainstem to 6 mm at the level of T2 cord. The large displacement in the lower cord levels (below C3/C4) led to an increase of 2.2 % in the cord maximum dose and 1.1 % in its D_1. Another study (Wang et al., 2007) demonstrated the setup errors, which was < 3 mm in NPC cases, could increase significantly when patients lost > 5 % of their body weight. These studies showed the lower neck region where the lymph node targets usually located was vulnerable to movement. Therefore, the patient motion due to weight loss and loosen of immobilization device may lead to cord

displacement and result in adverse dosimetric effect.

3.4 Radiotherapy techniques

Conventional 2D-RT and 3D-CRT are common radiotherapy techniques in treating NPC in the 1990s. In general, large radiation fields covering the faciocervical region are used aiming to encompass both the primary site and the neck nodes. It is known that radiation dose to the target volume is one of the prognostic factors for local control in NPC (Teo et al., 2006; Teo, Lee, & Yu, 1996). In addition, large tumor in advance stage usually requires higher tumoricidal dose for cell killing (Fang et al., 2001; Kwong et al., 2006; Kam et al., 2004). However, the complexity of the anatomic relationship between the tumor and various critical organs often induces target undercoverage and hinders meaningful dose escalation using these conventional methods (Waldron et al., 2003). Intensity modulated radiotherapy (IMRT) has been widely implemented in treating NPC since last decade. On top of this, the concerns in dosimetric consequences due to treatment uncertainties urge the rapid development of in-room imaging techniques and hence give rise to further advanced treatment techniques of image guided radiotherapy (IGRT) and adaptive radiotherapy (ART). All these are discussed below.

3.4.1 Intensity modulated radiotherapy (IMRT)

In IMRT, treatment fields consist of numerous small radiation beams (beamlets) with non-uniform intensities are applied. The intensities of these beamlets are calculated by an inverse planning algorithm, in which the dose-volume objectives and weighting factors for the targets and OARs are first assigned by the planner and followed by iterative computer optimization to generate an optimum beam intensity profile. This profile is then translated into a series of MLC motions for actual treatment delivery. IMRT allows complex shaping of the dose distribution for irregular shaped targets, providing highly conformal treatment with steep dose fall off outside the target volumes. It also allows differential doses to be delivered to different target volumes during treatment. The advantages of IMRT include radiation dose escalation without jeopardizing the surrounding OARs, and hence improve the local tumor control with OARs preservation (Cheng, Chao, & Low, 2001; Kam et al., 2003; Kodaira et al., 2009; Kwong et al., 2006; Lee et al., 2002; Pow et al., 2006).

Kam et al. (2003) study clearly demonstrated the dosimetric advantages of IMRT over conventional radiotherapy in treating all stages of non-metastatic NPC. IMRT provided best target coverage with increased conformity and homogeneity to the target volumes when compared to those conventional techniques. For all stages, the D_{95} of PTV was improved from 52.5–62.0 Gy in 2D-RT and 3D-CRT to 67–68 Gy in IMRT. Better sparing of various OARs like brainstem, spinal cord, temporal lobes and temporomandibular joint was achieved by IMRT. In particular, the mean doses to the parotid glands were

significantly reduced from 49.6–69.7 Gy in conventional radiotherapy to 32.7–41.4 Gy in IMRT. Another study (Cheng, Chao, & Low, 2001) also found that the target coverage and parotid sparing were significantly better with IMRT. The V_{70} of the lymph nodes GTV was 46.2 % in 3D-CRT compared to 87.7 % in IMRT, whereas the V_{30} of the parotid gland was 93.2 % in 3D-CRT but only 48.4 % in IMRT. The feasibility of dose escalation by IMRT was also demonstrated in various studies (Kam et al., 2003; Kam et al., 2004; Kwong et al., 2006). Using IMRT, total dose of up to 76–80 Gy could be delivered to the targets with all OAR doses stayed well within tolerance. This subsequently led to an improved therapeutic ratio.

Some studies emphasized the impact of IMRT on parotid sparing in NPC cases. Lower parotid dose as achieved by IMRT can decrease damage to the salivary function which in turn improves patient's QOL. Pow et al. (2006) showed that 83.3 % early staged NPC patients who were treated with IMRT had recovered at least 25 % of parotid saliva flow 12 months after radiotherapy. However, only 9.5 % patients who treated with conventional radiotherapy had the same level of recovery. Moreover, the QOL score for patients in IMRT group was significantly higher than those using conventional techniques, indicating the IMRT group suffered less from xerostomia-related symptoms. The encouraging result is not limited to early staged cases. Another study (Hsiung et al., 2006) on advance staged NPC patients recorded the results of parotid scintigraphy and showed the mean maximal excretion ratio was only 0.6 % in 6–12 months after conventional radiotherapy. This value was dramatically higher in the IMRT group and presented as 23.3 %. In 9 months after radiotherapy, 94% patients in the

conventional group suffered from grade 3 xerostomia, whereas only 50 % patients had grade 2 xerostomia in the IMRT group.

Centres worldwide had showed promising treatment outcomes with IMRT on NPC. Aichi Cancer Centre showed a 10-month progression-free survival of 79.7 % and overall survival of 95 % in NPC patients treated with helical tomotherapy (Kodaira et al., 2009). In the University of California, San Francisco, the rate of local progression-free, locoregional progression-free, distant metastasis-free and overall survival rates were 97 %, 98 %, 66 % and 88 % respectively in 4 years (Lee et al., 2002). In Hong Kong experience, the 3-years actuarial rates were 92 %, 98 %, 79 % and 90 % for local relapse-free, nodal relapse-free, distant metastasis-free and overall survival respectively (Kam et al., 2004). Despite multiple dosimetric benefits given by IMRT, the sharp dose gradient at boundaries between targets and OARs inherently increases the treatment sensitivity to setup errors and anatomic changes, in which a small deviation from the treatment plan may greatly alter the actual dose being delivered. The potential consequences will be insufficient dose coverage to tumors and/or overdose to adjacent OARs (Hansen et al., 2006; Kuo et al., 2006). This concern brings about the introduction of IGRT.

3.4.2 Image guided radiotherapy (IGRT)

Recently, IGRT has been promoted to detect and correct treatment uncertainties. IGRT refers to continuous improvement of treatment delivery quality using in-room images to better achieve the goals of radiation therapy (Mackie et al., 2003a). In particular, radiotherapy using CT image guidance gains most popularity as they provide volumetric images for online treatment verification. Compared to 2D orthogonal portal vision, the better soft tissue visualization in volumetric images allows direct measurement of organ/target variation instead of using bony structures as surrogates (Borst et al., 2007; Morin et al., 2006). Moreover, the verification CT is readily comparable to the planning CT in a slice-by-slice fashion in different viewing planes. Precise correction of setup errors can be performed by assessing the coordinate changes and make corresponding couch translation and rotation.

Most common IGRT techniques used in Hong Kong include kilovoltage cone-beam (kVCB) CT (Oelfke et al., 2006) and megavoltage (MV) CT (Schubert et al., 2009). kVCBCT system is mounted on a conventional linear accelerator (LINAC). It consists of a kV x-ray tube and an amorphous silicon flat panel detector attached on the gantry perpendicular to the radiation beam direction (Mackie et al., 2003a; McBain et al., 2006; Meyer, 2007). During image acquisition, the gantry with the kV x-ray tube is rotated once around the patient in treatment position. Image projections are acquired by the detector and reconstructed using the Feldkamp filtered back-projection algorithm (Feldkamp,

Davis, & Kress, 1984) to give volumetric image set. Helical MVCT imaging is provided by the TomoTherapy System (TomoTherapy Inc., Madison, WI, US), which is an integration of a LINAC plus a CT scanner. Same MV x-ray source is used with a xenon detector positioned oppositely inside the ring gantry for MVCT imaging. The image acquisition process is analogous to CT scanning: patient in treatment position is continuously translated through the gantry with x-ray fan beam rotates about the patient (Forrest et al., 2004; Mackie et al., 2003a; Meyer, 2007). After image acquisition, the pre-treatment kVCB/MV CT images are manually or automatically registered to the planning CT images in transverse, coronal and sagittal planes for setup errors adjustment (Forrest et al., 2004; Kaiser et al., 2006; Mackie et al., 2003a; Pouliot et al., 2005; Xing et al., 2006;). The inherent differences in physical properties between kV and MV energies govern the imaging performances of these two techniques. In general, the Compton scattering effect on MV energies results in relatively poorer soft tissue contrast, but good at showing metal implants e.g. dental filling with only slight degradation in the MVCT images. In contrast, the dominant photoelectric radiation effect on kV energies depends on atomic number, which allows better soft tissue visualization but develops beam hardening and clipping artifacts around metallic objects which results in signal loss or dramatic streaks in the kV images (McBain et al., 2006; Meyer, 2007; Figure 3.1). Nevertheless, the image qualities of both techniques are good enough for instant detection of various treatment uncertainties (Mail et al., 2009; Meeks et al., 2005).

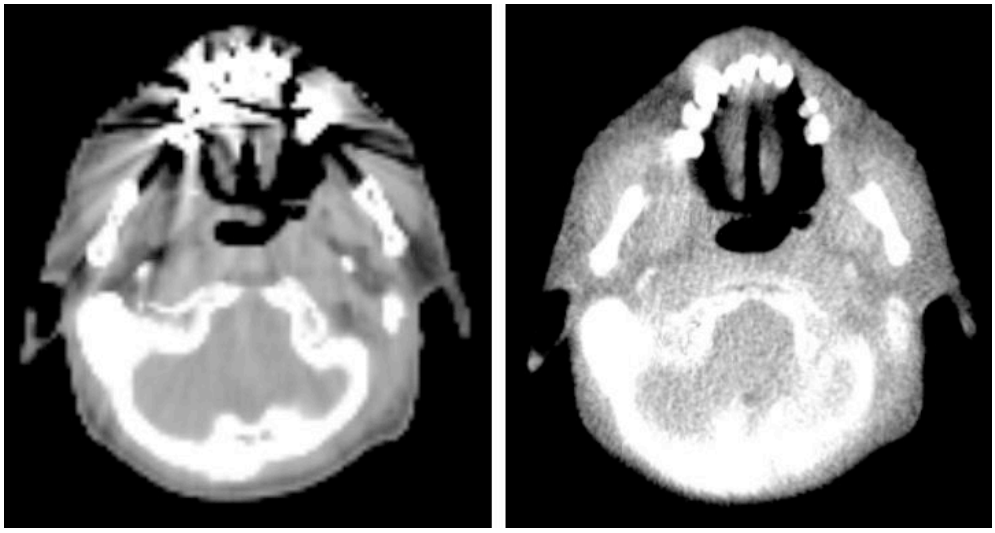

Figure 3.1: Transverse CT images of the head and neck region demonstrating the image quality differences between the kV (left) and the MV (right) images with dental filling.

IGRT is readily adopted in treating head and neck region because of the good image contrast between bones, soft tissues and air cavities enabling precise image registration. Although MVCT images are grainer compared to kVCBCT images, the tumor volume site is fairly visible especially for those situated in air-filled sinus. In addition, the surrounding bony landmarks can also be used as reliable surrogates for treatment verification owing to their stable relationship to the tumor (Pouliot et al., 2005). Due to accurate registration, IGRT can effectively reduce setup variations that may lead to undesirable dose discrepancies between treatment and planning (Burnet et al., 2010; Han et al., 2008; Li et al., 2007a; Schubert et al., 2009). Sheng et al. (2008) showed that the

mean setup error was reduced from 3.6 mm (without image guidance) to 1.7 mm (weekly image guidance) in head and neck patients using MVCT. This in turn improved the dose coverage to the PTV, which suffered from 2.1 % EUD loss without image guidance to only 1.4 % EUD loss with weekly guidance. In terms of OARs, the EUD increment was 1.8 Gy compared to 0.8 Gy without and with weekly guidance respectively. Unlike systematic errors which can be effectively minimized by different imaging protocols, random errors basically cannot be reduced in any fraction that is not image guided (Mechalakos et al., 2007; Zeidan et al., 2007). These random errors, though occasionally occur in small number of patients, can be of large deviation and project to tragic dosimetric consequences (Sheng et al., 2008). Daily image guidance is therefore always preferable in preventing day-to-day random errors (Li et al., 2007a).

The advantage of IGRT in precise tracking and correction of patient-specific variations over the head and neck treatment course provides chances to significantly reduce the CTV-PTV margin (Feng & Eisbruch, 2007; Schwartz & Dong, 2011). This is particularly helpful in treating NPC cases as the target volume is very close to various critical organs. Small CTV-PTV margin allows unprecedented tumor dose escalation and OARs sparing which is not available with IMRT alone. All these can ultimately maximize the local tumor control with minimal normal tissues toxicity (Meyer, 2007; Xing et al., 2006; Yan et al., 2005). In particular for head and neck region, IGRT also allows one to monitor the substantial radiation-induced organ changes throughout the treatment course (Barker et al., 2004, Han et al., 2008; Lee et al., 2008a; Lee et al., 2008b). Unfortunately, these non-rigid anatomic deformations cannot be corrected solely

by geometric couch offset calculated by the image guidance system. Therefore, the problem of fraction dose deviation and violation of the original dose-volume relationship may exist (Yan et al., 2005). Plan modification is required to accommodate such deficits, which gives rise to ART.

3.4.3 Adaptive radiotherapy (ART)

ART, which is an advanced mode of IGRT, refers to the modification of treatment plan based on tumor response and normal tissue anatomic changes during a course of radiotherapy (Meyer, 2007; Nath et al., 2009; Yan et al., 1997). Basically, ART involves (1) rescanning of patient, (2) recontouring of targets and OARs, and (3) replanning. ART is accomplished by the use of the CT image set acquired at any time during a treatment course. The tumors and OARs are contoured according to their changes on this scan. Any deviation from the original plan is being assessed and a new treatment plan is generated for subsequent fractions. Theoretically, ART that applies on a daily online basis, that is a new plan is generated everyday and executed immediately prior to a fraction, will be ideal to adapt daily anatomic changes. However for centres without in-room CT facilities, repeat CT scan requires patient to be transferred from the treatment room to the CT-scanner. Moreover, daily manual contouring and plan optimization can be tedious especially in head and neck cases with multiple target volumes and many OARs. As described, organ changes in head and neck cases were shown to follow a progressive trend rather than in a random manner (Barker et al., 2004; Fang et al., 2001; Lee et al., 2008a). Therefore it is possible for head and neck cases to deploy ART in interval basis, in which the

plan modification is done whenever significant changes are observed in any time point during the radiotherapy course. This approach potentially reduces the departmental resources e.g. related overheads, time and manpower needed with improved dosimetric results.

In the lights of a landmark report by Hansen et al. (2006) on the potential benefits of ART in head and neck cancer that published in 2006, some similar studies were carried out with different clinical settings and plan modification protocols. Hansen et al. repeated CT scan after 19 (mean, ± 6) fractions of treatment for 13 patients who experienced clinically observable changes or weight loss and a new plan was generated for subsequent fractions. Dosimetric analysis was done between the new plan (replanning) and the hybrid plan, which was computed by applying the original plan to the second CT (without replanning). Without replanning, the D_{95} of the PTV decreased in 92 % of patients (0.2–7.4 Gy). Conversely, the maximum doses to spinal cord and brainstem increased in 100 % and 85 % of patients, with the increased doses ranged from 0.2–15.4 Gy and 0.6–8.1 Gy respectively. Moreover, the doses to both the parotid glands and mandible increased without replanning, though some of their dose endpoints did not reach statistical significance. Kuo et al. (2006) performed a study in 10 patients with enlarged neck lymph nodes. The replanning was carried out after 25 fractions. It was observed in the second CT that the substantial lymph node regression (> 50 %) led to the medial translation of parotid glands into the high dose region, which caused a significant increase in the parotid mean doses. Replanning according to the parotid shift could provide a dosimetric benefit of > 3 Gy reduction in the mean doses.

Some trials were done specifically on NPC patients. Wang et al. (2010) repeated the CT for 15 NPC patients after 18 fractions of radiotherapy and compared the anatomic and dosimetric changes between the new plan and the hybrid plan. In this study, the lymph node target volume decreased 40.2 %. Nevertheless, the target coverage was maintained with increased high dose region. Again, the parotid glands decreased in volume and shifted medially, which led to increased mean doses of 2.57–2.97 Gy. Without replanning, the maximum doses to spinal cord and brainstem increased in 86.7 % and 80 % of patients, with the increased doses ranged from 0.05–7.8 Gy and 0.08–6.51 Gy respectively. Consistent results were found in Kim et al. (2009) study, in which 16 NPC patients had follow-up CT according to their treatment responses after receiving 30–50 Gy of radiotherapy. Again volumetric and dosimetric comparisons were made between the initial plan and the hybrid plan. Volume reduction of 37 % and 9 % was noted in GTV and CTV respectively, but the dose coverage to these targets was not changed significantly. The parotid gland volume decreased 34 %, which translated to a mean dose increment from 26.13 Gy in the initial plan to 31.62 Gy in the hybrid plan. The maximum doses to spinal cord and brainstem also increased from 42.79 Gy and 51.99 Gy in the initial plan to 44.96 and 53.59 Gy in the hybrid plan respectively. Nishimura et al. (2010) showed excellent clinical result of a two-step IMRT scheme with concurrent chemotherapy for NPC cancer. Thirty-five patients were treated with a new adaptive plan after 23–25 fractions. The 5-year overall survival and loco-regional rates were 83 % and 87 % respectively.

The above studies have clearly demonstrated that applying ART in the mid-course of head and neck or NPC treatment can overcome the dosimetric defects due to organ deformation. ART minimizes the unintended normal tissue toxicity and maintains the tumor coverage such that the advantages of IMRT will not be compromised. Considering the fact that the tumor and OARs have significant anatomic changes, ART with multiple replanning on different stages throughout the treatment course may be more beneficial. Some studies focused on the application of ART schemes for head and neck radiotherapy (Jensen et al., 2012; Schwartz et al., 2009; Zhao et al., 2011). In these studies, the frequency of replanning ranged from 1 replan to 3 replans. The selection criteria for the replan date were centre-specific without concrete guidelines, which might not be applicable to other institutions. To-date, the definition of optimum ART scheme for head and neck or specifically for NPC cases remains vague, more clinical proofs from systematic investigations are eagerly awaited.

3.5 Helical tomotherapy

Helical tomotherapy, which provided by the TomoTherapy HiArt System (TomoTherapy Inc.), is a specialized technique of delivering IMRT. The machine generates a modulatable fan beam from a 6 MV radiation source that is rotated around the patient in a helical manner. The beam intensity is modulated by sliding the binary 64 MLC leaves into and out of the path of the fan beam across its width, at the same time as the radiation beam rotating 360° around the patient and the treatment table advancing toward the gantry along the patient's cranio-caudal direction (Mackie et al., 2003b; Figure 3.2). Delivering radiation

in helical manner reduces the problem of junction matching for elongated treatment volume. The field length provided by the fan beam is 40 cm, and the field width of 1 cm, 2.5 cm or 5 cm is defined by the setting of movable jaws situated longitudinally below the radiation source (Mackie et al., 2003b). Unlike other LINACs, the radiation dose delivery for tomotherapy machine is based on time instead of monitor units. The typical beam on time for a NPC case is about 10 minutes.

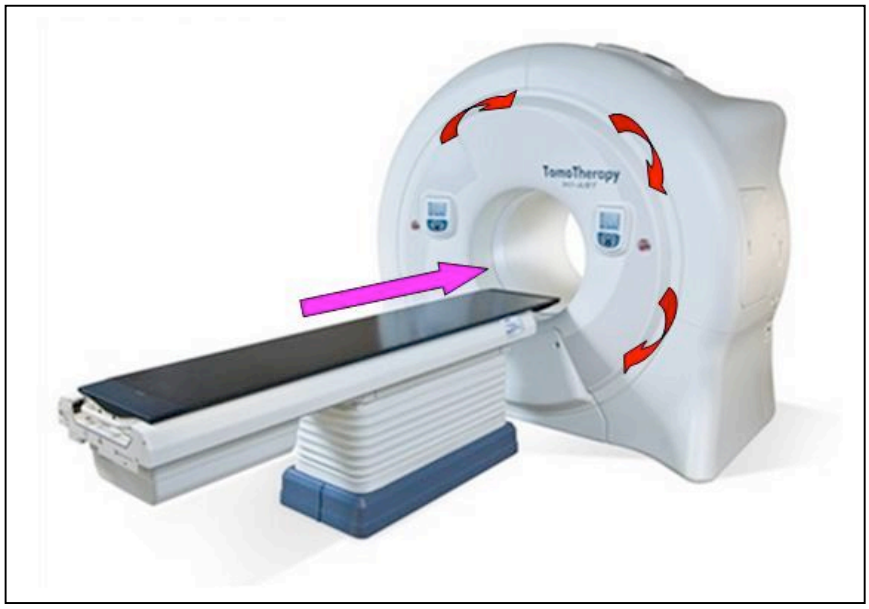

Figure 3.2: Tomotherapy machine manufactured by the TomoTherapy Incorporated (Madison, WI, US) for helical tomotherapy treatment.

Tomotherapy system also uses inverse planning algorithm for plan generation. In the optimization process, the 360° treatment delivery angle is approximated to 51 distinct beam directions with about 7° spacing (Burnet et al., 2010). In particular, the field width, pitch and modulation factor are set before dose optimization. The pitch is defined as the distance traveled by the couch in one complete rotation divided by field width, which determines the degree of overlapping between each helix. The modulation factor is defined as the ratio of maximum leaf opening time to average leaf opening time, which affects the flexibility of intensity modulation process during plan optimization (Burnet et al., 2010). These parameter settings affect the plan quality and the treatment delivery time. Basically, smaller field width, lower pitch, and higher modulation factor allows finer dose optimization and in turn higher quality of the plan but longer treatment time is required for the delivery. For NPC cases, the field width, pitch value and modulation factor are usually set as 2.5 cm, 0.287–0.3 and 2–4 respectively.

As stated, the tomotherapy system equipped with MVCT imaging ability allows IGRT to be performed with online correction of setup uncertainties. In imaging mode, the beam energy is detuned to 3.5 MV and full gantry rotation in a speed of about 6 second/rotation is employed (Forrest et al., 2004; Meyer, 2007). The maximum field-of-view is 40 cm in diameter (Jeraj et al., 2004). Three pitch modes can be selected for MVCT imaging: the coarse, normal and fine modes respectively produce MVCT slice thickness of 6 mm, 4 mm and 2 mm. The image acquisition time (number of slices x gantry rotation speed) for NPC cases is about 4 minutes (Mackie et al., 2003a). The imaging dose dissipated to patient

in general is about 1–3 cGy (Burnet et al., 2010; Forrest et al., 2004). The risk of secondary malignancies is relatively low with this dose range, which is therefore outweighed by the benefits of MVCT that allows setup verification and thus ensures the critical organs not fall into the high dose region.

The build-in software in the tomotherapy system allows rapid automatic registration between the MVCT and the planning CT images. The two image sets are superimposed with different color display for manual refinement of the matching results (Forrest et al., 2004; Figure 3.3). Rigid alignment is done in 3 translational and roll directions (Mackie et al., 2003a). The pitch and yaw adjustments, though available in the software, are not used in current practice because of the couch limitation in these directions (Schubert et al., 2009). One can validate the registration result by matching the anatomical landmarks on two image sets or by displaying the contours as well as isodose cloud on the MVCT image set to ensure correct dose is delivered to the intended area (Meyer, 2007). According to the registration result, the couch and the initial gantry angle are adjusted for the subsequent treatment.

In the Department of Radiotherapy of Hong Kong Sanatorium & Hospital, a three-phase radiotherapy protocol (i.e. two replannings in between the treatment course) for NPC treated with helical tomotherapy has been adopted since 2005. Daily MVCT prior to each treatment fraction is routinely performed for patient setup correction. All detected errors are corrected before each fraction. Including patient setup, treatment verification and delivery, the total patient on-couch time is about 20 minutes. Other than setup error correction, these daily MVCT image

sets also contain valuable anatomic information, which allows us to directly monitor and quantify the progression trend of tumor and OARs anatomic changes in NPC patients throughout a treatment course.

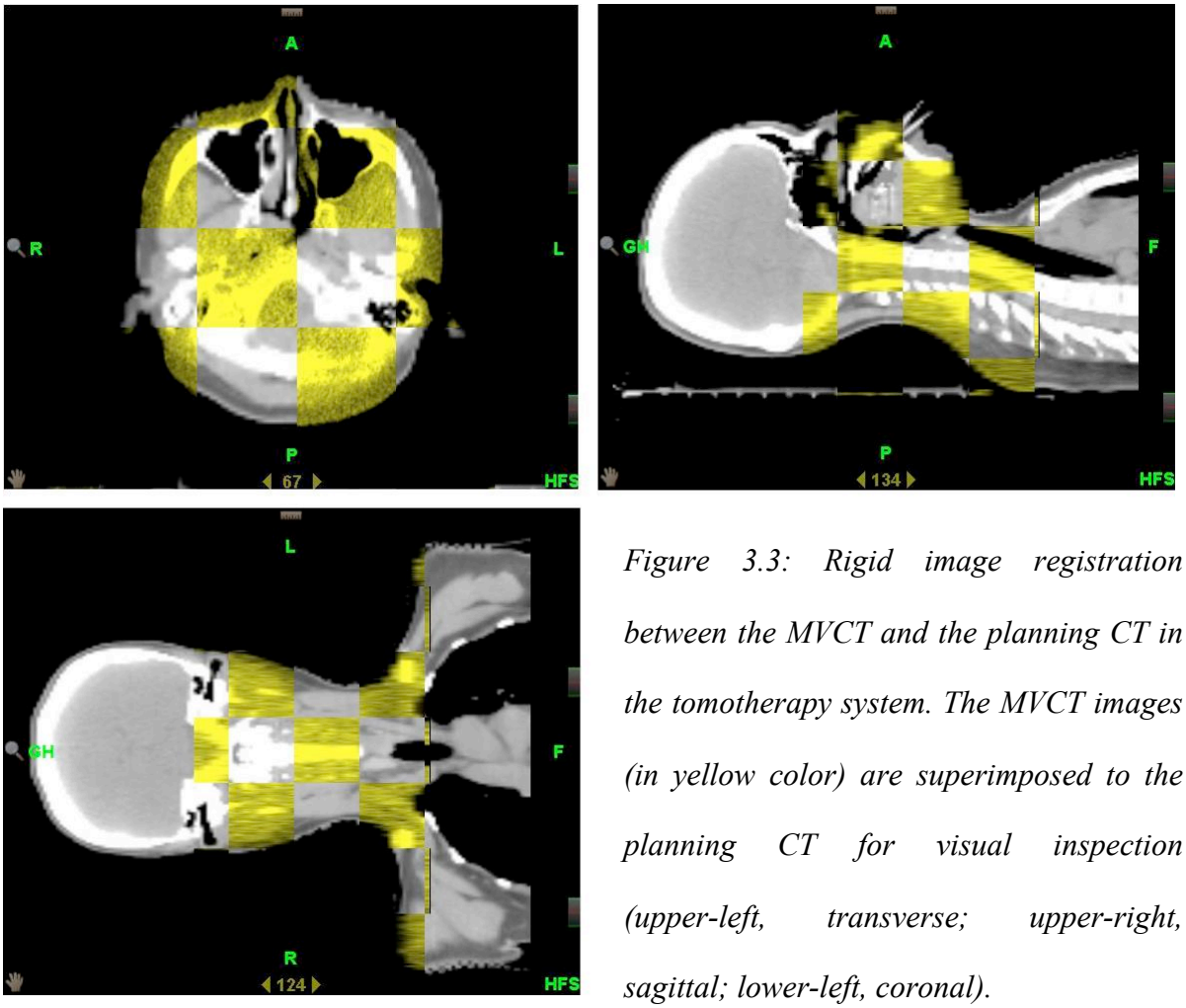

Figure 3.3: Rigid image registration between the MVCT and the planning CT in the tomotherapy system. The MVCT images (in yellow color) are superimposed to the planning CT for visual inspection (upper-left, transverse; upper-right, sagittal; lower-left, coronal).

CHAPTER FOUR

BASIS, OBJECTIVES AND CLINICAL SIGNIFICANCE OF THE THESIS

4.1 Basis of the thesis

The above literature review reveals that ART in interval basis can overcome the dosimetric consequences due to radiation-induced organ deformation in head and neck cancer. Nevertheless, research that focused on NPC is lacking. Most studies evaluated the tumor and organ regression trend on head and neck cancer where the primary treatment sites were heterogeneous. The dosimetric effect due to anatomic changes may vary according to different primary sites and so may not be representative for NPC. Published studies had showed that the target deformation in NPC cases might not necessarily lead to underdosage in target volumes as seen in head and neck cases. There are also insufficient reports of clinical experiences on ART strategies for head and neck cancer, even fewer for NPC. Besides, the sample sizes were small in all available studies. Most studies focused on ART involving 1 replan with the replanning day ranged from 18^{th}–25^{th} fractions. For those studies involved multiple replannings, the day and frequency of replanning ranged from 9^{th}–27^{th} fractions and 1–3 replans respectively. The great variety among studies reflected the controversy in when and how often the replanning should be deployed.

NPC is prevalent in Southern China including Hong Kong, ART implementation on this disease is therefore of particular interest. It is important for researcher to investigate the dosimetric outcomes of ART for NPC. In view of the progressive trends of anatomic changes in head and neck region during the radiotherapy course, it is possible to develop an ART strategy specifically for NPC by setting threshold to trigger a replan.

4.2 Objectives of the thesis

The first objective of the present study is to evaluate the potential dosimetric benefits of applying the current three-phase radiation protocol in NPC patients compared to the single phase treatment protocol. The second objective is to quantify and characterize the changes in volume and location of tumors and OARs in NPC patients using alternate day MVCT. The third objective is to establish an optimal ART strategy for NPC based on the above findings. This is done by defining various indicators and thresholds that signal the need for plan modification in a course of radiotherapy for NPC.

4.3 Clinical significance

This study emphasizes the ART advantages in NPC cases by hypothesizing the three-phase radiotherapy protocol should give better tumor dose coverage and sparing of adjacent critical organs when compared to those without replanning. ART is a technique heavily depends on the use of the image guidance systems that allow rescan, recontour and replan to be done. However, the lack of an

effective image guidance system as well as the manpower and time for increased workload hinder the ART implementation in some centres. In the second and third parts of this study, an ART strategy for NPC cases is established. By defining the optimal day(s) for replanning, ART performed in an interval basis can greatly reduce the needs of departmental resources. Moreover, it is practically feasible to apply in any centres regardless of the machines (tomotherapy system or LINAC) and image guidance methods being used in treating NPC. Most importantly, it is believed that the proposed strategy can effectively account for the anatomic changes that happen throughout a treatment course and bring about improvements in dosimetric and clinical outcomes.

CHAPTER FIVE

MATERIALS AND METHODS

The current study granted ethics approval from the Human Subject Ethics Sub-committee of the Hong Kong Polytechnic University and the Department of Radiotherapy, Hong Kong Sanatorium & Hospital. All data in this study were kept confidential and only used for study purpose.

5.1 Patient characteristics

This is a retrospective study recruiting 30 NPC cases treated with Hi-Art tomotherapy (TomoTherapy Inc.) at the Radiotherapy Department of Hong Kong Sanatorium & Hospital in 2005-08. The pre-treatment staging of the disease was done by clinical examination, endoscopic biopsy, CT and MRI. AJCC's 1997 staging system (Fleming et al., 1997; Table 2.1) was employed to define the disease stage. All patients received a three-phase radiotherapy protocol with a total of 37–38 fractions. Among them, 24 patients followed the routine treatment protocol of 25 fractions in phase one (PI), 10 fractions in phase two (PII) and 2–3 fractions in phase three (PIII). The other 6 patients received 25 or 30 fractions in PI, 5–9 fractions in PII and 2–4 fractions in PIII. All patients had repeat CT scanning and replanning for PII and PIII. In particular the first part of the present study, those patients who were not underwent routine treatment protocols were excluded. This was done to maintain the consistency of the replan schedule for better accentuation of the dosimetric differences between adaptive and non-adaptive approaches. In other words, only 24 patients with

same treatment protocol were included in the first part of the study, while all 30 patients were included in the second and third parts of the study for quantification of anatomic changes throughout the treatment course and establishment of optimal ART strategy for NPC.

Table 5.1 presents the main patient and disease characteristics in this study. All patients recruited were newly diagnosed with NPC without distant metastasis at the time of treatment. Majority (50 %) of patients suffered from Stage III disease. Histologically, all except 1 patient were diagnosed as undifferentiated carcinoma. Concurrent chemotherapy was given to those patients with Stage II to Stage IV disease. In particular, 73 % and 27 % patients received a total of 38 and 37 fractions of treatment respectively.

Table 5.1: Patient and disease characteristics

	No. of patient	%
Gender		
Male	23	77%
Female	7	23%
Tumor stage		
T1	9	30%
T2b	16	53%
T4	5	17%
Nodal stage		
N0	7	23%
N1	5	17%
N2	16	53%
N3a	1	3%
N3b	1	3%
Stage group		
I	3	10%
IIB	7	23%
III	15	50%
IVA	3	10%
IVB	2	7%
Histology		
Undifferentiated	29	97%
SCC	1	3%
Concurrent chemotherapy		
Yes	27	90%
No	3	10%
6 fractions/week		
Yes	20	67%
No	10	33%
Total no. of fractions		
37	8	27%
38	22	73%

5.2 Treatment planning and delivery

During CT simulation, all patients were immobilized with T-VacLok (Med-Tec Inc., Orange City, IA, US) under the head and neck region and covered with thermoplastic cast (Med-Tec Inc.; Figure 5.1). CT slices with thickness of 3 mm were acquired from the vertex down to the upper chest. The CT image sets were first sent to the Eclipse Treatment Planning System (Varian Medical Systems, Palo Alto, CA, US) for manual contouring. On each CT set, the oncologist delineated all target volumes and the radiation therapists delineated all OARs. For primary tumor, the GTV (NP-GTV) included all gross disease determined by CT, MRI, PET and endoscopic findings. The CTV of the nasopharynx (NP-CTV) included the parapharyngreal space, uvula, pterygo-maxillary fissure, outer table of clivus, basisphenoid, petrous tip, foremen ovale, foremen rotundum, inferior half of the sphenoid sinus, anterior vertebral body of C1 and prevertebral muscle/fascia, posterior 1–2 cm of maxillary antrum and nasal septum. In case of T3 disease, the inner table of skull was included into the NP-CTV. In T4 disease, the para-cavernous sinus and the orbits would be included in the NP-CTV depending on the location and the content of NP-GTV involvement. The PTV of the nasopharynx (NP-PTV) was generated automatically by the planning software with 3 mm margin added to the NP-CTV without any extension beyond the body surface to account for setup errors. This margin was decreased to 1 mm in posterior aspect if the NP-CTV was in close proximity to critical structures like brainstem. For the neck region, the GTV of the lymph nodes (LN-GTV) included any nodes > 1 cm and the nodes with necrotic centres. The CTV of the lymph nodes (LN-CTV) in PI covered the whole neck bilaterally which included

lymph nodes of surgical level II-V. For PII, the LN-CTV included the nodes at surgical level II-III, upper portion of level IV and the mid portion of level V. The LN-CTV in PIII included any residual lymph nodes plus 3 mm margin. Similarly, a 3 mm margin was again added automatically to the LN-CTV without extending beyond the body surface to generate the lymph nodes PTV (LN-PTV). The target volumes in the neck region were defined separately for left (L) and right (R) side. The same oncologist was responsible for all target delineation for all patients. After contouring, The CT sets were then transferred to the TomoTherapy Planning Station (Version 2.2.1) for helical tomotherapy treatment planning. The optimization options including the pitch, field width and modulation factor were set during the planning process and kept constant in all plans for the same patient.

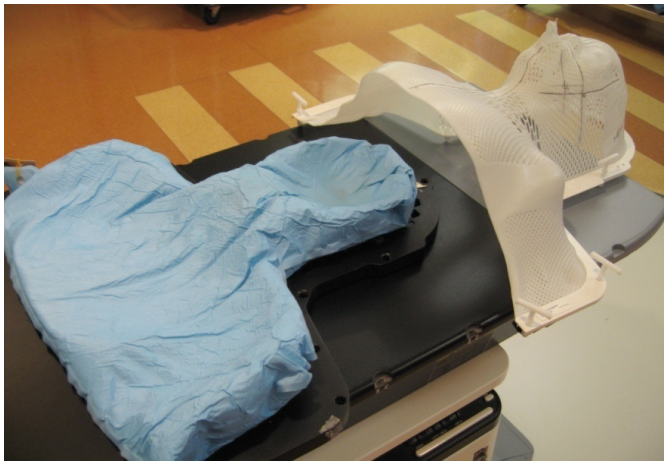

Figure 5.1: Customized T-VacLok (left) and thermoplastic cast (right) used for patient immobilization during CT simulation and also during treatment.

5.2.1 PII-ART and PIII-ART

Repeat CT scanning for PII and PIII treatments were scheduled within 1 week prior to the beginning of the corresponding phase. Same cast with original isocentre was used to set up the patient for image acquisition and subsequent treatment. In these repeated scans, the targets and OARs were recontoured based on their up-to-date anatomic changes. The target contouring was performed by the same oncologist. Two new treatment plans, denoted as PII-ART and PIII-ART, were optimized based on the modified contours on these CTs for subsequent PII and PIII treatments respectively. Table 5.2 shows the standard dose prescription for the routine treatment protocol. All target doses were prescribed at 95 % isodose level. According to the patient clinical condition and later on radiation response, the actual prescribed doses could be variable according to oncologist's decision.

Table 5.2: Standard dose prescription of the routine NPC treatment protocol; fr = fraction.

Target volumes	**Dose prescription**		
	PI	**PII**	**PIII**
NP-CTV	52.5 Gy / 25 fr	21.0 Gy / 10 fr	7.4 Gy / 2 fr or 10.5 Gy / 3fr
NP-PTV	51.5 Gy / 25 fr	20.6 Gy / 10 fr	7.0 Gy / 2 fr or 10.5 Gy / 3fr
LN-PTV (L/R)	50.0 Gy / 25 fr	20.0 Gy / 10 fr	7.0 Gy / 2 fr or 10.5 Gy / 3fr

5.2.2 PII-NART and PIII-NART

For the 24 patients treated with routine treatment protocol, two hybrid plans were generated to simulate the dosimetric effect as if no replanning had been applied in PII and PIII. These 2 plans, denoted as PII-NART and PIII-NART, were optimized by pasting the original contours from the initial CT sets on the PII and PIII CT sets by CT-CT fusion. In this way, these plans would visualize the isodose distribution when no modification was done and the doses delivered to the actual target volumes and OARs in these two phases could be obtained. During optimization, the qualities of the PII- and PIII-NART plans were made consistent with the initial plan to ensure the dosimetric differences between NART and ART, if any, would be mainly due to the anatomic changes of the structures in these phases.

5.2.3 MVCT

For all 30 patients prior to each treatment, MVCT was conducted and registered to the corresponding planning CT for verification of patient setup accuracy. Coarse mode was set to obtain MVCT slices with 6 mm thickness. The scan range was set to just encompass the target volumes and the bilateral parotid glands in order to minimize radiation dose to patient and patient on couch time. With reference to Shah et al. study (2008), the total dose contributed by 38 MVCTs using coarse imaging mode was estimated as 0.51–0.89 Gy, which was relatively low when compared to the prescribed dose to target volumes. Alternate day MVCTs starting from the first treatment were exported to the

Eclipse Treatment Planning System (Varian Medical Systems) for contouring. Altogether there were 19 MVCT images exported for each patient which would give a total of 570 MVCT image sets. On each set of MVCT, the posterolateral wall of nasopharynx (P-NP), the bilateral parotid glands and the neck volume covering the whole cervical spine level were manually contoured using consistent window and level settings. The P-NP basically included the soft tissues at the posterior pharyngeal wall, the prevertebral muscle, the fossa of Rosenmuller, the torus tubarius, opening of the eustachian tube, and the tensor and levator veli palatini. Since NPC frequently arises from the lateral and the superoposterior wall of nasopharynx, the anatomic changes in P-NP could directly reflect the changes of the nasopharyngeal gross tumor. On the other hand, the vertebral canals on the CT slice level of 3 cm (VC3), 6 cm (VC6) and 9 cm (VC9) inferior to the base of skull were also outlined (Figure 5.2). The geometric changes of these three slices of contours demonstrated the changes in the upper, middle and lower portion of the cervical cord as well as the corresponding neck region respectively. To eliminate the interobserver variance, one oncologist was responsible for the contouring of the P-NP and the same radiation therapist performed all the normal structure delineation in each MVCT set for all patients.

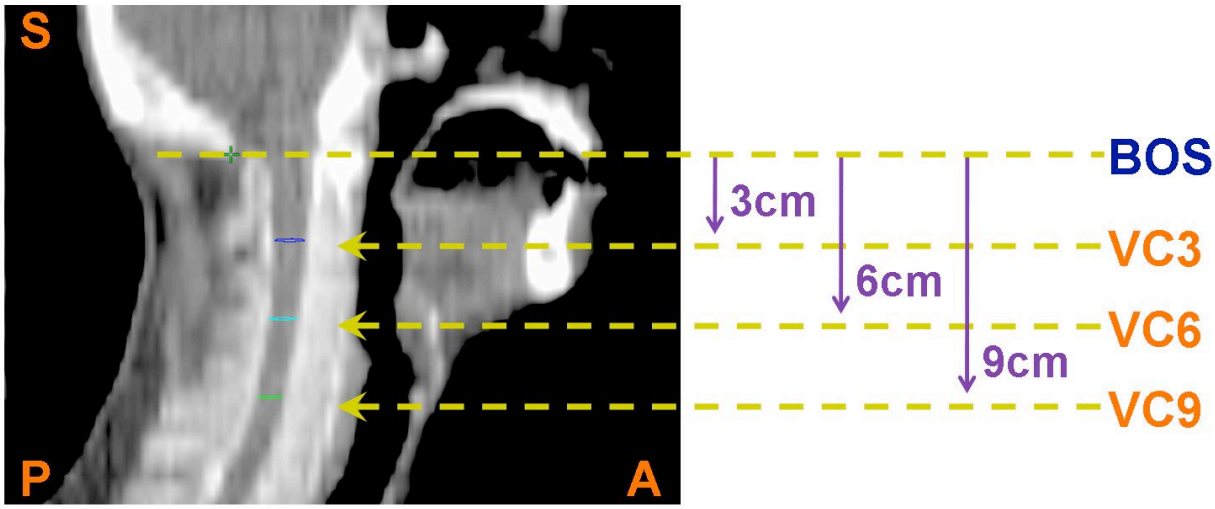

Figure 5.2: Schematic diagram showing the definitions of VC3, VC6 and VC9. BOS = base of skull; A = anterior; P = posterior; S = superior.

5.3 Dosimetric comparison between NART and ART plans

Dosimetric comparison was performed on the 24 patients who had 2 additional NART plans generated. Dose volume histograms (DVHs), which use a graphical method to show the amount of organ volume receiving a dose within a specified dose interval, were calculated for all target volumes and OARs in all plans. For both PII and PIII, The DVHs of the NART plans were compared to that of the corresponding ART plans to investigate the dosimetric effect due to anatomic changes in these two phases. Dose evaluation was done on all prescribed target volumes and selective OARs. These OARs were the brainstem, spinal cord, optic chiasm, pituitary gland and bilateral parotid glands. Other than the maximum (D_{max}), mean (D_{mean}), and minimum (D_{min}) doses of these structures, the dose received by 95 % target volumes (D_{95}) and the doses received by 1 % of the brainstem and spinal cord (D_1) were also recorded.

To assess the target conformity and homogeneity in each plan, two indices were employed. The conformation number (CN), proposed by van't Riet et al. (1997), was calculated for each target volume and is defined as:

$$CN = \frac{TV_{RI}}{TV} \times \frac{TV_{RI}}{V_{RI}}$$

where TV_{RI} = target volume covered by the reference isodose i.e. its prescribed isodose; TV = target volume; and V_{RI} = volume of the reference isodose.

The first fraction of the CN quantifies the degree of target coverage, whereas the second fraction quantifies the degree of healthy tissues irradiation. The CN value ranges from 0 to 1, with the value of 1 indicates perfect target dose conformity. The homogeneity index (HI) was also calculated for each target volume (Grzadziel, Grosu, & Kneschaurek, 2006). The value of HI decreases with increased target homogeneity and ultimately reaching 0 when the target dose is perfectly uniform. The HI is defined as:

$$HI = \frac{D_{max} - D_{min}}{D_{mean}}$$

In order to demonstrate the possible dosimetric outcome throughout the 37–38 fractions of radiotherapy course, the recorded dose endpoints were summed from all three phases under the no-replanning or two-replanning approach for dosimetric comparison. For example, the total maximum dose received by the brainstem after the whole course of treatment with adaptive measures would be equal to the summation of its maximum doses from PI, PII-ART and PIII-ART.

5.4 Volumetric and geometric analysis of tumors and OARs throughout the treatment course

In the alternate day MVCTs of each patient, the volumes of the P-NP, bilateral parotid glands and neck were calculated by the treatment planning system and recorded. The locations of the P-NP, bilateral parotid glands, VC3, VC6 and VC9 were monitored throughout the treatment course. For every patient, a reference point was defined at the level of skull base in the mid-sagittal plane in each MVCT and was set as the origin of a coordinate system *(0, 0, 0)*. This reference point was defined on rigid bony anatomy rather than external mark e.g. laser-defined isocentre therefore it was easily reproducible to correlate the whole series of alternate day MVCT sets and free from the effect of setup variation. To quantify the geometric changes, the centre of each structure mass (COM) was calculated by the planning computer and was expressed in positional vectors *(x, y, z)* relative to the origin. In this way, the structure movement in lateral (left, x_{+ve}; right, x_{-ve}), longitudinal (superior, y_{+ve}; inferior, y_{-ve}) and vertical directions (anterior, z_{+ve}; posterior, z_{-ve}) were followed over time. An illustration of the coordinate system using parotid contours as an example is shown in Figure 5.3. For VC3, VC6 and VC9, the evaluation of changes in longitudinal direction were excluded.

For all measured parameters in volumetric and geometric analysis, graphs together with trend lines were plotted to visualize the specific patterns of changes over time. The rates of changes were calculated for those that experienced substantial anatomic deviation at the end of the treatment course.

Correlations between various parameters were also studied.

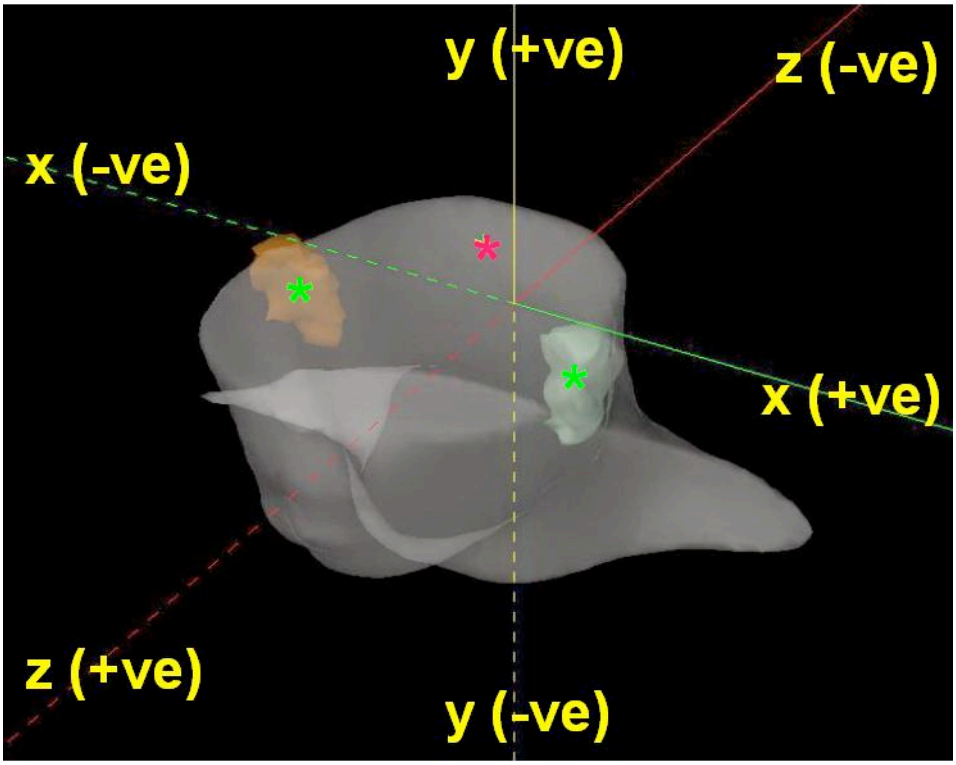

Figure 5.3: Schematic diagram of the coordinate system used for quantifying the geometric changes of various structures. The bilateral parotid glands are used here as an example. in red color indicates the origin (0, 0, 0) that is defined at the skull base level in mid-sagittal plane; * in green color indicate the COMs of the parotid glands in each side.*

5.5 Defining optimum ART strategy for NPC cases

During volumetric and geometric analysis, any parameters that showed progressive anatomic changes were under consideration for setting the ART strategy in NPC cases. For each selected parameter, threshold(s) that indicate a significant anatomic change during the treatment course was defined by statistical test. To begin, the data in the first treatment fraction was compared to those in subsequent fractions separately until the result reached statistical difference. For example, if significant difference (i.e. significant anatomic change) was seen between the data in the 9^{th} and the 1^{st} fraction, the 9^{th} fraction would be the first threshold point that replanning was assumed. The data in the 9^{th} fraction was then compared to those in subsequent fractions in order to define the next threshold point and so on. In this way, the threshold points in each selected parameter throughout the treatment course could be identified. An optimal schedule for ART was ultimately established by accounting all thresholds appeared in all parameters in terms of efficiency and efficacy.

5.6 Statistical analysis

All statistical tests were performed using GraphPad Prism (Version 5.00, GraphPad Software, San Diego, CA, US). The dosimetric differences between the ART plans and the NART plans were tested by two-tailed paired *t* test or Wilcoxon matched pairs test. In the volumetric and geometric analysis, two-tailed paired *t* test or Wilcoxon matched pairs test was applied to all data to demonstrate any significant deviations at the end of the radiotherapy course.

Linear regression was used to quantify their rates of changes throughout the treatment course, and the correlations between parameters were investigated using the two-tailed Pearson correlation or Spearman correlation tests. One-way repeated measure analysis of variance (ANOVA) with post-hoc multiple comparison using bonferroni criterion was used to indicate the specific time point(s) of significant anatomic changes which required plan modification. A p value < 0.05 was considered statistical significant in all tests.

CHAPTER SIX

RESULTS

6.1 Dosimetric comparison

In general for the NP-CTV and NP-PTV, the D_{95} were increased with a lower HI in the NART plans when compared to those in the corresponding ART plans. However, the D_{95} and the HI of the bilateral LN-PTVs were comparable in both approaches. For all target volumes, the CN was found to be lower in the NART plans. In terms of OARs, all of their endpoint doses were significantly higher in the NART plans when compared to those in the ART plans. The standard dose prescription is reprinted in this chapter for easy reference (Table 5.2).

Table 5.2: Standard dose prescription of the routine NPC treatment protocol; fr = fraction.

Target volumes	**Dose prescription**		
	PI	**PII**	**PIII**
NP-CTV	52.5 Gy / 25 fr	21.0 Gy / 10 fr	7.4 Gy / 2 fr or 10.5 Gy / 3fr
NP-PTV	51.5 Gy / 25 fr	20.6 Gy / 10 fr	7.0 Gy / 2 fr or 10.5 Gy / 3fr
LN-PTV (L/R)	50.0 Gy / 25 fr	20.0 Gy / 10 fr	7.0 Gy / 2 fr or 10.5 Gy / 3fr

6.1.1 PII-NART vs PII-ART

Table 6.1 shows the dosimetric, CN and HI differences between PII-NART and PII-ART. In PII-NART, the mean D_{95} of the NP-CTV and NP-PTV increased 1.15±4.37 % and 4.30±5.60 % respectively, while a slight decrease of 0.58±6.72 % and 0.12±5.20 % was observed in the mean D_{95} of the LLN-PTV and RLN-PTV respectively when compared to PII-ART. Among them, only the result in NP-PTV showed significant difference (p = 0.0006). Majority of patients received higher target doses in PII-NART. In individual cases, 68 %, 75 %, 75 % and 75 % of patients had their D_{95} of NP-CTV, NP-PTV, LLN-PTV and RLN-PTV increased by 0.03–2.50 Gy, 0.14–3.55 Gy, 0.02–0.82 Gy and 0.02–0.85 Gy in PII-NART respectively. The mean CN of all targets in PII-NART were significantly lower than that of PII-ART, with 19.33±15.66 %, 27.61±19.33 %, 28.55±21.55 % and 31.04±21.04 % reduction in NP-CTV, NP-PTV, LLN-PTV and RLN-PTV respectively (all $p < 0.0001$). When viewed individually, except 1 patient had higher CN in NP-CTV (18.37 %) and 1 patient had higher CNs in bilateral LN-PTVs (5.66 % and 8.16 %), all others had lower CNs in all 4 target volumes in PII-NART when comparing to PII-ART. The mean HI in PII-NART was lower in NP-CTV, NP-PTV and LLN-PTV with a respective decrement of 32.53±25.77 %, 27.18±23.28 % and 0.04±91.51 % when compared to PII-ART. In particular, the results in NP-CTV and NP-PTV reached statistical significance ($p < 0.0001$ & p = 0.0003 respectively). The percentage change of the mean HI of RLN-PTV in PII-NART was calculated as 3.91±103.22 % higher than that in PII-ART. Nonetheless, the absolute mean in PII-NART was lower. In individual cases, 91 %, 88 %, 75 % and 75 % of

patients had their HIs of NP-CTV, NP-PTV, LLN-PTV and RLN-PTV reduced by 6.36–68.05 %, 3.68–61.01 %, 5.26–75.30 % and 2.09–85.85 % in PII-NART respectively. The above dosimetric results indicated that the target volumes in PII-NART experienced better dose uniformity with increased high dose region, but target conformity was worsen when compared to the PII-ART.

While increased target doses were delivered in PII-NART, the OARs also received higher doses than those in PII-ART. The mean D_1 of brainstem and spinal cord significantly increased 24.41±30.69 % ($p = 0.0041$) and 38.23±37.80 % ($p < 0.0001$) respectively in PII-NART. The brainstem dose was increased in 75 % of patients and spinal cord dose was increased in 83 % of patients. The optic chiasm and pituitary gland also received significantly higher maximum doses in PII-NART, with a mean increase of 27.61±31.02 % and 28.14±24.80 % respectively (both $p < 0.0001$). In particular, 83 % and 95 % of patients had respective increase of their chiasm and pituitary doses. The mean dose of left parotid gland increased 10.37±16.25 % and the right one increased 8.27±17.60 % on average in PII-NART, both showed significant difference ($p = 0.0037$ & 0.0350 respectively) when compared to PII-ART. The left and right parotid doses were increased among 79 % and 66 % of patients respectively. It was noted that the absolute dose increments in these OARs could be even greater in individual cases. Using PII-NART, the end point dose increments to the brainstem, spinal cord, optic chiasm, pituitary gland, left and right parotid gland could be as high as 5.84 Gy, 7.42 Gy, 8.86 Gy, 8.19 Gy, 4.34 Gy and 4.61 Gy respectively when compared to that in PII-ART.

Table 6.1: Dosimetric, CN and HI comparison between PII-NART and PII-ART.

** indicates the result with statistical significance.*

End points (mean)	PII-NART	PII-ART	*p* value
Targets - D_{95}			
NP-CTV	21.00±0.55 Gy	20.79±0.88 Gy	0.2737
NP-PTV	20.27±0.74 Gy	19.48±1.10 Gy	0.0006*
LLN-PTV	19.84±1.31 Gy	19.97±0.35 Gy	0.0789
RLN-PTV	19.97±1.05 Gy	19.99±0.28 Gy	0.1096
Targets - CN			
NP-CTV	0.59±0.14	0.74±0.14	< 0.0001*
NP-PTV	0.48±0.17	0.66±0.15	< 0.0001*
LLN-PTV	0.40±0.15	0.56±0.12	< 0.0001*
RLN-PTV	0.39±0.15	0.56±0.10	< 0.0001*
Targets - HI			
NP-CTV	0.17±0.07	0.28±0.13	< 0.0001*
NP-PTV	0.27±0.14	0.38±0.13	0.0003*
LLN-PTV	0.20±0.13	0.24±0.10	0.0839
RLN-PTV	0.22±0.16	0.28±0.16	0.0268*
OARs			
Brainstem D_1	12.11±1.75 Gy	10.19±2.59 Gy	0.0041*
Spinal Cord D_1	10.21±1.92 Gy	7.66±1.57 Gy	< 0.0001*
Optic Chiasm D_{max}	13.96±3.51 Gy	11.26±3.12 Gy	< 0.0001*
Pituitary Gland D_{max}	15.97±3.34 Gy	12.68±2.85 Gy	< 0.0001*
Left Parotid Gland D_{mean}	9.90±2.15 Gy	8.97±1.48 Gy	0.0037*
Right Parotid Gland D_{mean}	9.94±2.10 Gy	9.22±1.44 Gy	0.0350*

6.1.2 PIII-NART vs PIII-ART

Table 6.2 shows the dosimetric, CN and HI differences between PIII-NART and PIII-ART. Overall, the mean D_{95} of NP-CTV, NP-PTV and RLN-PTV in PIII-NART increased 2.53±4.75 %, 4.90±5.81 % and 1.27±3.92 % respectively, whereas the LLN-PTV dose had a marginal decrease of 0.19±8.29 % when compared to PIII-ART. The changes in NP-CTV, NP-PTV and LLN-PTV reached statistical significant levels (p = 0.0080, p = 0.0007 & p = 0.0419 respectively). In individual cases, the D_{95} of NP-CTV, NP-PTV, LLN-PTV and RLN-PTV were increased among 81 %, 87 %, 81 % and 76 % of patients in PIII-NART by 0.00–1.57 Gy, 0.05–1.70 Gy, 0.00–0.71 Gy and 0.00–0.72 Gy respectively. All patients had lower CN in all 4 target volumes in PIII-NART compared to PIII-ART. The mean CN of NP-CTV, NP-PTV, LLN-PTV and RLN-PTV in PIII-NART were 40.57±28.20 % (p = 0.0003), 56.14±25.61 % (p = 0.0001), 73.88±14.93 % (p < 0.0001) and 73.18±15.99 % (p < 0.0001) lower than those in PIII-ART respectively. In PIII-NART, the mean HI was again lower when compared to PIII-ART, with 31.85±29.10 %, 35.91±30.93 %, 12.09±59.46 % and 5.56±74.89 % reduction in NP-CTV, NP-PTV, LLN-PTV and RLN-PTV respectively. The results in NP-CTV and NP-PTV reached statistical significance (p = 0.0002 & p < 0.0001 respectively). In individual cases, 86 %, 83 %, 62 % and 67 % of patients had their HI of NP-CTV, NP-PTV, LLN-PTV and RLN-PTV reduced by 2.32–74.67 %, 19.52–68.42 %, 0.51–76.99 % and 1.22–81.25 % in PIII-NART respectively. Using PIII-NART, better dose uniformity with increased high dose region to the target volumes could be achieved. However, target conformity was again lower when compared to the

PIII-ART.

Similar to PII, higher doses was delivered to the OARs if PIII-NART had been applied. The mean D_1 of brainstem and spinal cord was significantly increased in PIII-NART by 51.09±35.73 % and 54.93±46.36 % respectively (both $p < 0.0001$). The brainstem dose was increased among all patients and spinal cord dose was increased in 87 % of patients. The average maximum doses of the optic chiasm and pituitary gland in PIII-NART also increased significantly by 84.38±132.93 % and 66.87±106.64 % respectively (both $p < 0.0001$). In individual cases, all and 95 % of patients had respective increase of their optic chiasm and pituitary doses. The mean dose of left parotid gland increased 20.92±29.89 % and the right one increased 15.96±30.80 % on average in PIII-NART, both showed significant differences ($p = 0.0018$ & $p = 0.0269$ respectively) when compared to PIII-ART. The left and right parotid doses increased among 74 % and 65 % of patients respectively. In individual cases, the end point doses in all OARs had an even greater increment if PIII-NART was used. Using PIII-NART, the dose increments to the brainstem, spinal cord, optic chiasm, pituitary gland, left and right parotid gland could be as high as 3.13 Gy, 3.67 Gy, 5.58 Gy, 5.20 Gy, 2.74 Gy and 2.97 Gy respectively.

Table 6.2: Dosimetric, CN and HI comparison between PIII-NART and PIII-ART.

** indicates the result with statistical significance.*

End points (mean)	PIII-NART	PIII-ART	*p* value
Targets - D_{95}			
NP-CTV	9.80±1.80 Gy	9.55±1.71 Gy	0.0080*
NP-PTV	9.22±1.86 Gy	8.80±1.75 Gy	0.0007*
LLN-PTV	8.19±2.35 Gy	8.17±2.14 Gy	0.0419*
RLN-PTV	8.28±2.23 Gy	8.16±2.10 Gy	0.0521
Targets - CN			
NP-CTV	0.49±0.28	0.76±0.17	0.0003*
NP-PTV	0.30±0.22	0.65±0.13	0.0001*
LLN-PTV	0.10±0.06	0.40±0.13	< 0.0001*
RLN-PTV	0.11±0.07	0.40±0.11	< 0.0001*
Targets - HI			
NP-CTV	0.14±0.04	0.24±0.10	0.0002*
NP-PTV	0.21±0.08	0.37±0.13	< 0.0001*
LLN-PTV	0.31±0.33	0.34±0.23	0.4240
RLN-PTV	0.31±0.34	0.33±0.23	0.3305
OARs			
Brainstem D_1	5.99±1.38 Gy	4.04±0.89 Gy	< 0.0001*
Spinal Cord D_1	4.58±1.37 Gy	3.14±1.12 Gy	< 0.0001*
Optic Chiasm D_{max}	6.44±2.22 Gy	4.12±1.82 Gy	< 0.0001*
Pituitary Gland D_{max}	7.05±2.07 Gy	5.10±2.38 Gy	< 0.0001*
Left Parotid Gland D_{mean}	4.58±1.41 Gy	3.87±1.13 Gy	0.0018*
Right Parotid Gland D_{mean}	4.50±1.38 Gy	4.02±1.27 Gy	0.0269*

6.1.3 No replanning vs two replannings

The possible treatment outcome throughout the radiotherapy course with no replanning or twice replanning strategy is illustrated in Table 6.3. The overall mean D_{95} of NP-CTV, NP-PTV and RLN-PTV increased by 0.57±1.60 %, 1.65±1.73 % and 0.03±1.62 % without any plan modification respectively, with the dose change in NP-PTV demonstrated a significant difference (p = 0.0002). For LLN-PTV without replanning, a slight decrement of 0.25±2.43 % in the mean D_{95} was observed. Again when viewed individually, most patients received a higher target doses if there was no replanning applied. In individual cases without replanning, 67 %, 83 %, 71 % and 67 % of patients had their overall mean D_{95} of NP-CTV, NP-PTV, LLN-PTV and RLN-PTV increased by 0.05–3.65 Gy, 0.13–4.02 Gy, 0.03–1.83 Gy and 0.02–1.08 Gy respectively.

All OARs received significantly higher total doses when there was no replanning. The overall mean D_1 of brainstem and spinal cord increased by 9.19±7.40 % and 11.84±8.87 %, and the overall maximum doses to the optic chiasm and pituitary gland increased by 11.46±8.10 % and 10.36±8.62 % respectively when compared to those with adaptive measures (all $p < 0.0001$). The overall mean doses to the left and right parotid glands also increased by 4.73±5.92 % (p = 0.0006) and 3.57±6.5 % (p = 0.0184) respectively without replanning. In particular, 91 %, 87 %, 96 %, 100 %, 78 %, 70 % of patients were suffered from an increase in the total end point doses of brainstem, spinal cord, optic chiasm, pituitary gland, left and right parotid gland, which could be as high as 9.85 Gy, 9.75 Gy, 13.37 Gy, 12.24 Gy, 5.08 Gy and 5.43 Gy respectively. Table 6.4

compares the number of patients who would have their critical organ doses exceeding tolerance with or without replannings. The result showed that fewer patients would have their brainstem, spinal cord, optic chiasm and pituitary being overdosed when two relpans were applied. However regardless of the planning approaches, the parotid mean doses of all patients exceeded the typical tolerance of 26 Gy.

Table 6.3: Dosimetric comparison between no replanning and two replannings.

** indicates the result with statistical significance.*

End points (mean)	No Replan	Two Replans	*p* value
Targets - D_{95}			
NP-CTV	83.18±2.56 Gy	82.72±2.46 Gy	0.1303
NP-PTV	78.74±2.97 Gy	77.49±3.27 Gy	0.0002*
LLN-PTV	78.02±3.28 Gy	78.21±2.42 Gy	0.6538
RLN-PTV	78.28±2.91 Gy	78.24±2.29 Gy	0.9033
OARs			
Brainstem D_1	49.18±6.47 Gy	45.23±6.61 Gy	< 0.0001*
Spinal Cord D_1	38.87±5.90 Gy	34.77±4.69 Gy	< 0.0001*
Optic Chiasm D_{max}	49.56±11.43 Gy	44.50±10.16 Gy	< 0.0001*
Pituitary Gland D_{max}	58.87±12.68 Gy	53.63±12.05 Gy	< 0.0001*
Left Parotid Gland D_{mean}	36.60±5.36 Gy	34.90±4.40 Gy	0.0006*
Right Parotid Gland D_{mean}	37.14±4.86 Gy	35.88±4.30 Gy	0.0184*

Table 6.4: Number of patients with their critical organ doses exceeding tolerance with or without replannings.

Typical dose tolerance	No. of patients		
	No Replan	Two Replans	Difference
Brainstem $D_1 > 54$ Gy	4	2	2
Spinal Cord $D_1 > 45$ Gy	3	1	2
Optic Chiasm $D_{max} > 54$ Gy	7	3	4
Pituitary Gland $D_{max} > 60$ Gy	11	8	3
Left Parotid Gland $D_{mean} > 26$ Gy	24	24	0
Right Parotid Gland $D_{mean} > 26$ Gy	24	24	0

6.2 Volumetric and geometric analysis

6.2.1 P-NP

Progressive P-NP volume reduction was observed in all patients throughout the course of radiotherapy (Figure 6.1). The P-NP tended to lose volume faster in the first half of the treatment course. This was manifested by the steeper slope of the mean percentage volume loss in the first 19 fractions of treatment when compared to that in the latter part of the treatment course in Figure 6.1. At the end of the treatment course, the mean P-NP volume dropped significantly by 35.70±20.06 % ($p < 0.0001$). Using linear regression, the mean rate of volume

loss was estimated as 0.99±0.55 %/day. Majority (66 %) of patients had a volume regression < 40 %, while 20 % and 13 % patents had a regression of 40–60 % and > 60 % respectively. Though substantial volume reduction was seen in P-NP, there were no significant changes regarding the geometric location of its mean COM during the treatment course. The mean position of the COM had no specific trends in the longitudinal direction (Figures 6.3). However, it had a slight tendency of shifting to the left and posterior direction (Figure 6.2 & 6.4). At the end of the treatment course, the mean left and posterior displacement of the P-NP COM were 0.08±0.40 cm (p = 0.4581) and 0.05±0.24 cm (p = 0.1413) respectively. The initial volume of the P-NP was found to have a mild negative correlation with its percentage volume loss at the end of the treatment course (Correlation coefficient = -0.4522; p = 0.0138), indicating larger primary tumors tended to regress in a relatively slower progress.

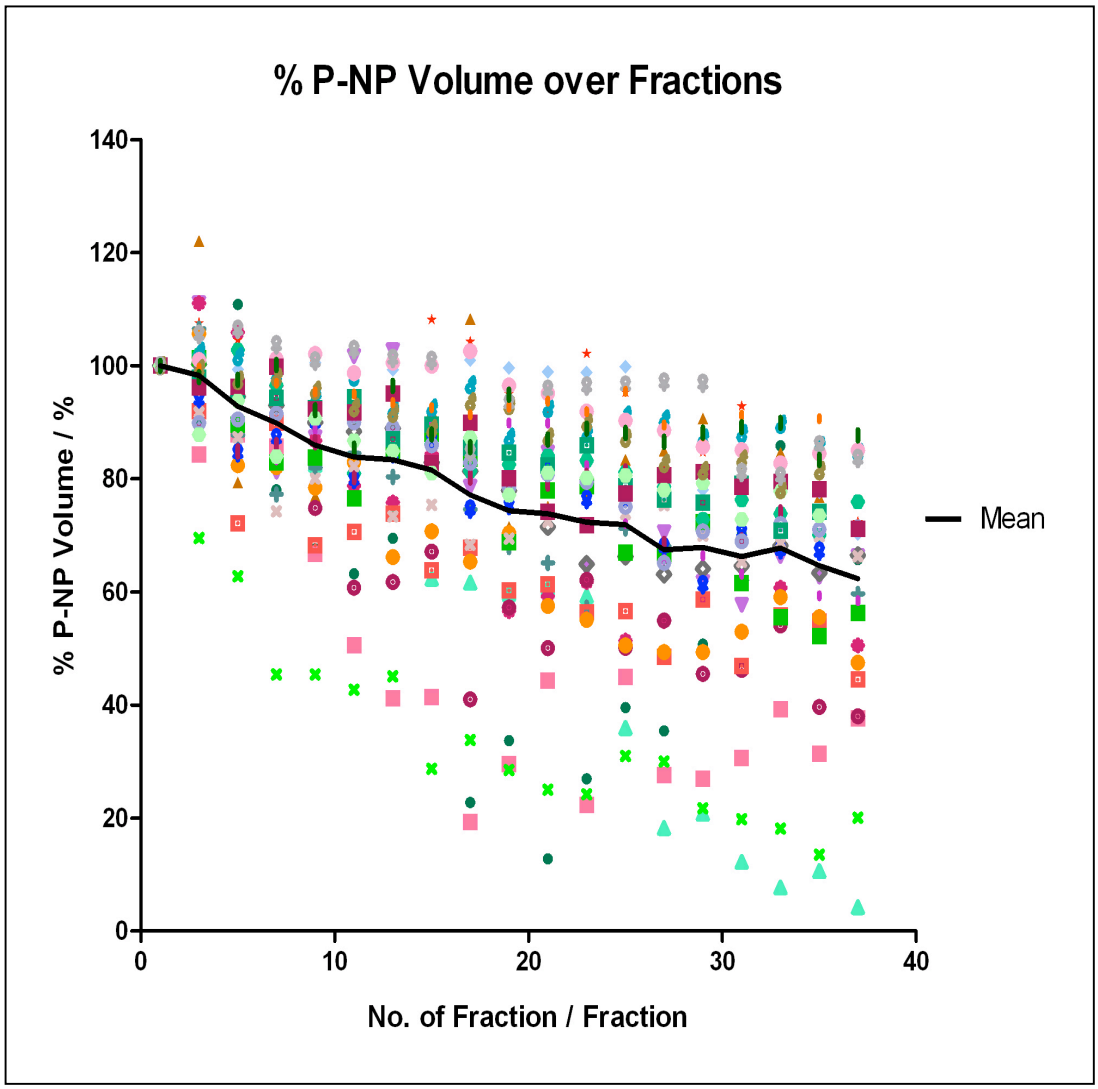

Figure 6.1: Relative P-NP volume over the treatment course.

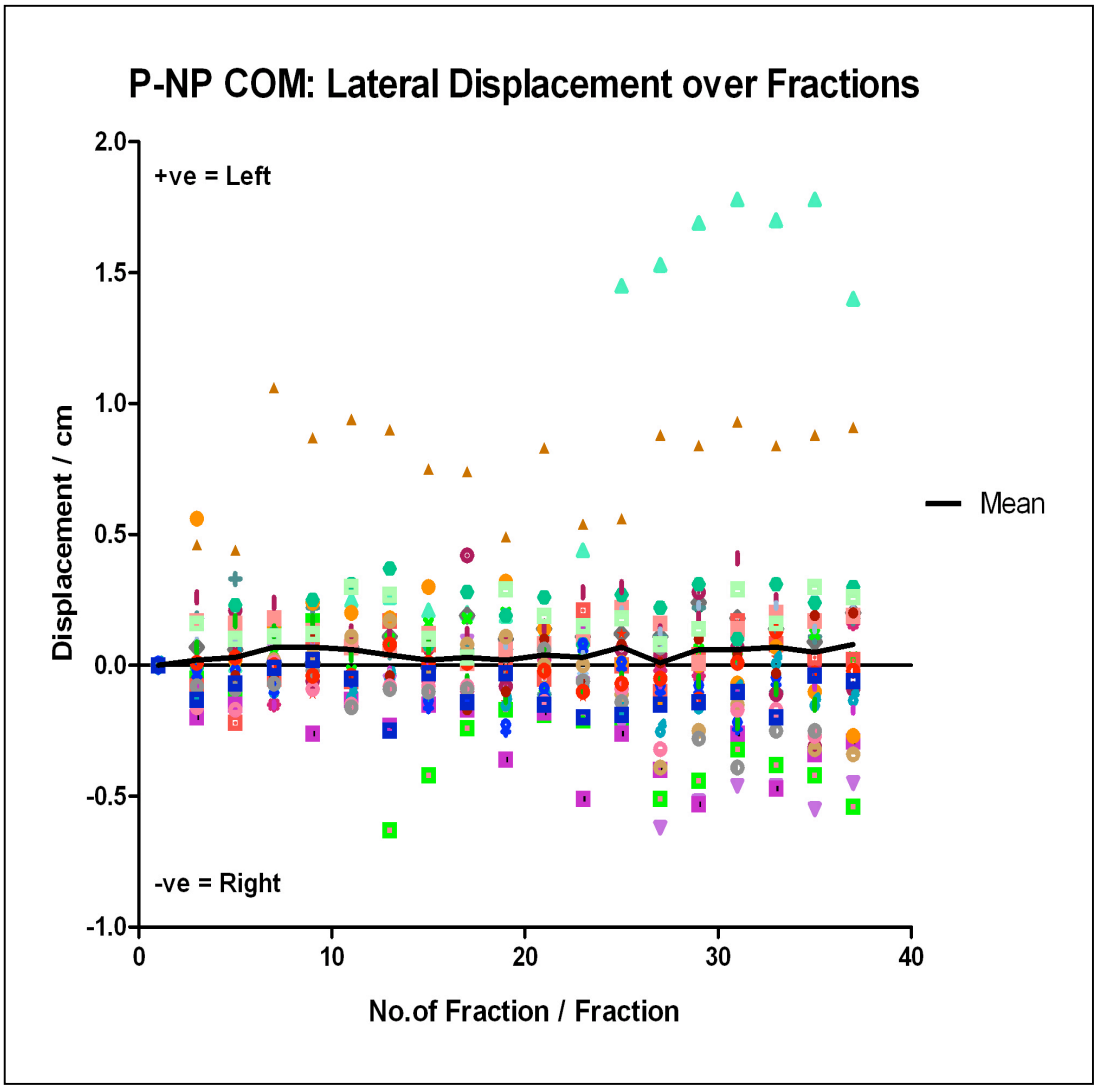

Figure 6.2: Relative COM displacement of P-NP in lateral direction over the treatment course.

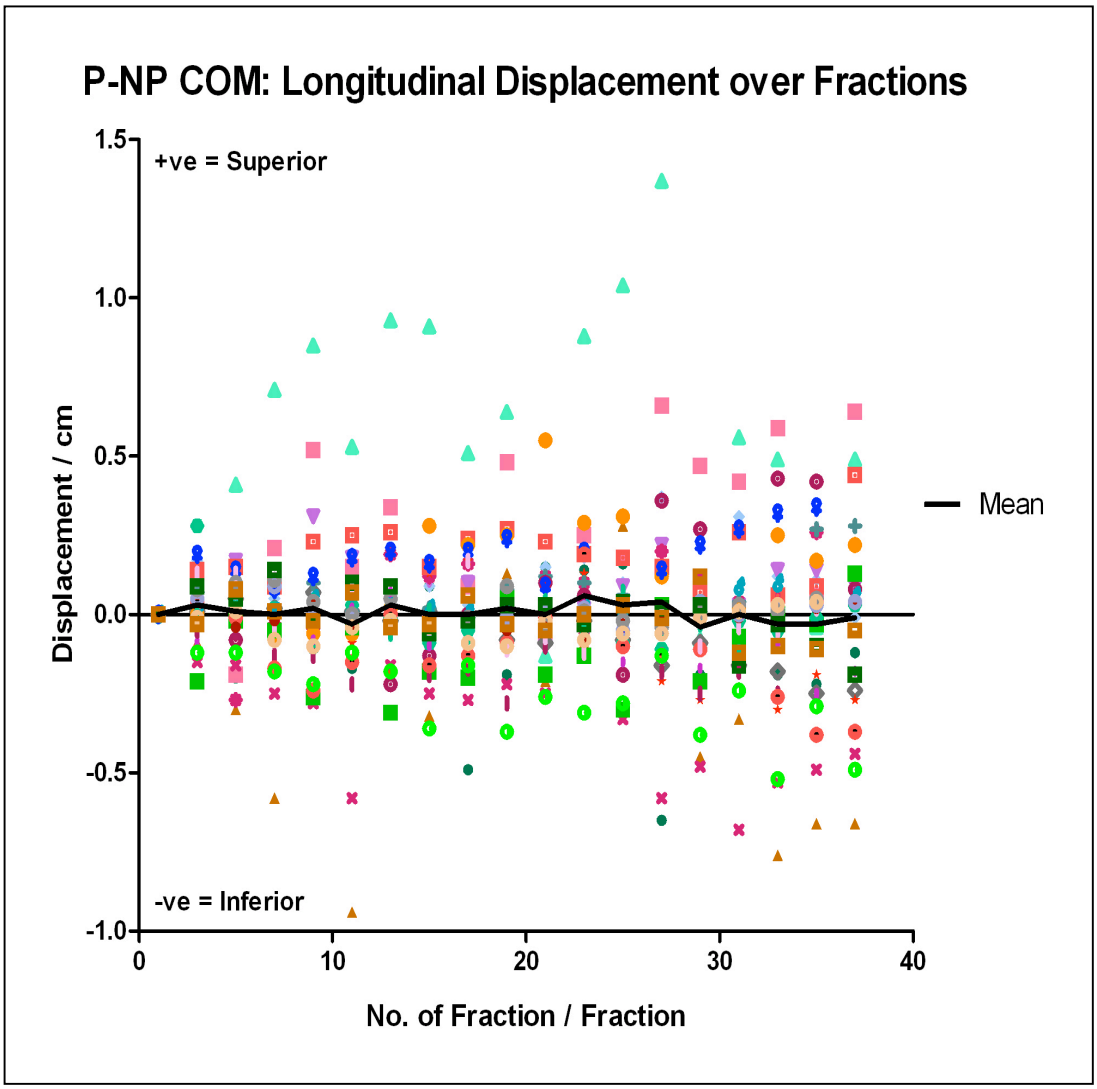

Figure 6.3: Relative COM displacement of P-NP in longitudinal direction over the treatment course.

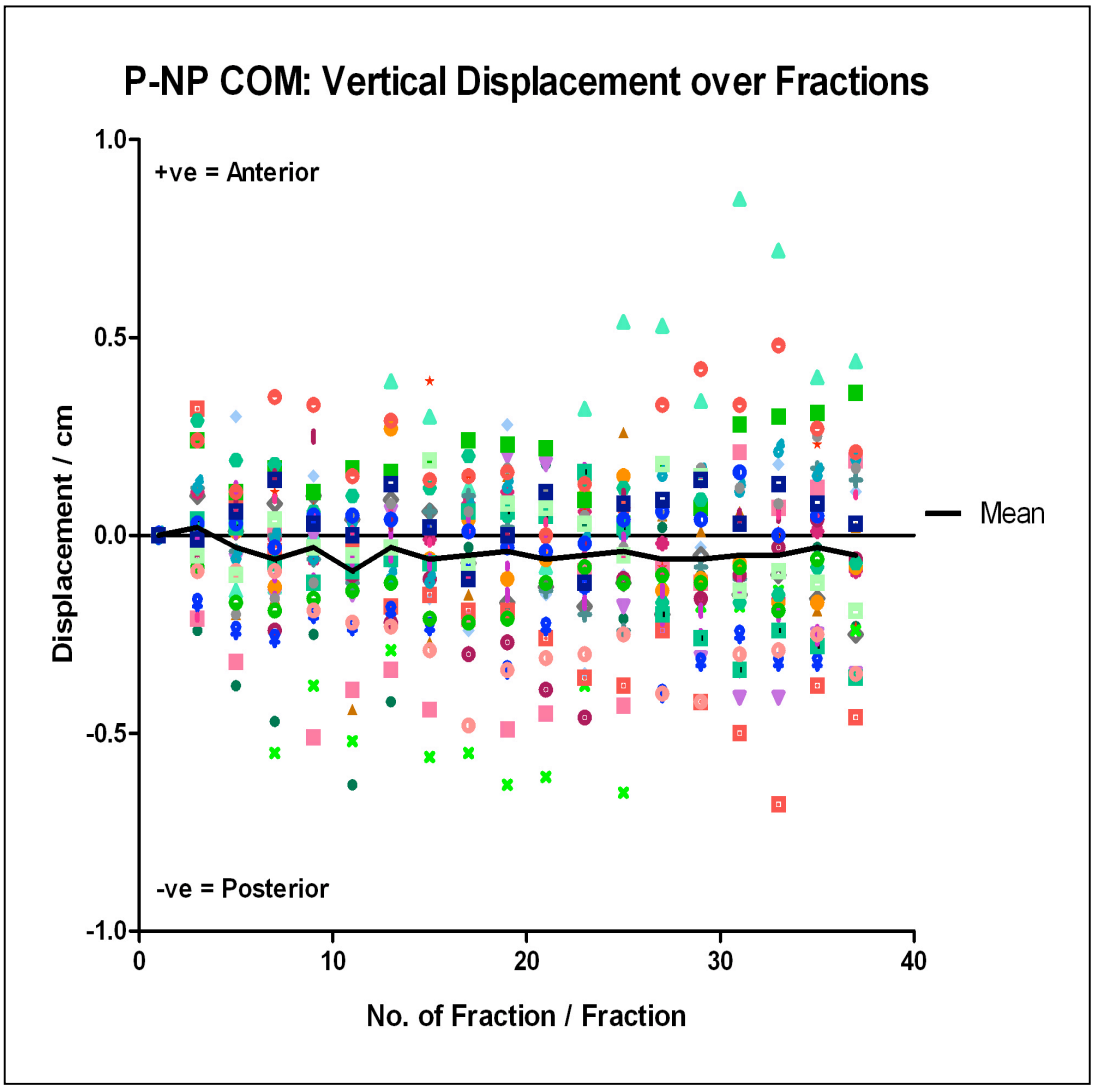

Figure 6.4: Relative COM displacement of P-NP in vertical direction over the treatment course.

6.2.2 Parotid glands

Figure 6.5 shows the relative parotid gland volumetric changes over time. All parotid volumes demonstrated similar reduction trends throughout the radiotherapy course. Gradual reduction was observed from the beginning of the course towards the treatment end. The mean percentage volume loss was 47.54±14.27 % ($p < 0.0001$) at treatment completion. Using linear regression, the mean rate of volume loss was estimated as 1.35±0.39 %/day.

The mean COM of the parotid gland shifted significantly to the medial direction during the treatment course. As shown in Figure 6.6, the mean parotid COM was displaced gradually to the medial side from the beginning to 29th fraction and kept fairly constant until the end. At the end of treatment, the mean medial displacement was 0.34±0.27 cm ($p < 0.0001$). Using linear regression, the mean rate of medial shift was estimated as 0.01±0.01 cm/day. The mean parotid COM also shifted significantly to the superior aspect, with a gradual increase of displacement till 23rd fraction and became settled towards the treatment end (Figure 6.7). The mean rate of change to the superior direction was 0.01±0.01 cm/day and the mean displacement was 0.24±0.39 cm ($p < 0.0001$) at the end of the treatment course. In individual cases, 90 % and 75 % parotid glands respectively shifted to the medial and superior aspects. There was no specific trend of the mean parotid COM displacement in the vertical direction (Figure 6.8).

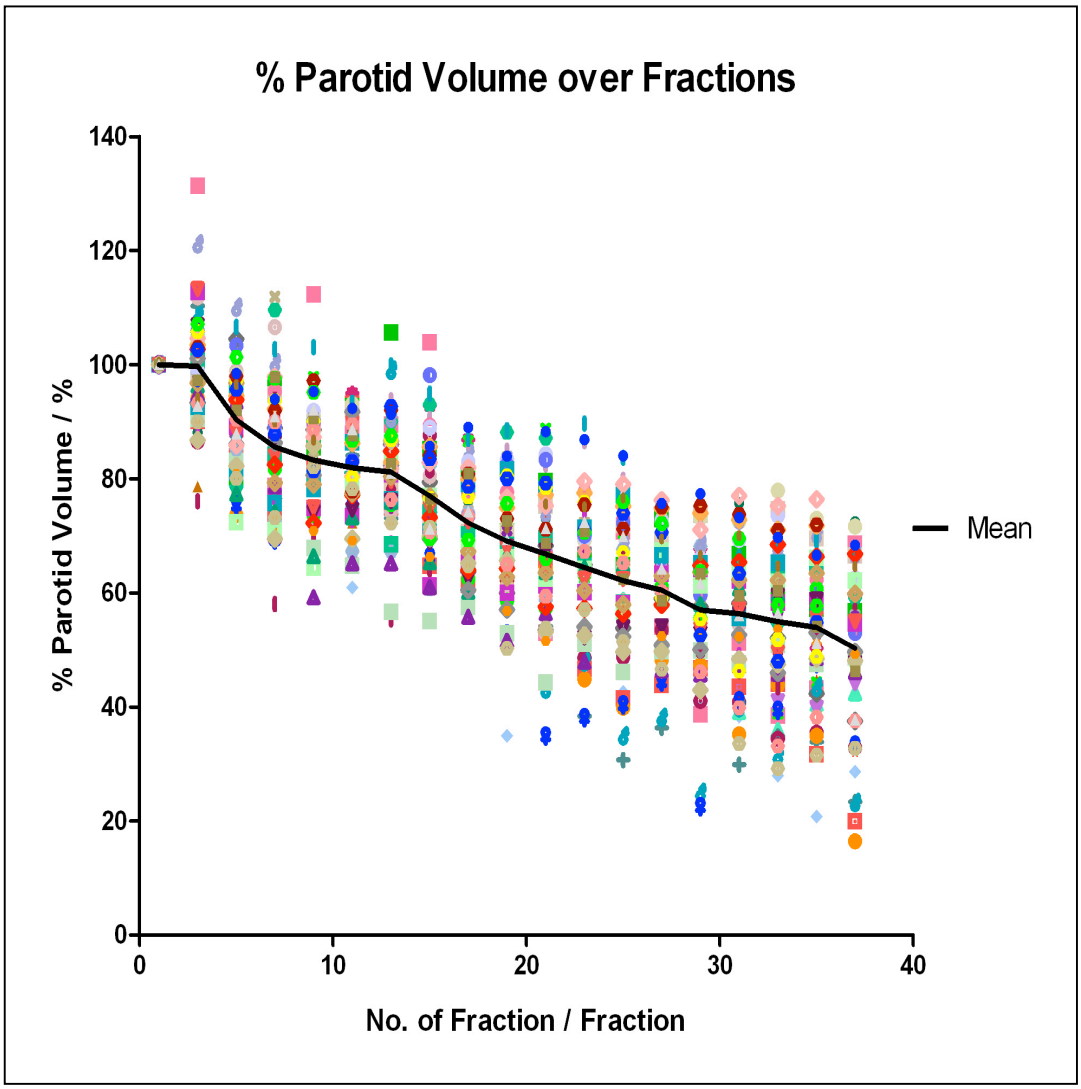

Figure 6.5: Relative parotid volume over the treatment course.

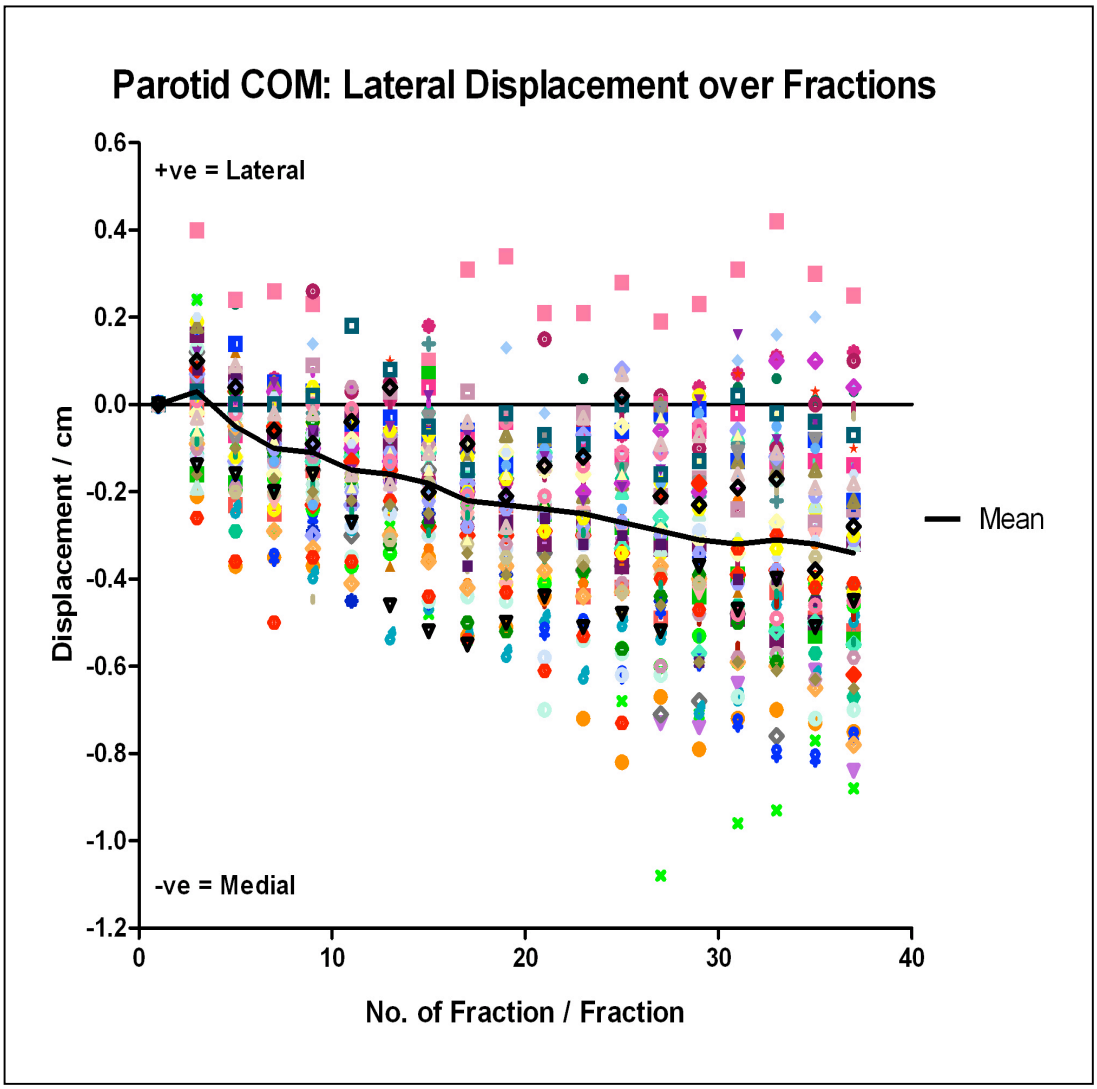

Figure 6.6: Relative COM displacement of parotid gland in lateral direction over the treatment course.

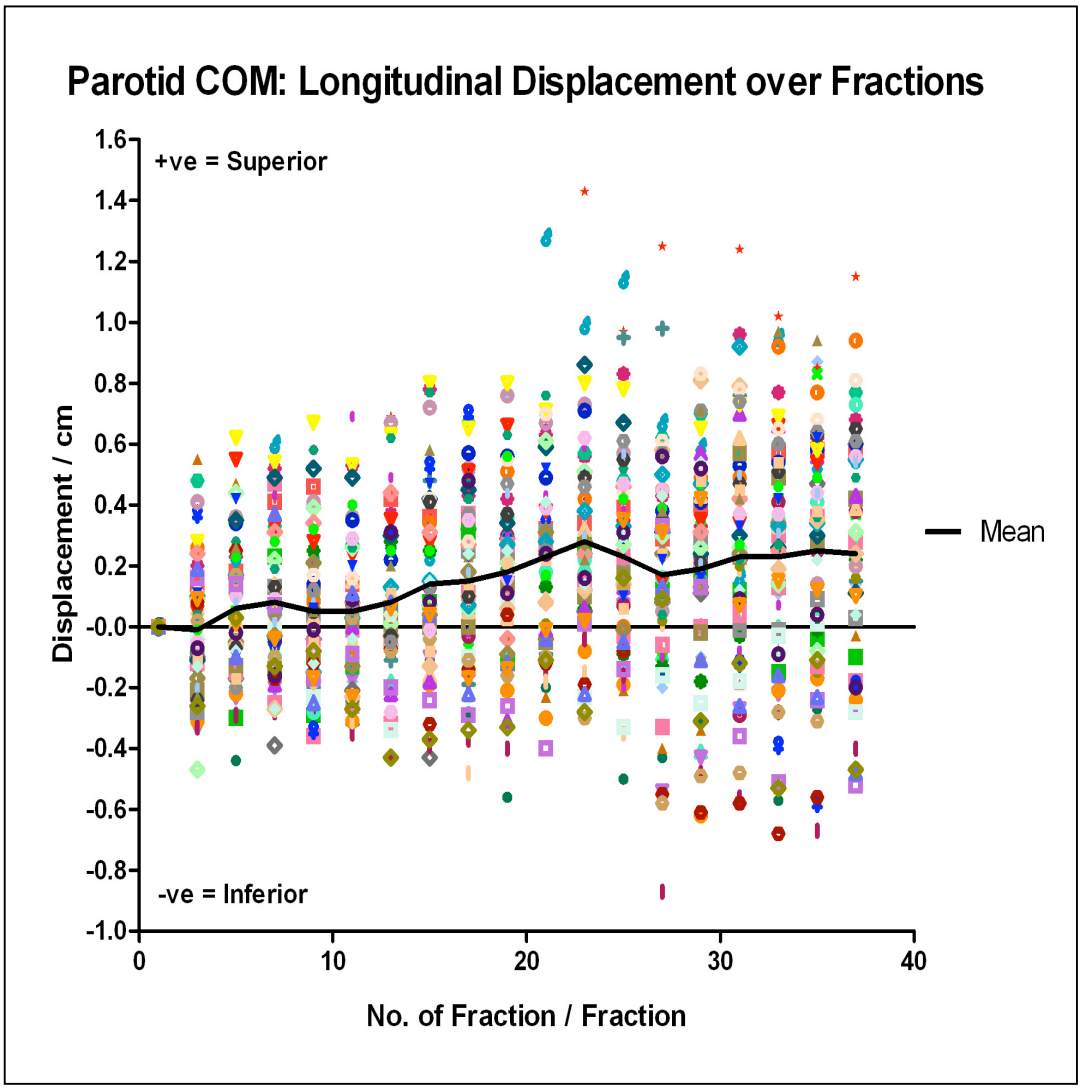

Figure 6.7: Relative COM displacement of parotid gland in longitudinal direction over the treatment course.

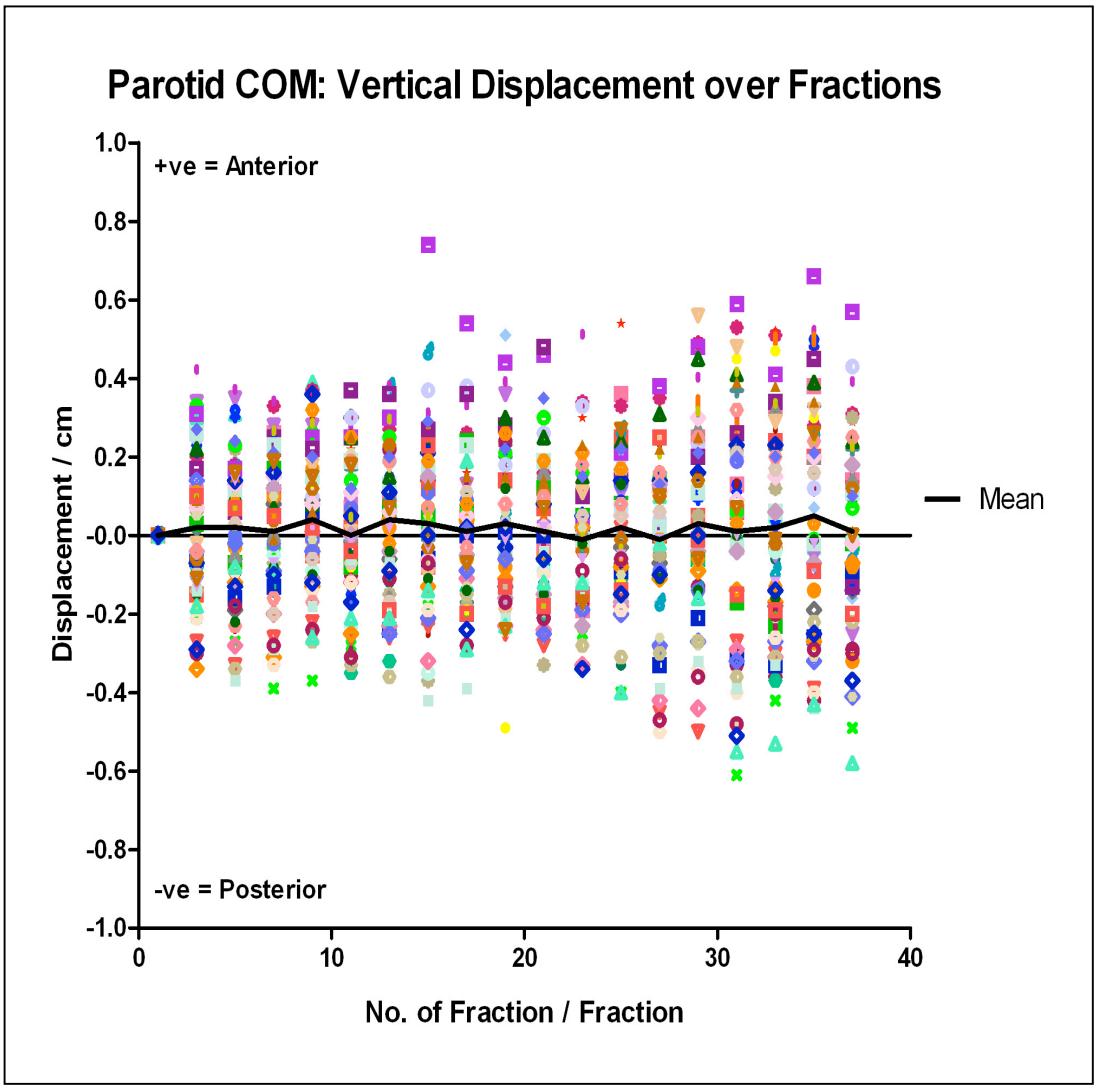

Figure 6.8: Relative COM displacement of parotid gland in vertical direction over the treatment course.

The percentage parotid volume loss correlated strongly with its medial and superior displacement during the treatment course (Correlation coefficient = 0.9914 & 0.9291 respectively; both $p < 0.0001$). With linear fit, a 5 % loss in the parotid volume indicated a 0.04 cm shift to the medial direction and 0.03 cm shift to the superior direction (Figure 6.9). There was a positive relation between the initial volume of the parotid gland and its absolute volume loss at the end of the treatment (Correlation coefficient = 0.7769; $p < 0.0001$). Apparently larger initial parotid volume would lead to a greater volume loss at treatment completion. It was also found that the mean percentage volume reduction in the parotid volume and the P-NP volume were linearly correlated (Correlation coefficient = 0.9943; $p < 0.0001$) during the radiotherapy course, with 5 % shrinkage of parotid volume would indicate 3.70 % decrement of the P-NP volume (Figure 6.10).

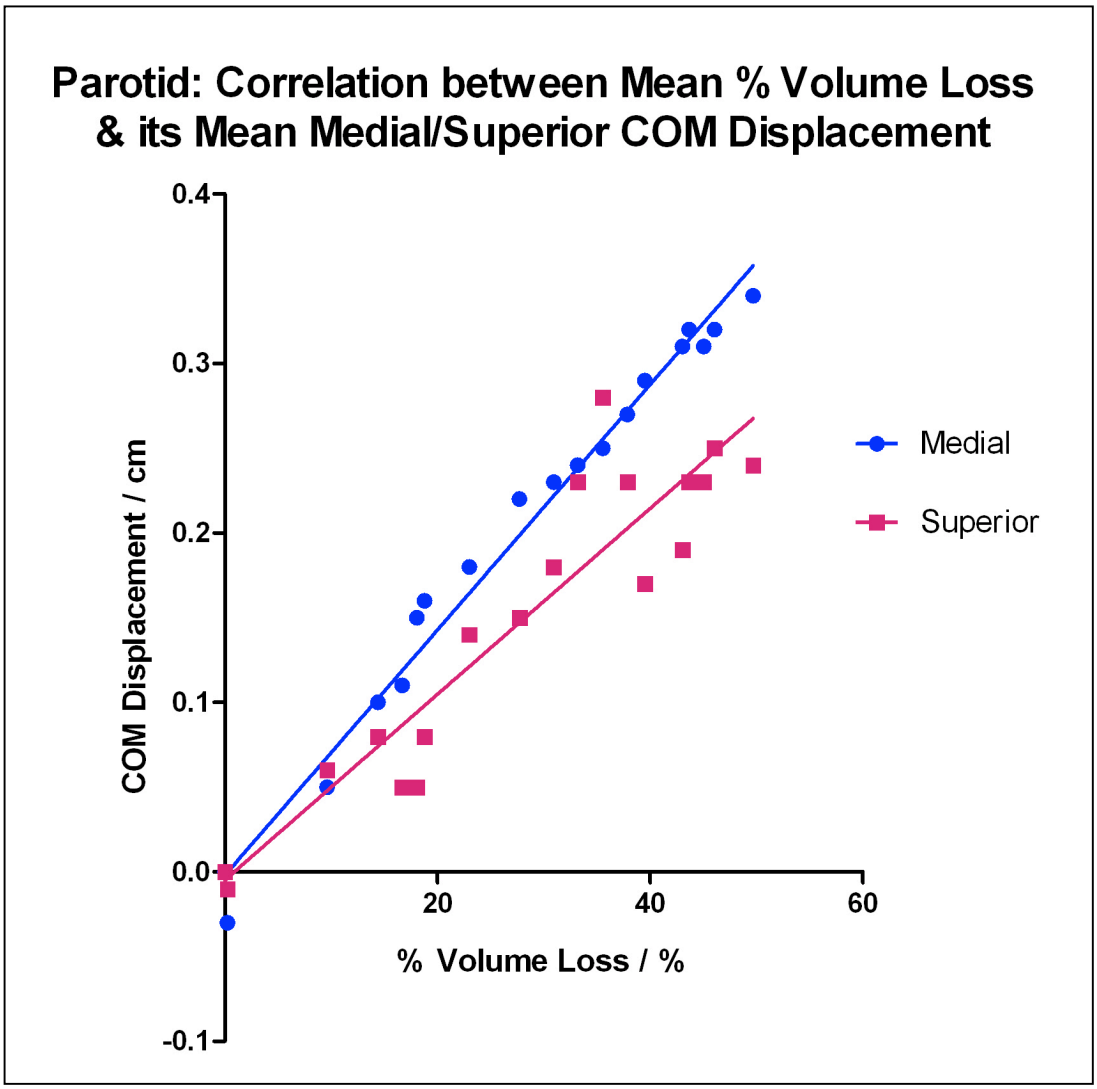

Figure 6.9: Correlation between the mean percentage loss of parotid gland volume and the mean medial or superior displacement of its COM throughout the treatment course (Linear fit displayed).

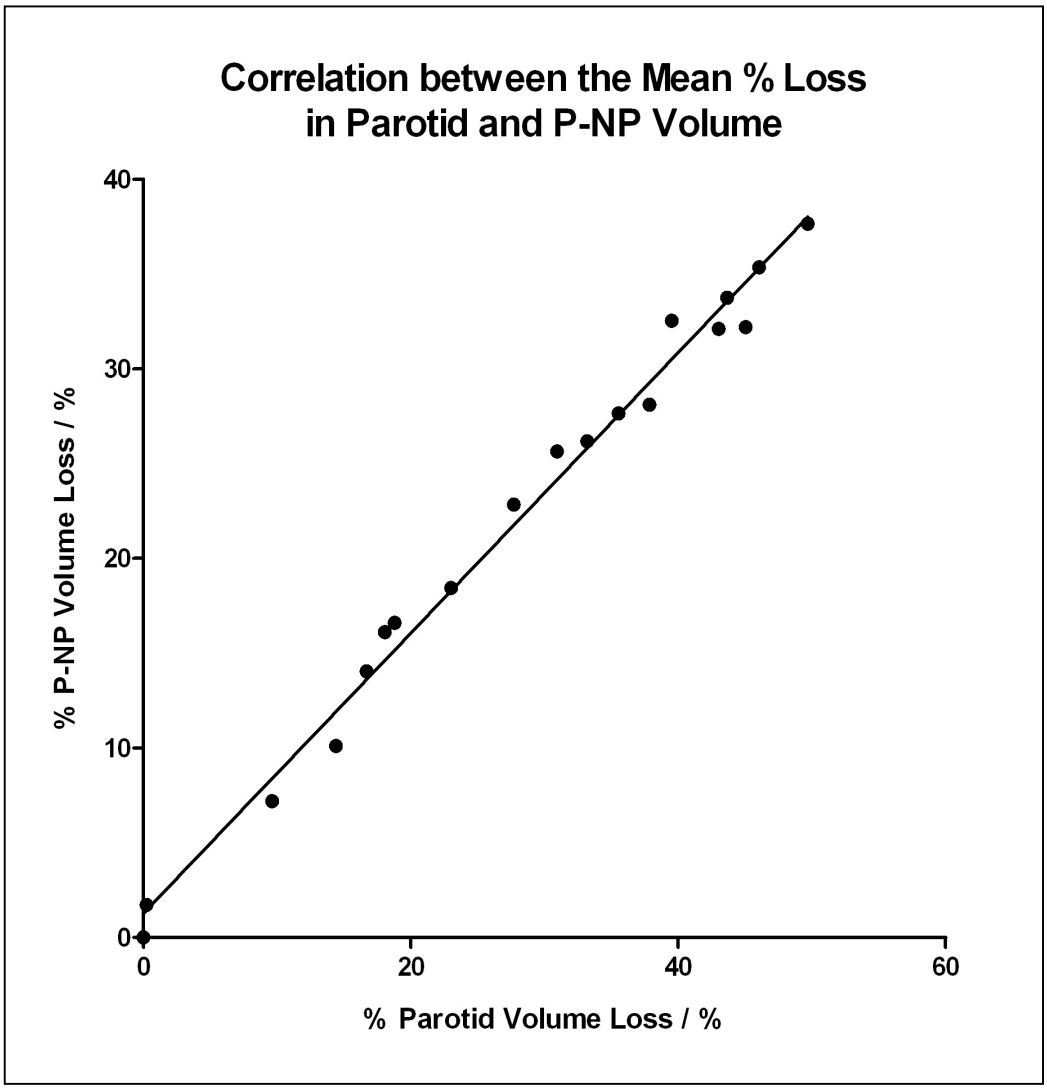

Figure 6.10: Correlation between the mean percentage loss of the parotid gland and the P-NP volumes throughout the treatment course (Linear fit displayed).

6.2.3 Neck volume

All patients experienced changes of habitus in the neck region, manifested by a progressive reduction trend in the mean neck volume throughout the treatment course (Figure 6.11). The neck volume dropped slightly faster in the first half of the course. Towards the end of treatment, the mean reduction was 11.91±5.57 % ($p < 0.0001$). When fit into the linear model, the neck volume decreased in a mean rate of 0.39±0.15 %/day.

The mean percentage reduction in the neck volume and the parotid volume were linearly correlated (Correlation coefficient = 0.9923; $p < 0.0001$) during the radiotherapy course, with 1 % decrease in the neck volume would indicate a 3.53 % decrease in the parotid volume (Figure 6.12). The percentage neck volume loss also correlated strongly with medial and superior displacement of the parotid gland (Correlation coefficient = 0.9812 & 0.9364 respectively; both $p < 0.0001$) over the treatment course. With linear fit, a 5 % loss in the neck volume would indicate a parotid shift of 0.13 cm to the medial direction and 0.10 cm to the superior direction (Figure 6.13).

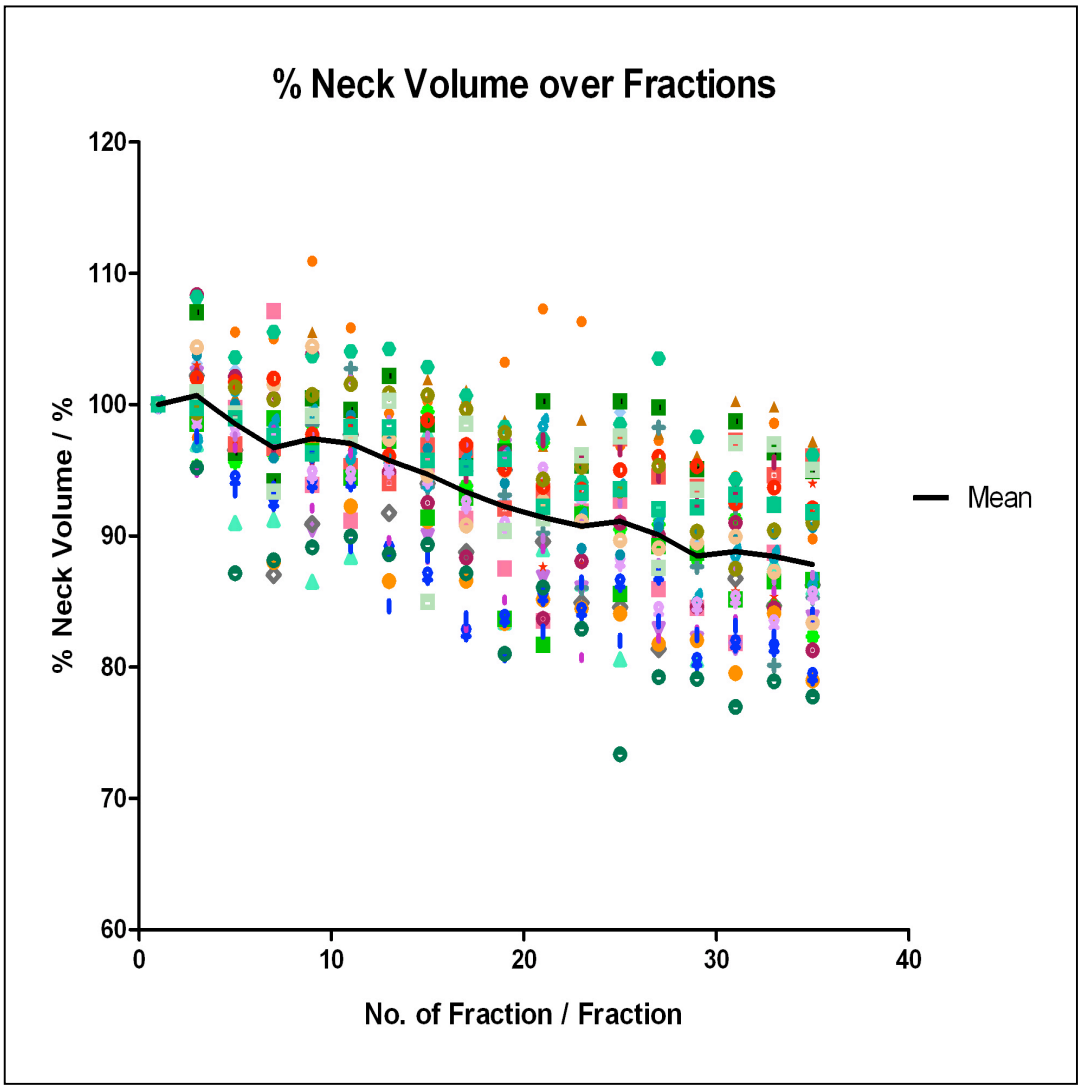

Figure 6.11: Relative neck volume over the treatment course.

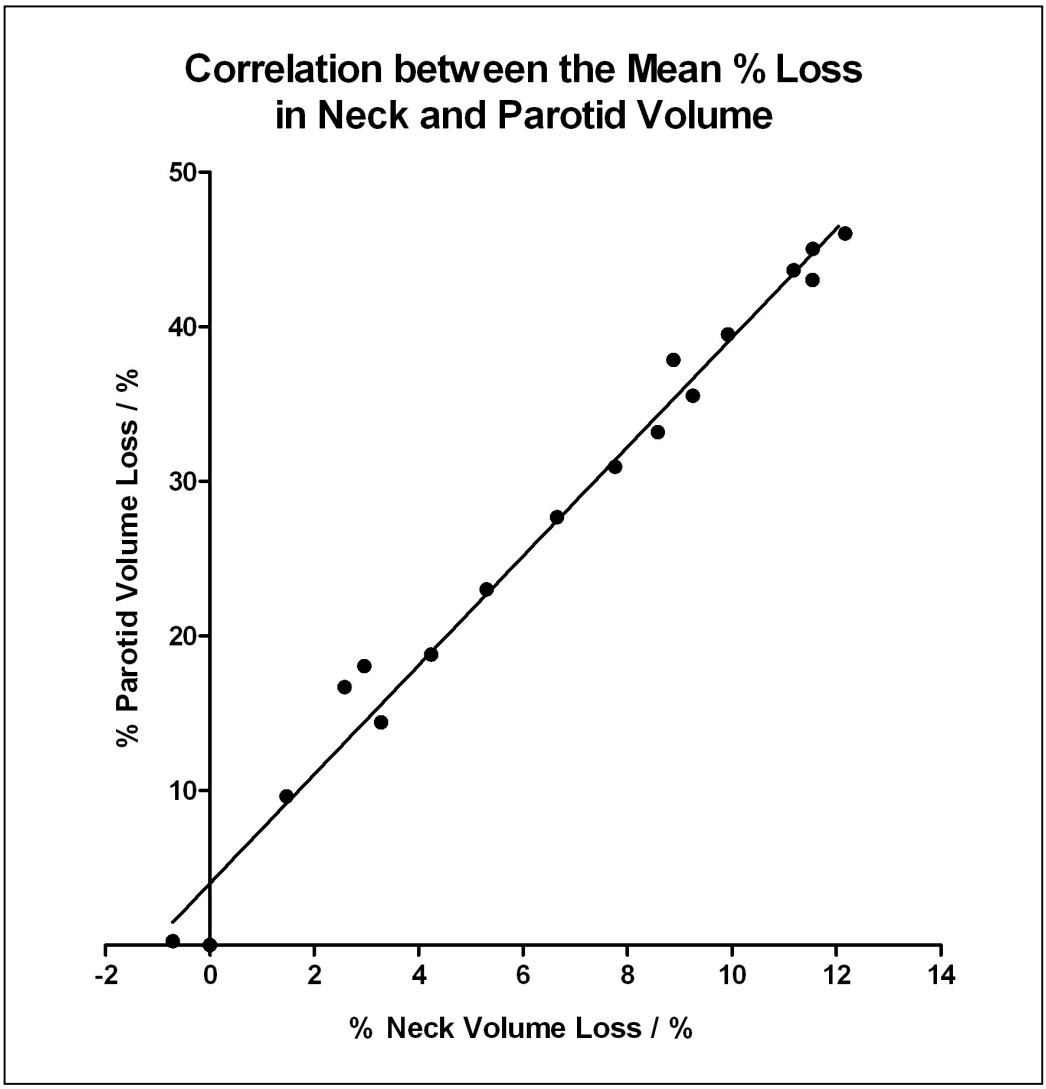

Figure 6.12: Correlation between the mean percentage loss of the neck and parotid gland volumes throughout the treatment course (Linear fit displayed).

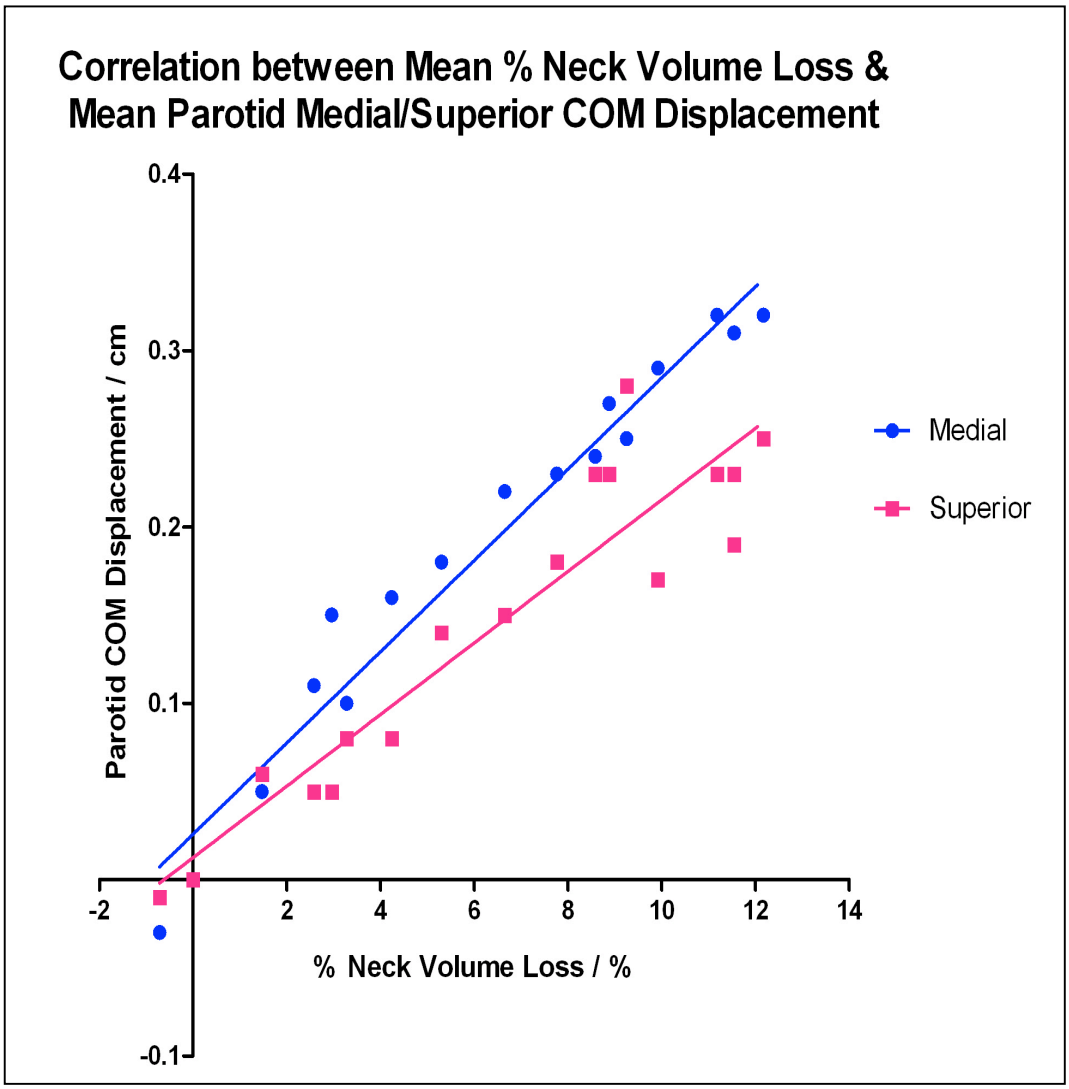

Figure 6.13: Correlation between the mean percentage loss of neck volume and the mean medial or superior displacement of the parotid COM throughout the treatment course (Linear fit displayed).

6.2.4 COM positions of VC3, VC6 and VC9

There were no significant changes in the mean COMs of VC3, VC6 and VC9 in the lateral aspect, though they showed a mild tendency of shifting towards the patient's right side during the treatment course (Figure 6.14). The mean displacements of the VC3, VC6 and VC9 COMs were 0.03±0.14 cm (p = 0.2489), 0.04±0.26 cm (p = 0.3679) and 0.03±0.36 cm (p = 0.3570) to the right side respectively at the treatment end. Nevertheless, the mean COMs of all VCs shifted significantly to posterior direction (Figure 6.15). Progressive downward trends were noted in all these vertebral levels, in which the mean COM displacements increased with time especially after two-third of the treatment course. Moreover, the magnitude of the mean COM shifting also increased from VC3 towards VC9, which implied there was a greater variation in lower neck position throughout the treatment course. At treatment completion, the mean displacements of the VC3, VC6 and VC9 COMs were 0.04±0.22 cm (p = 0.2210), 0.18±0.31 cm (p = 0.0064) and 0.24±0.36 cm (p = 0.0008) to the posterior direction respectively.

It was observed that the percentage neck volume loss was highly correlated with the posterior displacement of VC6 and VC9 COMs during the treatment course (Correlation coefficient = 0.8397 & 0.9127 respectively; both $p < 0.0001$). Using linear regression, a 5 % neck volume reduction would indicate the posterior displacement of 0.06 cm and 0.08 cm in the COMs of VC6 and VC9 respectively.

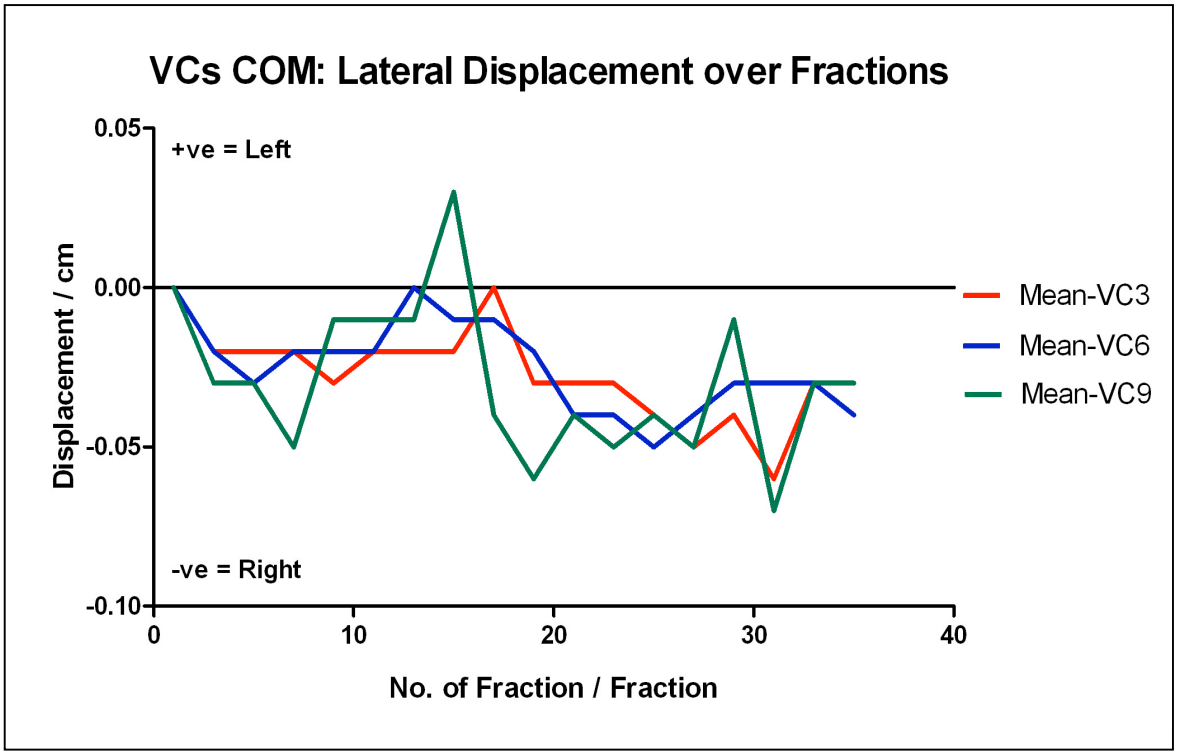

Figure 6.14: Relative COM displacement of VC3, VC6 and VC9 in lateral direction over the treatment course.

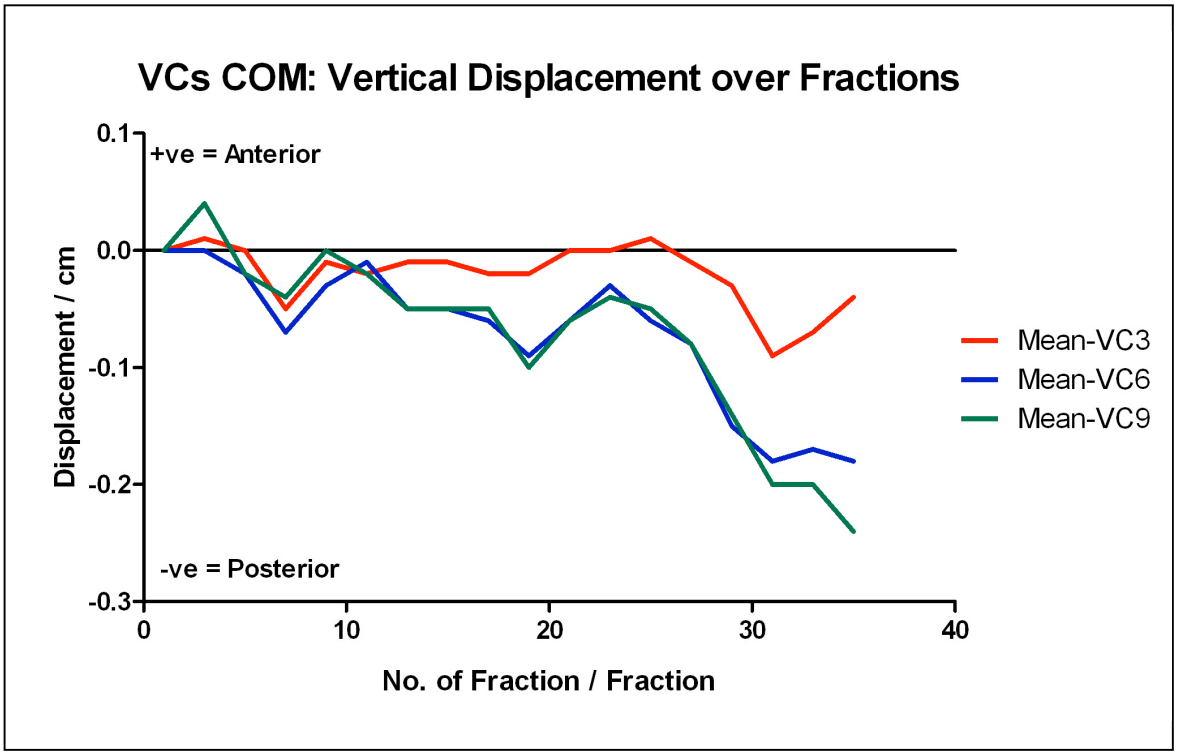

Figure 6.15: Relative COM displacement of VC3, VC6 and VC9 in vertical direction over the treatment course.

6.3 Optimum ART strategy for NPC cases

From the volumetric and geometric analysis, the P-NP volume, the parotid volume, the medial and superior displacement of the parotid COM, the neck volume, and the posterior displacement of COMs of VC6 and VC9 demonstrated significant progressive changes during the treatment course. These parameters were under consideration for setting the optimum ART strategy in NPC cases. Table 6.5 lists the threshold points in each parameter throughout the treatment course based on the ANOVA results. Each threshold represented a statistical significant anatomic change that replanning was preferred. According to the table, the frequency of replanning (threshold occurrence) varied among different parameters. It ranged from 1 replan in VC6 and VC9 position to 6 replans in parotid volume. In practical consideration, 3 replans at 9^{th}, 19^{th} and 29^{th} fractions were proposed as most of the thresholds appeared in these time points. The corresponding degrees of anatomic changes (mean) are shown in Table 6.6. This proposed replanning strategy can optimally accommodate the dosimetric consequences due to anatomic deviations over the treatment course and should be clinically feasible.

Table 6.5: Replanning schedules for selected parameters. Med. = medial; sup. = superior; post. = posterior.

** indicates threshold occurrence on a particular fraction of treatment, in which replanning is suggested.*

Week	Treatment fraction	P-NP % volume	Parotid % volume	Parotid COM med. shift	Parotid COM sup. shift	Neck % volume	VC6 COM post. shift	VC9 COM post. shift	Total no. of thresholds
wk 1	1st								0
	3rd								0
	5th		* (-9.63%)						1
wk2	7th			* (0.10cm)					1
	9th	* (-14.05%)	* (-16.70%)						**2**
wk3	11th								0
	13th					* (-5.30%)			1
	15th		* (-23.02%)						1
wk4	17th			* (0.22cm)					1
	19th	* (-25.64%)	* (-30.94%)			* (-7.76%)			**3**
wk5	21st				* (0.23cm)				1
	23rd								0
	25th		* (-37.86%)						1
wk6	27th								0
	29th			* (0.31cm)		* (-11.54%)	* (0.15cm)		**3**
wk7	31st		* (-43.66%)						1
	33rd								0
	35th							* (0.24cm)	1
wk8	37th								0

Table 6.6: Degrees of anatomic changes (mean) of selected parameters at the proposed replanning fractions. Med. = medial; sup. = superior; post. = posterior.

	Treatment fractions		
	9th	**19th**	**29th**
P-NP % volume loss	14.05 %	25.64 %	32.11 %
Parotid % volume loss	16.70 %	30.94 %	43.03 %
Parotid COM med. shift	0.11 cm	0.23 cm	0.31 cm
Parotid COM sup. shift	0.05 cm	0.18 cm	0.19 cm
Neck % volume loss	2.58 %	7.76 %	11.54 %
VC6 COM post. shift	0.03 cm	0.09 cm	0.15 cm
VC9 COM post. shift	0.00 cm	0.10 cm	0.14 cm

CHAPTER SEVEN

DISCUSSION

7.1 Dosimetric comparison

This study emphasized the dosimetric importance of implementing ART strategy in NPC cases by comparing the treatment plans between replanning and without replanning. In PII and PIII without replanning, the doses to the NP-CTV and NP-PTV were increased with significantly better dose homogeneity due to radiation-induced target volume shrinkage. As shown in Table 7.1, there were substantial volume losses in the NP-CTV and NP-PTV in both phases. Consistent result was also noted when monitoring the volumetric change of the P-NP throughout the treatment course (Figure 6.1). Indeed, the target volume shrinkage mostly took place within the initial planned high dose region (Figure 7.1). As a result, the regressed target volumes became away from the dose fall off area around the original target edge resulted in an increased proportion of the target volumes receiving the prescribed doses. Therefore even without replanning, the dose coverage to the NP-CTV and NP-PTV was still maintained. In addition, the dose homogeneity was improved among these target volumes. When comparing the dosimetric results between the NP-CTV and NP-PTV, it was found that the differences in D_{95} between replanning and without replanning reached statistical significant level in NP-PTV in both PII and PIII but not in NP-CTV. Besides, the dose homogeneity and conformity of the NP-PTV were relatively poor when compared to those in NP-CTV in both phases. One possible reason for this observation was that the NP-PTV coverage was sometimes being

sacrificed during plan optimization in order to lower the doses to surrounding critical organs e.g. brainstem. It might also be due to the fact that the dose gradient at the PTV-normal tissue boundary would always be greater than that at the CTV-PTV boundary. All these consequently led to a more fluctuated dose to the NP-PTV and thus a greater dose difference in NP-PTV during comparison.

This study also demonstrated that the bilateral LN-PTVs suffered from substantial radiation-induced shrinkage (Table 7.1). Nevertheless, the doses to the LN-PTVs did not significantly change with similar dose uniformity between replanning and without replanning in both PII and PIII. Unlike the primary tumor, the lymph node targets were surrounded by less critical organs e.g. parotid glands. Therefore, adequate dose coverage to these lymph node targets was of higher priority than sparing the OARs, resulting in comparable dosimetirc outcomes between the two planning approaches. In PII, the mean HI of RLN-PTV without replanning was lower than that with replanning in terms of absolute value but was higher when presenting in terms of relative percentage. This contradicting result was probably due to the underdosage of RLN-PTV in PII-NART of 3 extreme cases. Particularly low minimum doses were received by the RLN-PTVs in PII-NART of these cases, which led to the substantially high HIs and in turn affected the calculation of the percentage change of mean HI in the overall population when compared to the PII-ART. Despite this, majority of patients had lower HIs i.e. better dose uniformity in RLN-PTV without replanning.

Table 7.1: Mean percentage volume losses of target volumes in PII and PIII relative to PI.

Target volumes	% Volume loss (mean)	
	PII	PIII
NP-CTV	17.97±25.42 %	51.73±21.00 %
NP-PTV	19.87±13.29 %	37.75±27.93 %
LLN-PTV	32.28±20.83 %	72.70±11.02 %
RLN-PTV	32.10±18.35 %	74.84±13.93 %

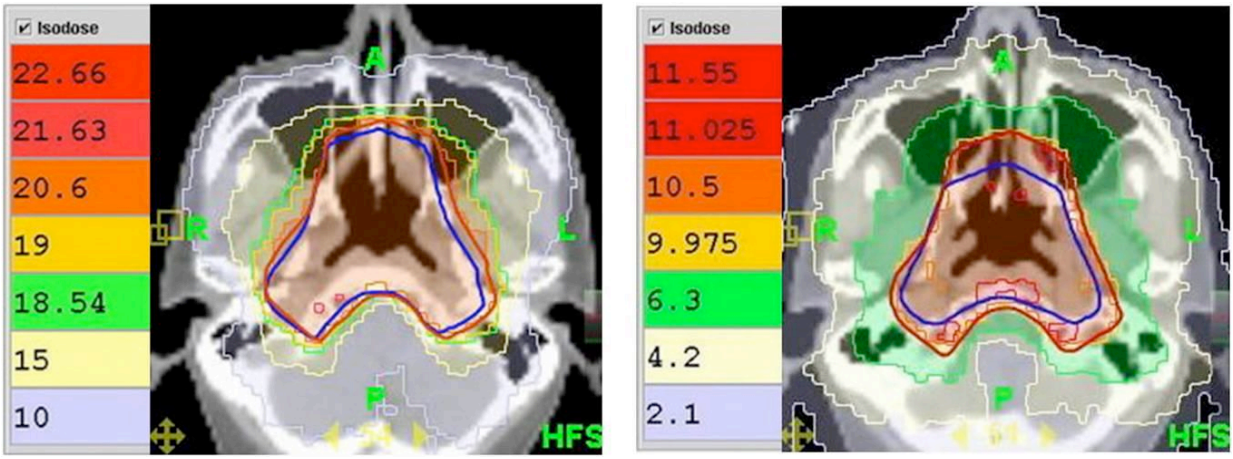

Figure 7.1: Transverse CT images of a patient from PII-NART (left) and PIII-NART (right) demonstrating target shrinkage and dose coverage throughout the treatment course. The actual NP-PTVs of PII and PIII (blue), after shrinkage, were enclosed by the high-dose region of the initial NP-PTV (red) without replanning.

Although adequate doses could still be delivered to the target volumes without plan modification, many abutting normal tissues were being unnecessarily irradiated with high dose due to target shrinkage. This explained why the dose conformity of all target volumes was deteriorated without replanning, as indicated by the significantly lower CNs in both PII and PIII when compared to those with replanning. To better illustrate the dose distribution with or without replanning, the two fractions of the CN were calculated separately (refers to Chapter 5.3). The first fraction, which quantifies the degree of target coverage, was close to the ideal value of 1 for all target volumes in both phases with or without replanning (Tables 7.2 & 7.3). This implied that adequate dose coverage was achieved by all target volumes, which was consistent with the findings in D_{95} and HIs. However the second fraction, which quantifies the degree of normal tissue irradiation, was significantly lower in all target volumes without replanning in both PII and PIII when compared to those with replanning (Tables 7.2 & 7.3). This indicated that a substantial volume of normal tissues would be under irradiation if no replanning was done to compensate the volume shrinkage in targets. As seen in this study, there was substantial volume loss in the neck region (Figure 6.11). The alteration in muscle mass and fat distribution resulted in distortion of the planned dose distribution in this region, consequently led to increased skin dose and hence more severe skin reaction if no replan was applied. On the other hand, the reduction in the lymph node targets and the neck volume caused the displacement of the parotid glands. In addition, the parotid glands themselves also suffered from radiation-induced shrinkage and medial migration towards the initial planned high dose region (Figures 6.5 & 6.6). All these led to an increase in the parotid mean doses if no replan was performed. The

dosimetric consequences due to anatomic changes in the parotid glands were also presented in Han et al. (2008) study on 5 NPC patients, in which the average median doses had increased 0.6 Gy at the end of the treatment course. In the present study, the absolute mean dose increments in parotid glands were relatively small (≤ 1.5 Gy) when compared to other OARs. Their average total mean doses after the whole treatment course were estimated as ~36.80 Gy if there was no replan and ~35.39 Gy if two replannings were applied (Table 6.3). In this dose range, xerostomia is usually resulted with modest recovery several months after the completion of the radiotherapy course (Hsiung et al., 2006; Li et al., 2007b). Nonetheless, the incomplete return of pre-treatment salivary level can still trigger patients' discomfort during mastication and swallowing thus resulting in loss of appetite and inadequate nutritional intake in long run. In view of the close proximity of the parotid glands to the target volumes and the concerns in sparing other more critical organs, it is difficult to limit the total parotid mean dose < 26 Gy as recommended by many authors (Blanco et al., 2005, Eisbruch et al., 2001; Eisbruch et al., 1999; Li et al., 2007b). Nevertheless, efforts should be put on keeping the parotid dose as low as possible because every Gy increase in parotid mean dose, as mentioned by Blanco et al. (2005), could lead to 5 % decrease in salivary function which dramatically decreased patient's QOL after treatment (Cooper et al., 1995; Li et al., 2007b).

Table 7.2: Comparison between PII-NART and PII-ART in terms of the degree of target coverage and normal tissue irradiation, which calculated based on the CN formula (van't Riet et al., 1997).

** indicates the result with statistical significance.*

End points (mean)	PII-NART	PII-ART	*p* value
Target coverage			
NP-CTV	0.94±0.09	0.95±0.06	0.8502
NP-PTV	0.96±0.06	0.95±0.04	0.2136
LLN-PTV	0.97±0.06	0.95±0.05	0.0228*
RLN-PTV	0.97±0.06	0.96±0.03	0.1051
Normal tissue irradiation			
NP-CTV	0.64±0.17	0.78±0.16	0.0007*
NP-PTV	0.51±0.18	0.70±0.15	< 0.0001*
LLN-PTV	0.42±0.16	0.59±0.11	< 0.0001*
RLN-PTV	0.41±0.16	0.58±0.10	< 0.0001*

Table 7.3: Comparison between PIII-NART and PIII-ART in terms of the degree of target coverage and normal tissue irradiation, which calculated based on the CN formula (van't Riet et al., 1997).

** indicates the result with statistical significance.*

End points (mean)	PIII-NART	PIII-ART	*p* value
Target coverage			
NP-CTV	0.96±0.07	0.96±0.03	0.2948
NP-PTV	0.99±0.02	0.96±0.03	0.0009*
LLN-PTV	0.95±0.10	0.96±0.02	0.6085
RLN-PTV	0.97±0.03	0.96±0.02	0.5114
Normal tissue irradiation			
NP-CTV	0.52±0.30	0.80±0.18	0.0003*
NP-PTV	0.31±0.22	0.68±0.12	0.0001*
LLN-PTV	0.11±0.06	0.42±0.13	< 0.0001*
RLN-PTV	0.11±0.07	0.42±0.11	< 0.0001*

It had been reported by Teo et al. (2006) that local disease control in NPC could be improved by target dose escalation. In our centre for most NPC cases, aggressive tumoricidal dose of up to 84 Gy can be prescribed. Such a high prescribed dose apparently increases the difficulty in sparing the adjacent critical organs. The present study demonstrated that there were potential risks of overdosing the brainstem, spinal cord, optic chiasm and pituitary gland if one single plan was used throughout the whole treatment course. Without any adaptive measures, the total doses to these organs could be dramatically increased by 9–13 Gy. As discussed in previous section (Chapter 3.2), overdose to the pituitary gland can lead to hypopituitarism that normal secretion of various pituitary hormones are decreased or prohibited. This consequently affects the body functions in terms of growth, development and reproduction. Depending on the specific types of hormonal deficiencies, patients may suffer from fatigue, weight loss, decreased sex drive, failure of lactation and constipation etc (Table 3.1). All these can severely influence the routine daily life of patients. Although hypopituitarism can be treated with hormone replacement therapy, lifelong supplement and surveillance are needed which significantly degrade patient's QOL. On the other hand, dose control to the brainstem, spinal cord and optic chiasm are particularly important during plan optimization as radiation damage to these organs can lead to various irreversible side effects like central nervous system injury, myelopathy and optic neuropathy. Injuries to brainstem can be manifested as loss of body coordination and motor weakness. In severe cases, it may cause paralysis, body numbness and death (Mayo, Yorke, & Merchant, 2010). Myelopathy which results from radiation-induced injury of the spinal cord can lead to paresthesia, sensory and/or motor deficits and may progress to

paralysis. In particular, patients with damage to the cervical cord region may lose control of the upper limbs (Martini et al., 2001). Radiation-induced optic neuropathy at the optic chiasm can be presented as unilateral or bilateral, temporary or permanent visual impairment (Danesh-Meyer, 2008; Mayo et al., 2010). If the entire chiasm is being damaged, complete irreversible blindness may be the consequence (Mayo et al., 2010). In this study when one single plan was applied, some patients would have the estimated total doses of brainstem, spinal cord and optic chiasm exceeding tolerance, in which the exceeded doses were 55–67 Gy, 47–54 Gy and 55–73 Gy respectively. It had been reported that the risk of brainstem injury increases greatly if the dose is > 64 Gy (Mayo, Yorke, & Merchant, 2010), the incidence of myelopathy is 0.2 % if the cervical cord dose reaches 50 Gy (Schultheiss, 2008), and the chance of developing optic neuropathy is 3–7 % for chiasm dose of 55–60 Gy and 7–20 % when the dose is > 60 Gy (Mayo et al., 2010). Treatment to these complications is limited and some of the symptoms can be life threatening. This study demonstrated that when the targets shrank during the treatment course, the physical distance between the targets and these critical organs increased. The new adaptive plans being generated in the three-phase treatment approach could therefore provide better sparing of these critical structures without compromising the target conformity and in turn the local tumor control. Figure 7.2 illustrates the effect of brainstem dose reduction in a patient when replanning strategy was applied. In this patient, replanning based on the regressed target allowed the dose to the portion of brainstem that near the target to be as low as 30 % of the prescribed dose. The dosimetric result may also be correlated to clinical outcomes by calculating the normal tissue complication probability (NTCP) and tumor control

probability (TCP). These radiobiological indices quantitatively predict the likelihood of normal tissue complication and tumor control according to the delivered dose and irradiated organ/target volume. By applying statistical and mathematical principles together with radiobiological data such as published normal tissue tolerances, tissue/tumor radiosensitivity and tumor cellular or organ type etc (Beyzadeoglu, Ozyigit, & Ebruli, 2010), these indices are computed to evaluate the potential clinical effectiveness of the treatment. In this study, the NTCP of the OARs and the TCP of the target volumes were not calculated based on the models suggested in various publications (Beyzadeoglu, Ozyigit, & Ebruli, 2010; Kutcher & Burman, 1989; Lyman, 1992; Lyman & Wolbarst, 1987; Niemierko, 1997; Webb & Nahum, 1993). Nevertheless, reduction in NTCP could be extrapolated by the fact that fewer patients had their OAR doses exceeding acceptable tolerance when replannings applied (Table 6.4). Although adequate target coverage was achieved in all phases with or without replannings (Table 7.2 & 7.3), the current study demonstrated that it was more feasible to deliver high tumoricidal dose when ART was used without risking the surrounding critical organs. This apparently increased the local disease control and in turn the TCP (Teo et al., 2006). All these should bring about overall improvement in the clinical outcomes. In this study, the dose differences between replanning and without replanning were much greater in the OARs than in the target volumes in both PII and PIII, which implied that the primary advantage of applying ART in NPC cases lies on limiting the doses to OARs than keeping the tumor coverage. This finding was consistent with those presented by Loo et al. (2011) study, which also suggested that replanning was not necessary for accommodating the tumor changes but would be beneficial in

sparing the OARs especially the parotid glands.

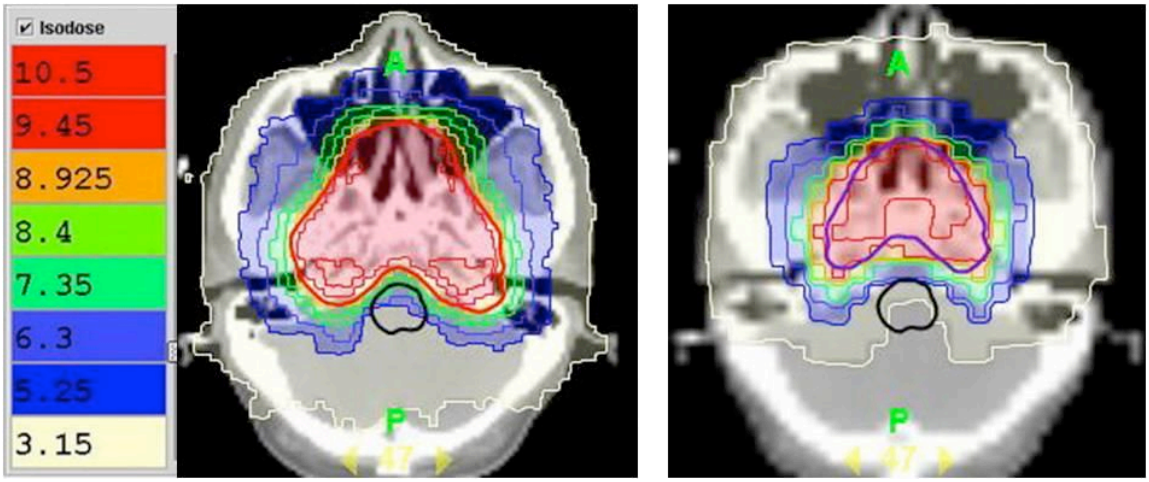

Figure 7.2: Transverse CT images of a patient from PIII-NART (left) and PIII-ART (right) demonstrating the brainstem dose reduction by replanning strategy. Without replanning, the brainstem (black) received over 50% of the prescribed dose because it was close to the initial NP-PTV (red). When replanning was applied, the brainstem dose could be reduced to 30% of the prescribed dose while keeping the dose conformity to the actual NP-PTV (purple).

As described, the purpose of ART is to resume the originally planned dose distribution by accounting the tumor response and normal tissue anatomic changes in between the treatment course. Therefore, the quality of the ART plans in terms of target coverage and OAR sparing should comparable to those of the baseline plans (i.e. using the initial CT and PI plan for the whole course of treatment). This is illustrated in Table 7.4, in which the target and parotid doses showed no significant difference between the baseline and the ART plans. Furthermore, by making use of the increased physical distance between the shrunken targets and surrounding critical organs during the treatment course, ART provides significantly better dosimetric results in all closely situated OARs such as the brainstem and optic chiasm when compared to the baseline plans (Table 7.4). In the current study, the potential statistical difference between early (T1/2) and late (T3/4) disease stages was not analyzed due to the small sample size in each subgroup. As discussed, ART is more advantageous in limiting the doses to OARs than keeping the tumor coverage. Moreover in concerns of the varying tumor size, the OAR sparing effect by ART might have a greater impact in late stage than in early stage disease. To illustrate, Table 7.5 lists the degree of target coverage based on the CN formula and the OAR doses of one T1 and one T4 NPC patients with or without adaptive measures. Adequate dose coverage to the actual target volumes could be achieved despite the treatment strategy used (NART/ART). However due to the extensive logo-regional infiltration and lymphatic spread, the initial target volumes for late stage disease would be much larger and very close to the critical structures when compared to that in early disease. When NART was applied to late stage disease, the OAR doses would inevitably receive high dose that more likely to exceed the tolerance.

Replannings in later stage of the treatment course allowed better sparing of the OARs and hence increased the chance of keeping the overall OAR doses within acceptable tolerance. For early stage disease, the initial targets were relatively small and distant from the surrounding critical organs. Therefore even without replannings, target dose could be safely delivered with OAR doses well within tolerance. Nonetheless, ART should still be promoted in treating early stage disease such that the OAR doses could be as low as possible.

Table 7.4: Dosimetric comparison between baseline plan and ART plan (two replans).

** indicates the result with statistical significance.*

End points (mean)	Baseline Plan	ART Plan	*p* value
Targets - D_{95}			
NP-CTV	82.97±2.48 Gy	82.72±2.46 Gy	0.3468
NP-PTV	77.65±3.20 Gy	77.49±3.27 Gy	0.4393
LLN-PTV	78.39±2.51 Gy	78.21±2.42 Gy	0.1063
RLN-PTV	78.44±2.38 Gy	78.24±2.29 Gy	0.0545
OARs			
Brainstem D_1	47.15±5.99 Gy	45.23±6.61 Gy	0.0013*
Spinal Cord D_1	35.21±3.64 Gy	34.77±4.69 Gy	0.0013*
Optic Chiasm D_{max}	46.48±11.45 Gy	44.50±10.16 Gy	0.0060*
Pituitary Gland D_{max}	56.63±14.46 Gy	53.63±12.05 Gy	0.0036*
Left Parotid Gland D_{mean}	34.79±4.29 Gy	34.90±4.40 Gy	0.7569
Right Parotid Gland D_{mean}	35.67±4.27 Gy	35.88±4.30 Gy	0.5945

Table 7.5: Comparison between NART and ART plans in terms of the degree of target coverage, which calculated based on the CN formula (van't Riet et al., 1997), and OAR doses of one early stage (T1) and one late stage (T4) NPC patient.

	T4 patient		T1 patient	
	NART	**ART**	**NART**	**ART**
Target coverage				
NP-CTV				
PII	0.98	0.95	0.96	0.94
PIII	1.00	0.98	0.95	0.93
NP-PTV				
PII	0.96	0.92	0.99	0.97
PIII	1.00	0.98	0.97	0.98
LLN-PTV				
PII	0.96	0.97	1.00	0.93
PIII	0.93	0.99	0.96	0.96
RLN-PTV				
PII	0.99	0.99	1.00	0.93
PIII	0.98	0.99	0.96	0.95
OARs				
Brainstem D_1	59.41 Gy	50.89 Gy	46.34 Gy	42.65 Gy
Spinal Cord D_1	39.49 Gy	32.47 Gy	32.44 Gy	31.53 Gy
Optic Chiasm D_{max}	73.08 Gy	61.32 Gy	53.46 Gy	47.93 Gy
Pituitary Gland D_{max}	n/a	n/a	35.03 Gy	28.23 Gy
Left Parotid Gland D_{mean}	28.47 Gy	28.22 Gy	30.46 Gy	31.37 Gy
Right Parotid Gland D_{mean}	33.00 Gy	31.54 Gy	33.27 Gy	33.19 Gy

As predicted, the result of the present study was different from those conducted on head and neck cancer patients. Hansen et al. (2006) showed a decrease in the PTV dose, while the present study demonstrated an increased or comparable target dose if no replanning was done. The discrepancy in the target dose changes was probably due to the heterogeneity of the primary treatment sites e.g. nasopharynx, base of tongue, and ispilateral tonsil that were included in Hansen et al. study. The radiation effect and shrinkage pattern could be largely different for different primary sites, which might lead to the discordant outcome. The present study focused on NPC patients, which reflected the dosimetric effect of applying ART specifically for this group. The findings in this study were largely consistent with those presented by Wang et al. (2010) and Kim et al. (2009), whose studies were also conducted on NPC patients. Regardless of the different replanning protocols, both studies showed that without replanning, the dose coverage to the regressed target volumes was maintained with no significant changes, but the doses to various OARs were increased. Compatible result was also seen in the present study. In Wang et al. study, the D_1 of the brainstem and spinal cord increased by 1.47 Gy and 2.06 Gy respectively. In Kim et al. study, the respective maximum doses to these organs increased by 1.40 Gy and 2.17 Gy. In the present study, the mean total D_1 of these organs increased 3.95 Gy and 4.10 Gy respectively. The magnitudes of dose differences were higher in the present study because the total doses from the whole course of treatment was recorded here but Wang et al. and Kim et al. only presented the mid-course doses of these structures.

When comparing the degree of dosimetric changes in PII and PIII in the present study, it was noted that the dose differences between PIII-NART and PIII-ART were greater than that between PII-NART and PII-ART especially in the OARs. In particular, the endpoint dose changes in brainstem and optic chiasm reached statistical significance. The dose difference for the mean D_1 of the brainstem was 24.41 % in PII but 51.09 % in PIII ($p = 0.0051$), while the dose difference for the maximum dose of the optic chiasm was 27.61 % in PII but 84.38 % in PIII ($p = 0.0059$). The dose variation was greater in PIII than in PII if no replanning was conducted. Moreover, the target volumes and the parotid glands also demonstrated progressive anatomic changes with greater volume losses in PIII. All these indicated that there were considerable volumetric changes and in turn resulted in dosimetric changes in later treatment fractions of the radiotherapy course, which could be overlooked if only one replanning was applied in the mid-course of treatment. Two replannings, as in the current three-phase radiation protocol, improved the overall dosimetric results by accounting also the anatomic variation in later fractions and was considered essential for NPC cases.

In the adopted three-phase radiation protocol, the same thermoplastic cast was used in all phases of the treatment course. Although a new cast that fit the patient up-to-date body contour for PII and PIII treatment should reduce patient motion inside cast, this also increased patient financial burdens and manpower needs for remouding. Using the same cast throughout the treatment course was considered justified due to several reasons. Because of the deep-seated anatomic location of the nasopharyngeal tumor, it was relatively stable regardless of the changes in patient facial contour. When compared to other body regions, the alternation of

facial habitus was bound by the presence of bony structures in the head. On the other hand, it was noted that the cast material underwent shrinkage over time. In fact, the cast would be very tight at the beginning of the treatment course and usually become just fit when patient loses some weight during the course. Moreover, the patient would always be aligned to the midline marked on the cast during daily setup. Together with the use of daily MVCT treatment verification, prescribed dose to the primary targets could be ensured.

The three-phase radiotherapy protocol showed improved dosimetric results to the critical structures while keeping satisfactory target dose coverage, which demonstrated the advantages of ART in helical tomotherapy of NPC. Rather than keeping adequate dose coverage to the target volumes, ART was more beneficial in terms of sparing the critical organs that surrounded the primary tumor and in turn minimized the risk of complications. The results also emphasized the necessity of multiple replannings throughout the treatment course to account for the anatomic variation during radiotherapy, which reinforced the need to develop an optimum ART strategy for NPC cases.

7.2 Volumetric and geometric analysis

With the use of daily MVCT scans, this part of the study investigated the trends of anatomic variations during the treatment course in NPC cases. The anatomic change of the nasopharyngeal gross tumor was assessed by quantifying the volumetric and geometric deviation of the P-NP. Figure 7.3 visualizes the progressive volume loss of the P-NP over time. Increased aeration of the nasopharyngeal region was observed when treatment proceeded, and the opening of the eustachian tube, the torus tubarius and the fossa of Rosenmuller were reappeared due to tumor shrinkage. In this study, the P-NP experienced volume loss with a mean loss rate at 0.99 %/day and a mean volume loss of 35.70 % at the end of the treatment course. Moreover, the initial P-NP volume was negatively correlated with its percentage volume loss. To my knowledge, only one study was conducted to monitor the gross tumor shrinkage trend in head and neck cases, while none was performed specifically for NPC cases. In Barker et al. (2004) study on head and neck patients, the GTV had a median volume loss of 69.5 % and a median loss rate at 1.7 %/day. They also showed that the initial GTV was positively correlated with its rate of volume loss, which was contradicted to the result in current study. These discrepancies might again be due to the heterogeneity of primary treatment sites in Barker et al. study, whose results might not represent the cases in NPC. This highlights the needs of characterizing the trends of anatomic changes particularly in NPC cases for precise establishment of optimum ART strategy in this group.

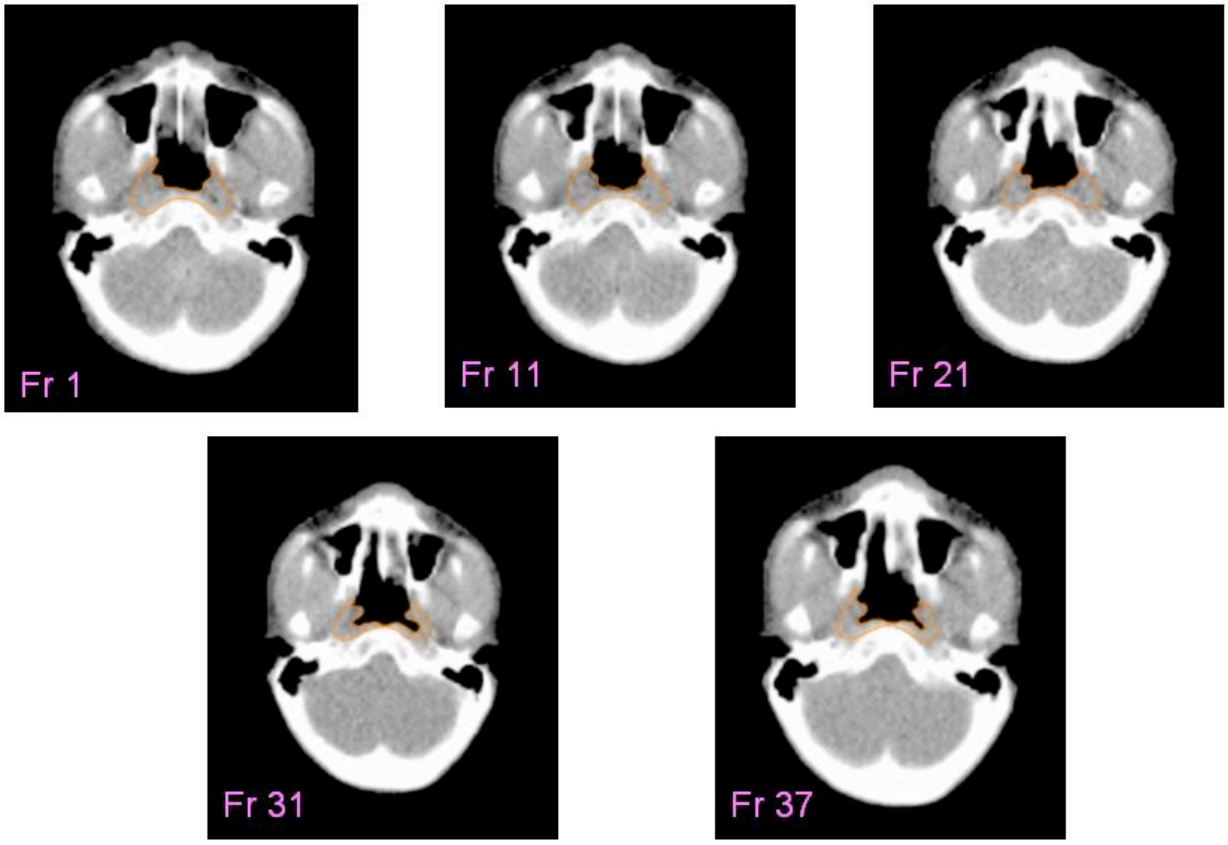

Figure 7.3: Transverse MVCT slices demonstrating the P-NP shrinkage over the treatment course. The fraction number is written on bottom left side of each image. Fr = fraction.

Some studies on NPC cases measured the degree of tumor shrinkage at different time points of or after the radiotherapy course (Fang et al., 2001; Kim et al., 2009, Kodaira et al., 2009). Fang et al. (2001) showed a mean primary volume regression rate of 70 % after 45 Gy, and Kim et al. (2009) showed a 37 % average decrease in the GTV after 30–50 Gy. These studies demonstrated a greater percentage loss in the tumor volume when compared to the present study. This might be due to the difference in the definition of the measured volume. The P-NP instead of the true gross tumor was being contoured because the oncologist could not define the tumor extent clearly in the MVCT images. To facilitate contouring, several prominent normal structures e.g. the prevertebral muscle was included in the P-NP. Although the volumetric changes of the P-NP presented in numerical data might be weakened due to the inclusion of normal structures, it could still reflect the significant shrinkage occurred in the GTV. Moreover, its regression trend throughout the treatment course provided valuable information for defining the optimum ART strategy for NPC cases.

Though the mean displacement of the P-NP COM was close to zero i.e. nearly no positional change in any direction throughout the treatment course, individual data were in great diversity. The lateral, longitudinal and vertical shifts were ranged from -0.54–1.4 cm, -0.66–0.64 cm and -0.36–0.44 cm respectively at treatment completion. In individual cases, the COM of the regressing P-NP changed position with varying displacement pattern over time. This implied that the P-NP volume loss was asymmetric, and every patient might have a unique regression pattern which could be unpredictable. In MVCT images, it was observed the anterior portion of the P-NP had noticeable volume regression i.e.

became thinner throughout the treatment course (Figure 7.3). This suggested that the asymmetric shrinkage of the P-NP volume might be predominant along the vertical axis. However, this effect was not great enough to be manifested as statistical significant deviation in the mean vertical displacement of the P-NP COM. As the estimation of the COM position was based on the volumetric changes of the entire P-NP volume, the regression effect in this direction was being weakened probably by the asymmetric changes occurred in lateral and longitudinal aspects. Regardless of the visual observation in the MVCT images, the exact shrinkage pattern of the P-NP remained vague. As no concrete conclusion could be drawn, the results of the P-NP COM displacement were not considered in this study for the establishment of the optimum ART strategy for NPC cases.

The GTVs of the bilateral lymph nodes were not contoured in this part of the study because the true nodes could not be defined clearly in the MVCT images. Although their patterns of volumetric and positional changes were not available, pronounced radiation-induced shrinkage throughout the treatment course was manifested by the mean percentage volume losses in bilateral LN-PTVs (Table 7.1). Some studies on NPC cases also demonstrated significant lymph node shrinkage during radiotherapy. The mean nodal regression rate was 70 % after 45 Gy of radiotherapy in Fang et al. (2001) study. In Wang et al. (2010) study, the lymph nodes regressed 40.1 % of its initial volume after 36 Gy of radiotherapy, with greater absolute volume loss seen in larger lymph nodes.

Unlike the study of Wang et al. (2009) who showed a faster drop of parotid gland volume in the first 3 weeks of radiotherapy, the present study demonstrated a gradual parotid volume loss over time. In addition, their systematic displacements to the medial and superior aspects were also noted throughout the treatment course. The decrease in parotid volume was due to the radiation-induced apoptosis which resulted in rapid depletion of the parotid acinar cells (Konings, Copes, & Vissink, 2005). Han et al. (2008) study was so far the only study that quantified the trend of volumetric changes on parotid glands specifically in NPC patients. They found that the parotid volume reduced at a mean rate of 1.1 %/day and had a mean loss of 40.2 % at the end of treatment, which was largely consistent with the current study that the parotid volume decreased 1.35 %/day and 47.54 % when treatment finished. Han et al. also showed a significant correlation between the average parotid volume and the average median parotid dose, in which a reduction in the parotid volume during the treatment course would indicate an increase in the parotid dose. This finding gave support of treating parotid volume as one of the considerations during the establishment of the optimum replanning strategy in the current study. The volumetric changes in the parotid glands would be a good indicator to signal any significant dose variation in the glands that required replanning.

Many studies quantified the medial displacement of the parotid glands in head and neck radiotherapy. Barker et al. (2004) and Lee et al. (2008a) demonstrated a median medial shift of 0.31 cm and 0.26 cm at the end of the treatment course respectively. The present study also showed a mean medial displacement of 0.34 cm. In addition, the glands tended to shift superiorly with a mean of 0.24 cm

after the treatment course. The geometric changes of the parotid glands were multi-factorial. Other than the fact that it could be displaced by the regressed lymph nodes or decreased neck volume, the asymmetric volume loss of the parotid might also contribute to the displacements predominantly in these directions. As seen in the MVCT images, the parotid shrinkage occurred mostly in the lateral and inferior portions throughout the treatment course (Figures 7.4 & 7.5). This observation was consistent with the results of those studies that investigated the parotid positional changes in terms of different regions of the glands. Vasquez Osorio et al. (2008) divided the parotid glands into 6 different subvolumes for investigation. They found that although all regions of the parotid tended to move inward when it shrank, the largest displacement occurred in the lateral and inferior regions. The mean displacements were 0.3 cm in the lateral region towards the medial aspect and 0.3 cm in the inferior region towards the superior aspect, whereas the medial region that partially adjacent to the bony structures showed least inward translation of 0.1 cm. Robar et al. (2007) also assessed the geometric changes separately in the medial and lateral aspects of the glands during the radiotherapy course. A systematic medial translation was clearly observed in the lateral aspect of the glands but not in the medial aspect. The variable degree of translation in different parotid segments in these studies reflected that the parotid volume loss was asymmetric. Although the changes in each portion of the parotid glands were not quantified, the present study also demonstrated the presence of asymmetric parotid volume loss during radiotherapy, which was manifested as significant displacement towards the medial and superior directions.

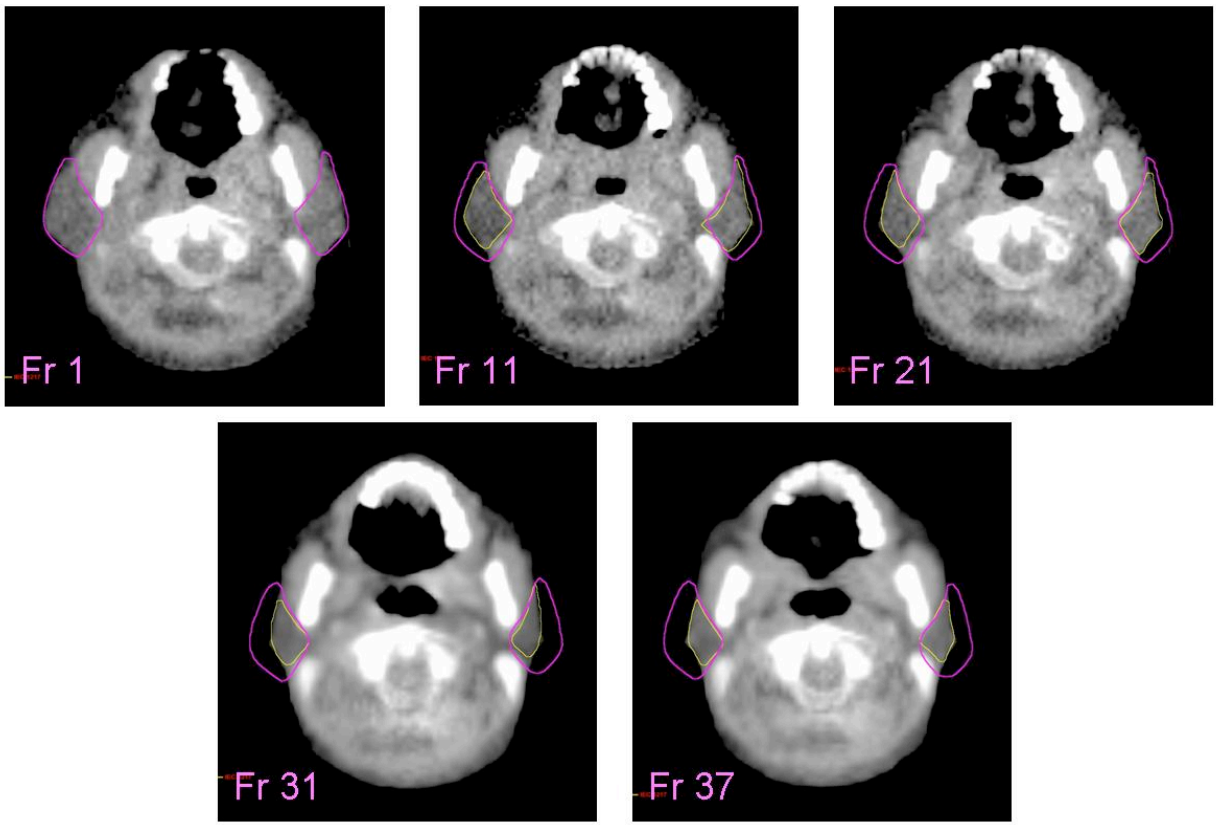

Figure 7.4: Transverse MVCT slices demonstrating the parotid shrinkage at the lateral portion over the treatment course. The initial volume is displayed in purple and the updated volume is in yellow. The fraction number is written on bottom left side of each image. Fr = fraction.

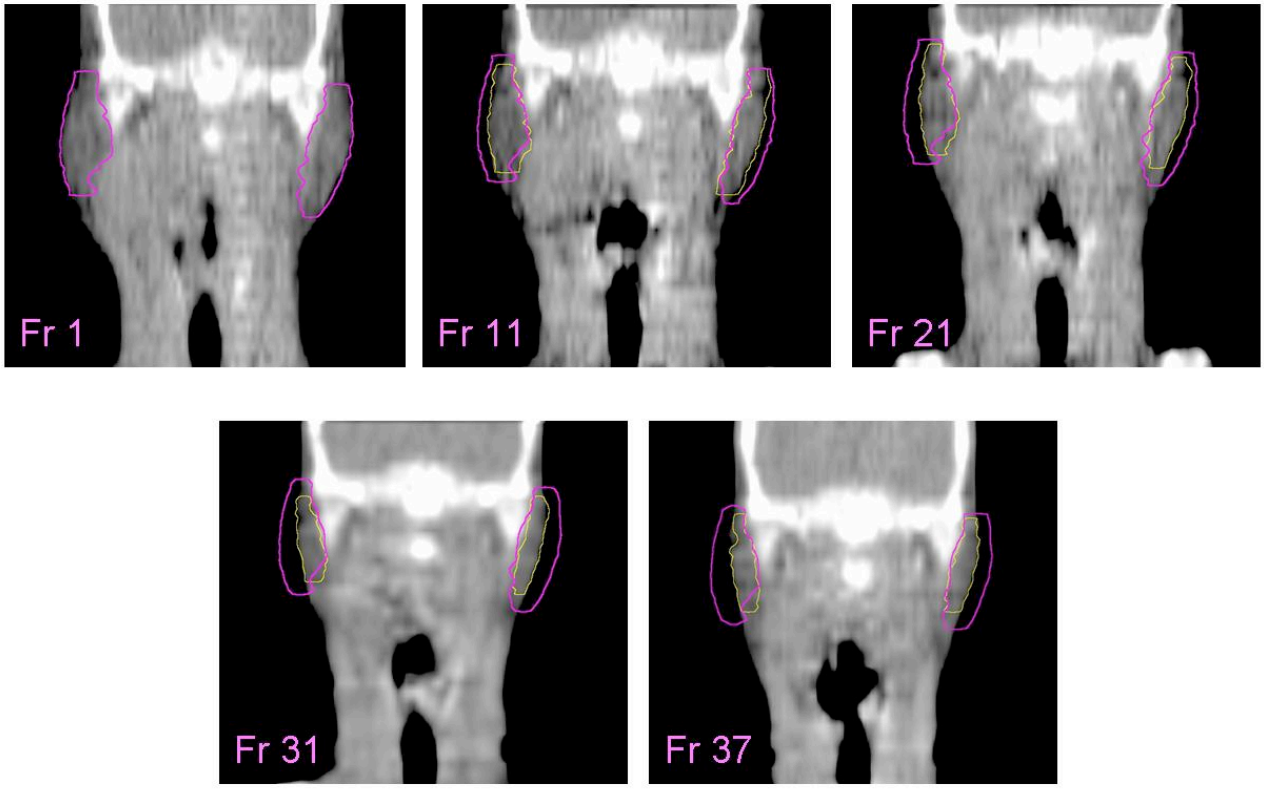

Figure 7.5: Coronal MVCT slices demonstrating the parotid shrinkage at the inferior portion over the treatment course. The initial volume is displayed in purple and the updated volume is in yellow. The fraction number is written on bottom left side of each image. Fr = fraction.

Barker et al. (2004) used the body weight loss to reflect the anatomic changes in the head and neck region by correlating the body weight to the skin volumes at C2 and skull base levels. The current study evaluated the volumetric change specifically in the neck region and the positional change of the cervical cord over the treatment period. Monitoring the neck volume should provide a better illustration on the weight loss particularly in the treatment region. Moreover, it could offer some clues in the lymph node shrinkage trend during radiotherapy. Figure 7.6 shows the alterations in the neck habitus throughout the treatment course in MVCT images. The neck volume decreased progressively over time and resulted in a significant drop at the end of the treatment course. The current study also found that the percentage neck volume reduction was highly correlated with the percentage parotid shrinkage as well as medial and superior shifting of the parotid glands. Similar finding was seen in Barker et al. (2004) study, which showed a close relationship between body weight loss and parotid medial displacement. Han et al. (2008) also showed the relative body weight loss was correlated with the relative parotid volume loss, although the relation was not strong in their study.

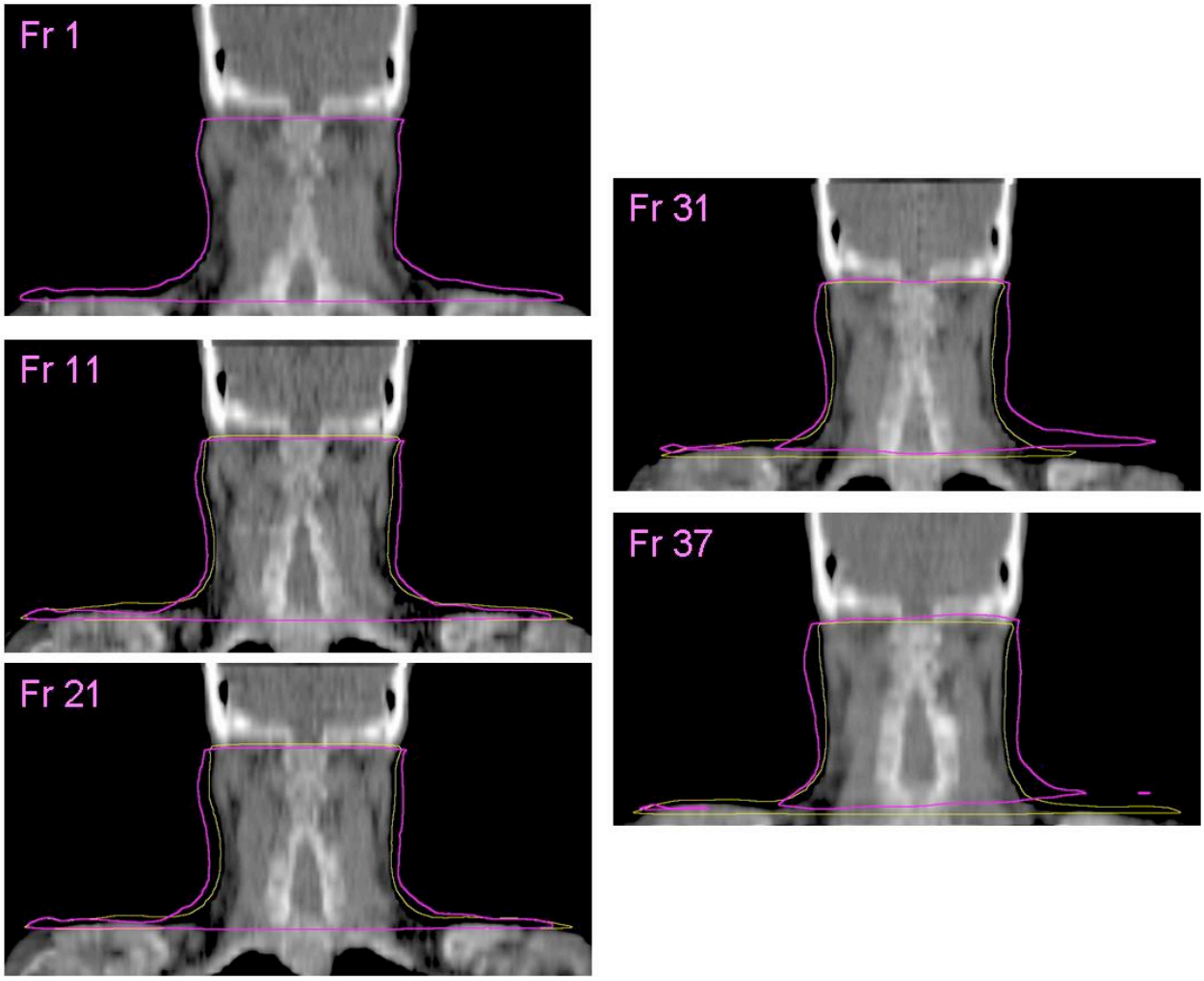

Figure 7.6: Coronal MVCT slices demonstrating the neck volume loss over the treatment course. The initial volume is displayed in purple and the updated volume is in yellow. The fraction number is written on upper left side of each image. Fr = fraction.

The reduction in the neck volume during treatment course obviously increased the risk of patient motion and mis-positioning inside the immobilization mask. Due to the loss of subcutaneous fat, patient frequently shifted backward which consequently led to cervical cord displacement as seen in the present study. The relatively insignificant cord displacement in the lateral aspect might be explained by the fact that during daily setup, the patients would always be aligned to the midline marked on the mask. This resulted in minimal shifting of the patients along this axis regardless of the volumetric change in the neck region. Nevertheless, the gradual decrease in the neck volume caused gradual displacement of the whole cervical spine towards the posterior aspect throughout the treatment course. In addition, differential changes were observed in the 3 monitored vertebral levels in the current study. The mean COM displacement was increased from the upper neck region (VC3) to the lower neck region (VC9). Consistent results were presented by Zhang et al. (2006) and Robar et al. (2007), in which both studies also demonstrated largest displacement in the lower neck region. These results implied that the geometric displacement of the cervical cord was non-rigid and therefore could not be completely corrected by couch offset even with IGRT approach. Replanning strategy was mandatory to adapt for these geometric changes.

In this study, significant correlations between various geometric parameters during the treatment course were being established and fitted with linear trends. These findings provided a more efficient way to estimate the underlying anatomic changes by using those easier-to-measure parameters as surrogates throughout the treatment course. For example, as the percentage parotid volume

loss was highly correlated with the percentage P-NP volume loss, monitoring the change in parotid volume could reveal the change in the P-NP volume. Because the percentage neck volume loss was closely related to the parotid medial and superior displacement, any significant changes in the neck volume could reflect a large parotid shift to these directions. As shown in the present study, the predicted loss in P-NP volume would be 3.70 % if 5 % reduction was seen in the parotid volume. When the neck volume decreased 5 %, a respective parotid shift of 0.13 cm and 0.10 cm to the medial and superior direction could be expected.

This study also investigated the potential predictive values of several pre/per-treatment parameters, which could be used to forecast the anatomic changes that might happen during the treatment course. The current study showed a negative correlation between the initial P-NP volume and its volume regression after the treatment course. Fang et al. (2001) also demonstrated that the initial primary tumor volume was negatively correlated to its regression rate, with the correlation coefficient highly consistent with the current study (-0.402 vs -0.4522 respectively). This gives a strong support to the phenomenon that large gross tumor tends to shrink slowly during the treatment course. In radiobiological aspect, the degree of tumor regression in response to irradiation basically depends on the net balance between the number of tumor cells growth, which affected by its proliferation kinetics and architecture, and the number of tumor cells being killed and absorbed. Therefore one possible explanation of the persistence of large tumor volume during or after radiotherapy may be due to the fact that the dead cells clearance in large tumors after irradiation is less efficient than that in small tumors (Fang et al., 2001). Fang et al. also showed that the

primary tumor regression rate was negatively correlated with the tumor stage but failed to correlate it with locoregional control or survival rates. These findings could not be verified in the present study but would worth an investigation in future. In addition, further studies on the relationship between the target dose and the tumor regression rate are also encouraged. The results of these prospective studies can give implication on whether altered dose scheme according to the degree of tumor shrinkage at the time of replanning will further improve the treatment outcome for NPC patients. The current study correlated the initial parotid volume to its volume reduction at the end of the treatment course, which suggested that large parotid glands tended to regress rapidly over time. Similar finding was seen in Broggi et al. (2010) study, in which multivariate analysis was conducted to define the possible predictors of parotid shrinkage during head and neck radiotherapy. They showed the parotid volume loss at treatment end was correlated with its initial volume as well as its planned mean dose. The relationship between the volume reduction of the parotid glands and their planned mean doses was also demonstrated in other papers (Vasquez Osorio et al., 2008 ; Wang et al., 2009), although such details were not investigated in the current study.

7.3 Optimum ART strategy for NPC cases

Capelle et al. (2012) pointed out that NPC patients should be targeted for routine adaptive replanning, as the large anatomic changes demonstrated in this group of patients derived greatest benefits from plan adaptation among all head and neck cancers. Based on the characteristic anatomic changes discussed in the previous sections, the current study established an ART strategy exclusively for NPC cases with three replans were proposed at 9^{th}, 19^{th} and 29^{th} fractions. Similar to the existing radiation protocol, multiple replannings in between the treatment course were deemed necessary. However, current study indicated 3 replannings that performed in earlier stage of the treatment course would be more beneficial in terms of accounting for the early anatomic response to treatment. The existing three-phase radiation protocol adopted in clinical practice was proved to give dosimetric advantages to NPC patients. Nevertheless, this protocol is merely set by oncologist based on clinical experience, therefore the designation of the frequency and time for replanning are rather subjective. In this study, an objective approach was used to define the ART strategy for NPC cases. Thresholds indicating significant anatomic changes and thus the needs of plan modification were spotted out for each selected parameters using statistical analysis. The ultimate ART strategy was established under practical consideration including efficiency and efficacy in clinical environment. The proposed replanning strategy i.e. replans at 9^{th}, 19^{th} and 29^{th} fractions is considered optimal, which allows rectification of the potential overdose to the critical organs due to substantial anatomic deformations. Moreover, replanning using appropriate schedule also guarantees a prompt reaction to the shrunk tumor

by conforming the dose straightly to the targets, thus providing opportunities for safe dose escalation without jeopardizing the surrounding OARs. All these should lead to an overall improvement in dosimetric and in turn clinical outcomes in NPC cases.

ART in interval basis is feasible in NPC cases because the organ changes, as shown in this study, follow progressive trends. The proposed ART strategy provides further dosimetric improvement on top of IGRT with acceptable increase of departmental workload and overheads. As the exact fractions for plan modification are already defined, the process of rescanning patient, recontouring structures and replanning will be repeated only 3 times within the whole treatment course. This is clinically feasible and also greatly reduces the needs of clinical resources e.g. machine occupancy and tedious workload that is added to the oncologists, physicists and dosimetrists when compared to daily adaptive approach. On the other hand, for centres without in-room CT facilities, the implementation of ART can be difficult because the patient anatomic changes during the treatment course cannot be effectively monitored. The proposed replanning strategy provides a standard guideline to these centres so that ART can be adopted easily to improve the dosimetric outcome to NPC patients. Although this study was conducted in the tomotherapy unit, the ART strategy can also be applied in NPC cases that treated with other LINACs.

Establishment of an optimum ART strategy in NPC cases is crucial because the timing to initiate a replan can greatly affects the efficiency of the ART process. If the plan modification is conducted too early (e.g. at 3rd fraction), probably no

apparent dosimetric benefits will be seen as the anatomic changes are still minimal but the manpower as well as clinical resources for replanning are wasted. If the plan modification is conducted in a very late stage of the treatment course (e.g. at 35th fraction), irreversible dose changes may result because the chance to accommodate the anatomic changes that appear in the mid-treatment course is missed. This study defined the proper timing for the initiation of ART procedure during a NPC treatment course. Replannings at these selected time points should maximize the benefits of ART application in NPC cases.

Wu et al. (2009) assessed the efficiency of different ART strategies by applying the single mid-course replanning, alternate week replanning (2 replans) and weekly replanning (6 replans) to 11 patients during head and neck IMRT. They concluded that significant dosimetric improvement could be achieved by increasing the replanning frequency from 1 to 2, but not from 2 to 6. Moreover, it was not recommended to conduct replanning more than once a week. These were consistent with the findings in the current study, which also emphasized the necessity of multiple replannings (i.e. > 1) with the suggestion of 3 plan modifications throughout the treatment course. Wu et al. additionally stated that rapid adaptation by using the new plan within the same week would further improve the dosimetric results. Schwartz et al. (2012) performed a study to deploy the ART procedure for 22 oropharyngeal cancer patients. The anatomic changes were assessed by the daily CT images which were used for setup verification. The replanning process was instigated whenever there were significant changes in anatomy which resulted in geographical miss in target or inadequate sparing of OARs during dose recalculation on the daily CT images.

In this study, all patients required one replan and the median trigger point was the 16th fraction. At the time of the first replanning, the bilateral parotid volumes and the CTV had shrunk by 16 % and 5 % respectively. Eight patients required two replans with the median trigger points at 11th and 22nd fractions respectively. At the time of the second replanning, the bilateral parotid volumes and the CTV had a respective decrease of 24 % and 14 %. Dosimetric comparison between replanning and without replanning showed a reduction in the mean doses of parotid glands by plan adaptation, with 2.8–3.9 % decrease in mean doses for one replanning and 3.8–9 % decrease for two replannings. This in turn facilitated post-treatment parotid functional recovery. Jensen et al. (2012) also reported their experience in implementing adaptive strategy in head and neck cancers. Weekly in-room CT scan for verifying the treatment position was used for replanning if unsatisfactory target volume and OAR position (deviation ≧ 1 cm) was noted in at least 3 representative slices (base of skull, C3 and supraclavicular fossa). In their study, 15 out of 72 patients required plan modification during the treatment course and the number of replanning ranged from 1–3. However, the exact time for replanning was not reported. This study also demonstrated that the adaptive planning process provided improvement in target coverage with decreased parotid doses over the non-adaptive plans, which resulted in reduction of xerostomia during patient's follow-up. Zhao et al. (2011) conducted an ART study on 33 NPC cases. The rescanning and replanning processes were applied to these patients because significant anatomic changes were noticed by inspection, palpation and/or direct endoscopy during the radiotherapy course. The adaptive procedure was triggered after an average of 15 fractions. In particular, 9 patients required a third CT scan and a second replan

after another 12 fractions. Other than the dosimetric benefits of ART strategy that had been well-reported in other papers, this study also showed comparable clinical results between replanning and without replanning in terms of survival rate.

The studies of Schwartz et al. (2012), Jensen et al. (2012) and Zhao et al. (2011) demonstrated a patient-specific way for implementing ART in interval basis. Instead of applying a standard protocol, individualized replanning schedule was tailor made for each patient according to his/her own changes in anatomy during treatment. The process of replanning was initiated once the significant change was being observed. This approach heavily depends on clinical judgment on the definition of "significant change", which can be varied among different centres and even among different oncologists. Moreover, the implementation of such strategy requires continuous monitoring of the organ changes throughout the treatment course, and the frequency and timing for plan modification is unpredictable. This certainly increases departmental burdens such as difficulties in the allocation of manpower. In contrast, the present study demonstrates a simpler way of ART implementation. By recognizing the trends of different organ changes in advance, the proposed replanning schedule can be applied in any centres for NPC cases, knowing that the unfavorable changes will always be adequately encountered even without the use of daily image guidance. On top of this, the pre/per-treatment predictors defined in this study provide additional information for the refinement of ART strategy in future. As suggested, tumors exceeding certain volume would have smaller volume loss and in turn smaller dose variation throughout the treatment course, therefore may require less

rigorous replanning strategy than for small tumors. Similarly, more plan modifications in between the treatment course may be needed for parotid glands larger than certain volume, thus to overcome the frequent dose changes due to rapid shrinkage. The planned mean doses of the parotid glands may also serve as an indicator for the determination of the replanning schedule. In general, these predictors can assist in classifying patients with high risk of significant anatomic and in turn dosimetric deviation during the treatment course. The proposed adaptive strategy may therefore be refined for specific groups of patients.

7.4 Recent development in ART

7.4.1 ART with dose correction

ART with dose correction is of great interest to the researchers recently, in which the plan adaptation is performed to compensate the changes in both anatomy and delivered dose. In general, the actual doses to various structures are determined daily by dose recalculation or dose reconstruction using the verification CT image set. For dose recalculation, the actual dose distribution is generated by applying the planned dose fluence to the daily CT images. For dose reconstruction, exit dosimetry recorded by the CT detector during treatment delivery is converted into delivered dose fluence and projected to the daily CT images to generate the actual dose distribution (Kapatoes et al., 2001; Langen et al., 2005; Mackie et al., 2003a; Ruchala et al., 2000). The daily delivered doses computed in either way are then summed up in a particular treatment period for dose evaluation. Any deviation in the cumulative dose e.g. under/overdose to the

targets and overdose to the OARs is being remedied in the new plan generated for subsequent fractions. Using this approach, the total dose delivered in the whole treatment course can resemble the initially planned one. It should however be noted that severe dose deviation in treatment is difficult to be corrected in one single subsequent fraction (Wu et al., 2002), which means that a too late replan can still lead to irreversible dosimetric effect. This again emphasizes the need of defining a properly timed ART strategy.

There are several prerequisites for successful deployment of ART with dose correction. First of all, in-room CT facilities are nearly a must for convenient acquisition of daily CT image set. Therefore, the quality of the CT images from the in-room CT scanners should provide sufficient anatomic details for accurate target and OAR delineation. This requirement is crucial because it is rather a fault than a merit to apply ART if uncertainties in contouring exist. kVCBCT and MVCT are the most common in-room CT modalities for IGRT in Hong Kong. However, both systems give relatively poorer soft tissue contrast in their images when compared to the conventional CT scanner (Meyer, 2007). This certainly affects their sensitivity in detecting the tumor extent. Although the parotid glands could be contoured with confidence, the current study demonstrated the inability of defining the true gross tumor and the lymph nodes precisely in the MVCT images of NPC cases. Similar problem was also seen in Loo et al. (2011) study, which also demonstrated uncertainties during tumor delineation on the MVCT scans. The blurring of the soft tissue boundaries especially in those between tumor and normal tissues can affect the clinical judgment on the definition of the OARs and target volumes, which in turn result

in wrong evaluation of their actual receiving doses and specification of remedied doses in the new plan. Efforts have been put on increasing the image quality of these in-room imaging tools so as to facilitate the clinical implementation of ART with dose correction. For example, the soft tissue contrast of the kVCBCT images can be improved by adding anti-scatter grid (Siewerdsen et al., 2004) or shaping filters e.g. bowtie filters (Graham et al., 2007; Mail et al., 2009) to reduce the scatters at the x-ray detector. For the TomoTherapy System (TomoTherapy Inc.), it recently provides a post-processing function of "TomoImage Filter" to help reducing the noise thereby increasing the image quality.

Another important issue is the accuracy of the CT number of kVCBCT and MVCT images, as a reliable CT number to electron density calibration curve is essential for precise dose recalculation/reconstruction and subsequent replanning process in ART. Numerous studies verified the CT number accuracy and stability in MVCT images (Kapatoes et al., 2001; Langen et al., 2005; Meeks et al., 2005). In particular, Langen et al. (2005) presented a phantom study and demonstrated the accuracy of dose calculation using MVCT images was similar to that using conventional CT images, suggesting reliable dose distribution can be obtained using the MVCT image set. For kVCBCT, scatter component in the images can cause CT number calibration problem thus introduce dose recalculation/reconstruction errors (Meyer, 2007). Nonetheless, studies showed that using bowtie filters could reduce the scatter and greatly improve the result (Ding et al., 2007; Mail et al., 2009). When compared the DVHs based on bowtie filtered kVCBCT and conventional CT images, the dosimetric difference

was clinically insignificant (< 3 %) for head and neck cases (Ding et al., 2007). Another phantom study (Mail et al., 2009) also demonstrated the application of bowtie filter on the kVCBCT images allowed almost 100 % CT number recovery at periphery.

Although the concept of ART with dose correction is inspiring, it remains to be an extremely time-consuming process due to repeat daily contouring and dose computation. Moreover, since the patient anatomy changes progressively during the treatment course, image registration with rigid fusion techniques may be insufficient for precise matching. This possesses errors in the alignment of the deformed targets and OARs, hence leads to inaccuracies in the calculation of cumulative doses in these structures. These concerns give rise to the introduction of deformable registration algorithms.

7.4.2 Deformable image registration

Basically, deformable registration is done by defining a voxel-to-voxel map between two CT image sets. In ART setting, this allows the voxel points in the planning image to be linked to their corresponding voxel points in daily/per-treatment images. The deformable registration algorithm can be used to transform the original structures in the planning image into the deformed structures in the subsequent images, thus allowing automatic delineation of targets and OARs. With the same deformation map, proper dose accumulation can also be achieved for treatment evaluation. The common way for deformable dose accumulation is to first deform the daily delivered dose to the planning CT

and then followed by the accumulation of these deformed delivered doses. In this way, the dose received by each voxel point can be integrated among all daily image sets for cumulative dose evaluation. These automated processes potentially reduce human interaction and thus greatly enhance the capability of implementing ART in routine care. Studies had been performed to test the validity of various registration algorithms (Castadot et al., 2008; Tsuji et al., 2010; Vasquez Osorio et al., 2008; Wang et al., 2005; Zhang et al., 2007). Some of them are discussed as follows.

Zhang et al. (2007) adopted a fast variational-based deformable image registration algorithm for atlas-based auto-segmentation in daily head and neck CT images. The planning image set with primary contours was used as the atlas for automatic propagation of contours in the subsequent daily images. Dice similarity index (DSI) that indicates the overlapping ratio between the reference contours and the test contours was used for evaluation, in which perfect match gives the DSI value of 1. In this study, the automatically generated contours for OARs were found to be consistent with the corresponding manually drawn contours in the daily images. The DSI for most OARs reached ~0.8. Nevertheless, the auto-segmented GTV was only visually inspected by the physician for validation but not quantitatively compared with the manually drawn contours. Castadot et al. (2008) examined 12 different deformable registration strategies using the images from head and neck cancer patients. The planning CT images were registered to the per-treatment CT acquired after an average of 36.8 Gy being delivered. They found that all deformable registration methods had significantly higher DSI when compared to rigid registration

technique. However, they also noticed the registration results could be deteriorated in several regions. When there were 1) only a small difference in the intensity gradient between organ boundaries e.g. thyroid gland; 2) a lack of significant features of a structure e.g. CTV; 3) a variability in the concentration of contrast medium inside an organ between the 2 CT scans e.g. veins; and 4) a thin structure e.g. hyoid bone in the images, the registration process could be affected with significant mismatch. Tsuji et al. (2010) used an alternative way to assess the automatically deformed contours in 16 head and neck cases. With the use of the mid-treatment CT image set, dosimetric comparison was made between the adaptive plan that was generated using the manual contours and the one generated using the automatic contours. It was found that the automatic contours were generally smaller than the manually delineated one, and the GTV from the 2 approaches were significantly different with lowest DSI among all contoured structures. Moreover, the adaptive plan with automatic contours had a significantly lower mean coverage of the GTV and CTV. Nevertheless, dosimetric parameters for the critical organs were generally consistent between the two approaches. The authors therefore concluded that auto-segmentation for ART could be applied to normal structures with confidence but might induce dosimetric errors for target volumes.

Quantitative evaluation of the accuracy of the auto-segmented target volumes is difficult. As the manually delineated targets are prone to contour subjectivity (Hong et al., 2004; Zhang et al., 2007), they may not serve as the gold standard for comparison. As shown in many studies, automatic segmentation by deformable registration is not robust enough for target delineation (Castadot et

al., 2008; Tsuji et al., 2010; Zhang et al., 2007). Moreover, the deformed target contours may exclude the tumor cells that are below radiographic detection threshold (Wu et al., 2009). Under this circumstance, the use of auto-segmented targets should be taken with caution. It is important for the oncologist and radiotherapist to perform a thorough slice-by-slice checking of the automatically generated contours before proceeding to the next steps of dose evaluation as well as subsequent replanning. Nonetheless, the deformable registration techniques will allow rapid segmentation of various structures with considerable reduction in human effort if properly used. Some studies also suggested that the auto-contouring approach using deformable registration could decrease the interobserver variability in target delineation. Chao et al. (2007) investigated the interobserver difference in delineating the CTVs with or without the use of non-rigid registration in 2 head and neck cases. They found that the variation in the CTVs that manually drawn by 8 oncologists was huge. However, when the CTVs were first auto-segmented based on the template contours deformed by the computer-assisted target volume delineation system and then modified by the oncologists, the variation was significantly reduced with improved geometric consistency. The average time saved when using the automatic-modification approach was 26–47 %. Similar results were seen in Stapleford et al. (2010) study on 5 head and neck cases. When comparing the differences between the contours of the lymph node CTVs that manually drawn or automatic-modified by 5 oncologists, the automatic-modified group was found to be more consistent with noticeable reduction in the range of contour volume and the percent false-positivity. The time for contouring was also reduced 35 % in average. Semi-automation is a desirable approach for structure delineation in ART

process, because it allows involvement of human checking while potentially reduces interobserver errors, hence increases contour efficiency without losing accuracy.

The performance of the deformable image registration highly depends on the quality of the image set being used. It is known that the presence of metal artifacts such as dental fillings can lead to localized mis-registration result (Lu et al., 2006; Zhang et al., 2007). For kVCBCT and MVCT images, their image qualities are inferior to that of the conventional CT images. In addition, their voxel intensities are different from the conventional one. All these may induce errors in relating the voxel points between these in-room CT images and the planning CT images, which consequently invalidates the deformable registration result. Specific deformable algorithm or conventional image preprocessing techniques may be used to increase the registration accuracy (Lu et al., 2006; Nithiananthan et al., 2011; Paquin, Levy, & Xing, 2009; Yang et al., 2009). Nithiananthan et al. (2011) developed an advanced deformation algorithm for registering the conventional CT to the kVCBCT. Iterative voxel intensity matching between the 2 images was done simultaneously during the deformable registration process to increase the registration accuracy. The robustness of this registration method had been thoroughly tested with the presence of various imaging defect e.g. scatter and object truncation as well as in 6 real cases, suggesting its validity in clinical use. Lu et al. (2006) applied an "edge-preserving smoothing" technique to the MVCT images prior to the deformable registration process. This technique could reduce the noise level while maintaining the contrast resolution in the MVCT images for subsequent

registration. The combined use of the "edge-preserving smoothing" technique with the deformable registration was validated by the similarity measures as well as visual inspection of the automatically deformed contours by oncologists. In addition, this study also demonstrated the feasibility of deformable dose accumulation among the daily MVCT images. Nevertheless, the authors emphasized that the accumulated dose could only be used as an approximation of the treatment outcome.

With proper validation, some studies applied deformable registration algorithm for ART implementation. O'Daniel et al. (2007) used in-house deformable registration software to quantify the differences between planned and delivered parotid gland and target doses in head and neck cancer patients. The daily dose distribution calculated using the in-room CT scans was mapped to the planning CT for cumulative delivered dose evaluation. Wu et al. (2009) used the deformable registration algorithm proposed by Zhang et al. (2007) between the planning CT and the 6 weekly CTs for contour propagation and dose accumulation in order to study efficiency of different ART strategy in 11 head and neck cases. Note that in their study, only the auto-segmented PTV instead of the GTV was used for replanning. In Schwartz et al. (2012) study, an in-house deformable registration algorithm was used to transform the baseline contours from the planning CT to the daily CT for dose recalculation and ART replanning in oropharyngeal cancer patients. They showed that the entire registration process only took seconds, but formal reviews of the transformed structures by oncologist should be done afterwards.

Deformable registration algorithm is absolutely essential for ART deployment, its application of auto-segmentation of the target and OARs provides basis for rapid checking on the anatomic changes throughout the treatment course. Together with its dose accumulating function, treatment evaluation in terms of dose conformity can be performed, which helps the oncologist to decide whether replanning should be initiated in between the treatment course. Though encouraging results have been reported, development in this technique is needed to improve the accuracy and robustness of the registration algorithms especially in multimodality image registration and dose accumulation. Continual studies should be conducted before the technique can be accepted as standard clinical practice.

7.4.3 Adaptive treatment plan generation

It is suggested that the dosimetric benefits will be further increased if the ART process can be completed and the new adaptive plan can be applied within the same week (Wu et al., 2009). Indeed, the time period between the CT acquisition and the plan adaptation should be as short as possible such that the dosimetric consequences due to the changes in anatomy can be corrected on time. On the other hand, rapid replanning is also a prerequisite for the implementation of daily online ART. Therefore, investigations have been focused on finding a practical way for rapid plan generation. Jensen et al. (2012) and Schwartz et al. (2012) applied a forward reoptimization method for fast replanning. Instead of full reoptimization, the treatment parameters as well as the optimization constraints of the initial plan were transferred to the per-treatment CT images as a starting

point of the optimization of the new plan. Refinement of the planning constraints could be made according to the actual contours. Jensen et al. demonstrated that the whole replanning process could be completed within 2 hours, thus avoiding the treatment break that might be needed in full reopimzation approach. Mohan et al. (2005) suggested a plan modification method of deforming the fluence map of each beam based on the deformed contours as seen in the field aperture, such that the doses to various structures in the new plan computed by newly deformed fluence map was the same as (or close to) the original treatment plan. Preliminary application on a head and neck case and a prostate case showed encouraging results, but technical issues such as the problem of organs moving out of the field due to significant geometric changes still remain unaddressed. Ahunbay et al. (2009) reported a similar approach as Mohan et al., with an additional step of putting the newly deformed fluence map into a segment weight optimization package for plan reoptimization. This two-steps algorithm had been tested in head and neck IMRT cases with equivalent plan quality to the original plan and the replanning process only take 5–8 minutes. With the continuous development in the fast reopitimization algorithm, immediate plan adaptation during the treatment course will become feasible which allows prompt reaction to the anatomic as well as possible dose deviation with minimal increase in workload.

7.4.4 TomoTherapy Planned Adaptive software

Recently, TomoTherapy System (TomoTherapy Inc.) has equipped with Planned Adaptive software for ART implementation using daily MVCT images. As the MVCT image set usually only covers the treatment volume, merged CT is generated by substituting the daily MVCT images into the corresponding portion of the planning CT (Figure 7.7). CT number to election density tables for both the kVCT and the MVCT are imported to the system for precise daily dose recalculation. After the targets and OARs are being delineated, daily dose distribution (verification dose) is computed by applying the original treatment plan in the merged CT images. Dosimetric comparison of various contoured structures can be done by displaying both the planned and verification dose curves on the daily DVH. Moreover, this software allows accumulation of the daily dose distribution (summation dose) by rigid registration, enabling the evaluation of the impact of the anatomic changes on delivered dose. Figure 7.8 shows the cumulative DVH of a NPC case, in which the daily doses calculated in 20^{th}, 25^{th}, 30^{th}, and 35^{th} fractions are summed for evaluation. It is shown that the summation doses for the target volumes closely match the planned doses, but significant increase in the parotid summation doses is observed. Adaptive replanning can then be initiated by converting the hot spots (cold spots as well) as seen in the CT image into a region-of-interest and applying specific constraint in the new plan for dose compensation.

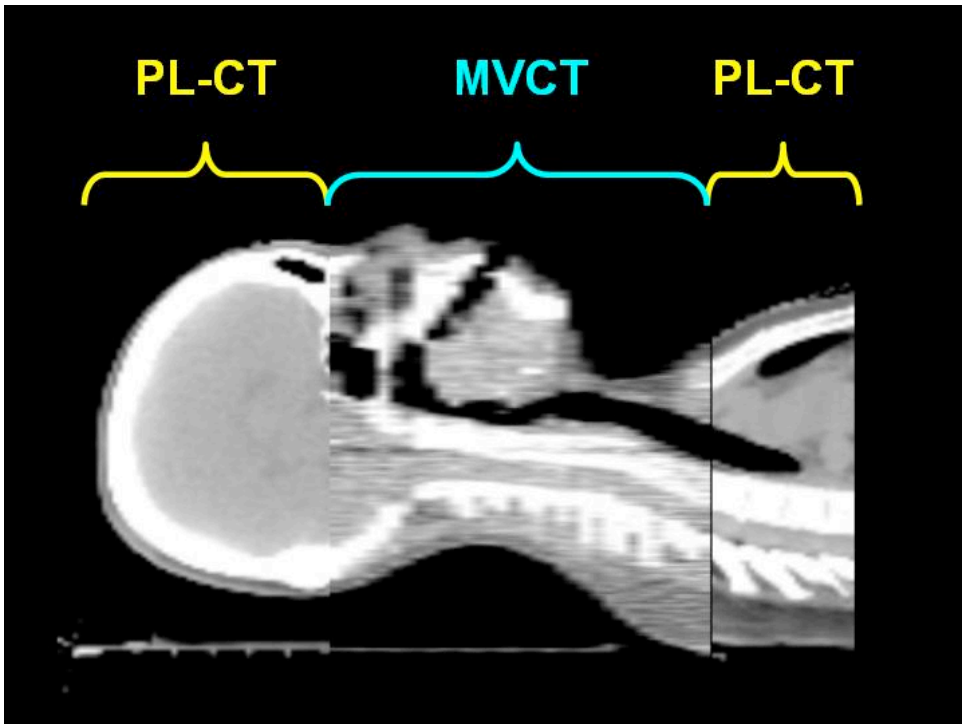

Figure 7.7: Merged CT image set of a NPC case generated by the TomoTherapy Planned Adaptive software (TomoTherapy Inc.).PL-CT = planning CT.

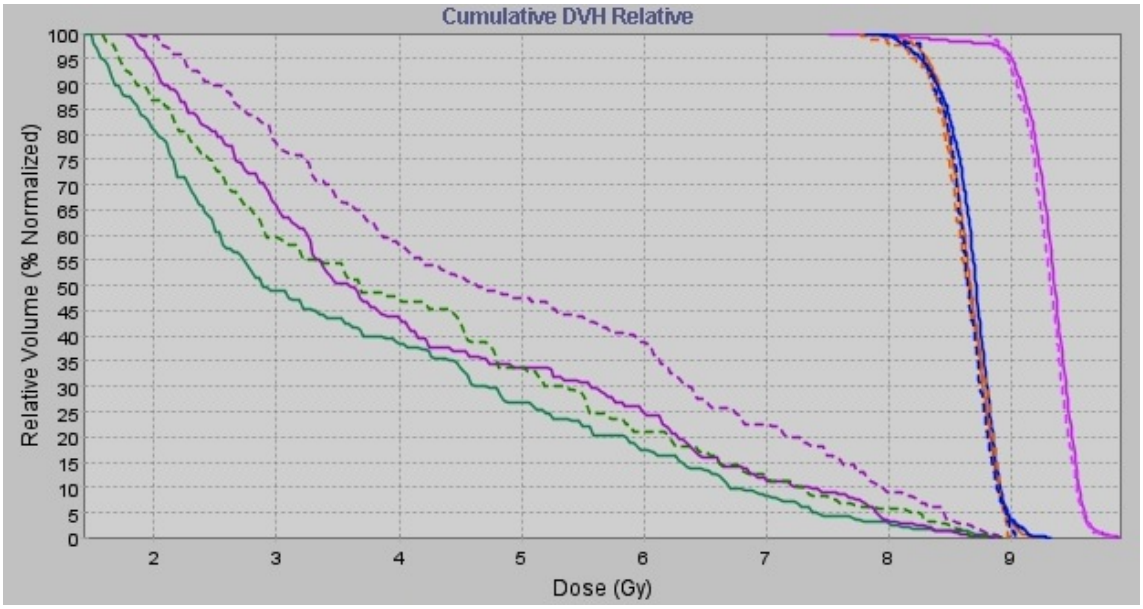

Figure 7.8: Cumulative DVH of a NPC case generated by the TomoTherapy Planned Adaptive software (TomoTherapy Inc.). The cumulative doses of NP-GTV (magent), LLN-GTV (orange), RLN-GTV (blue), left parotid gland (green) and right parotid gland (purple) are summed from 20th, 25th, 30th, and 35th fractions. The summation doses (dashed) and the planned doses (solid) are both displayed for treatment evaluation.

Though this feature sounds fascinating, one major drawback is the lack of deformable image registration algorithm built in to the Planned Adaptive software. As discussed, accumulated dose calculation of the deformed contours based on rigid image registration may induce errors. Therefore, the summation doses generated by the software may not accurately reflect the doses received by the organs. Moreover, manual contouring becomes a laborious task without computer aid. Temporary solution is to manually apply the existing deformable registration algorithm for auto-segmentation prior to daily dose calculation and for dose accumulation after the daily delivered dose being generated by the Planned Adaptive software. Lee et al. (2008b) employed the Planned Adaptive software in addition to the deformable registration algorithm developed by Lu et al. (2006) to evaluate the daily and cumulative dose changes in parotid glands with the use of daily MVCT in head and neck radiotherapy. Similar procedures were performed in 4 leukemia patients treated with total body irradiation using tomotherapy (Chao et al., 2012). The accumulated dose computation was accomplished with the use of deformable registration for total delivered dose verification. Regardless of this defect, the Planned Adaptive software is still a valuable tool for assessing the daily anatomic changes as well as daily dose variation throughout the treatment course (Han et al., 2008; Woodford et al., 2007). The summation dose generated by the software can provide a preliminary assessment of the overall dosimetric impact. Development of this feature is ongoing, new version with built in deformable algorithm is believed to be commercially available in near future.

7.5 Limitations and further studies

There were some limitations of this study that require future investigation. The formula for HI calculation employed in this study was most commonly used in other papers during the data analysis period. Recently, ICRU has suggested an updated formula for the calculation of HI (ICRU, 2010). Nevertheless, both approaches should be able to demonstrate the differences in target homogeneity between replanning and without replanning. On the other hand, as no deformable image registration software was available during the research period, the possible treatment outcome throughout the whole radiotherapy course could only be illustrated by simple summation of the endpoint doses in all three phases. Therefore, one should be reminded that the total endpoint doses shown in this study were only the best estimation of the possible treatment outcome when no replan or two replans was employed. These dose parameters could only be served as a reference but should not be treated as the actual total doses received by those structures at the end of the treatment course. Nevertheless, summation of the maximum doses in OARs demonstrated the worst scenario where the maximum dose points on the 3 CTs overlapped. Prospective study will be conducted to obtain solid conclusion when deformable image registration software is available in the department. Although this study clearly demonstrated the dosimetric benefits of applying ART in NPC cases, its effects on local control and survival rate as well as patient QOL did not quantitatively analyzed. Study can be performed to further relate the dosimetric results to the clinical outcomes with or without ART in the future.

Differentiation of subtle soft tissue contrast is difficult in MVCT due to the relatively low contrast resolution in the image sets. This hindered the accurate delineation of the gross tumors in the nasopharyngeal and the nodal regions as well as the spinal cord in this study. In views of the superb image contrast between the tissue/air and the tissue/bone, the posterolateral wall of nasopharynx and the vertebral canal were therefore selected as the surrogates for monitoring the anatomic changes in the primary gross tumor and the spinal cord respectively in the MVCT image sets in order to minimize the intraobserver variability. Nonetheless, the evaluation of the nodal changes had to be excluded in this study as there was no appropriate surrogate for the lymph node gross tumors in the MVCT images. Techniques for improving the contrast resolution in MVCT images are rapidly evolving, in which precise target delineation in these images will be soon achieved. Together with the use of the Planned Adaptive software provided by the TomoTherapy system (TomoTherapy Inc.), studies can be conducted on evaluating the actual daily dose-volume correlation of various structures in concerns. Furthermore, assessment on the feasibility of implementing ART in NPC cases with dose correction is suggested in coming future when the Planned Adaptive software is equipped with deformable registration. On the other hand, the need of refining the current proposing ART strategy based on the pre/per-treatment predictors found in this study can be investigated by sorting the patient samples into subgroups e.g. initial tumor volume and clinical staging for dosimetric evaluation when sample sizes increase.

CHAPTER EIGHT

SUMMARY OF MAJOR FINDINGS AND CONCLUSION

In the present study, the importance of implementing ART strategy in NPC cases was demonstrated. The application of the three-phase radiotherapy protocol in NPC cases using tomotherapy showed pronounced dosimetric benefits on normal tissue sparing while keeping the satisfactory target dose coverage. Without adaptive measures, the doses to all OARs were significantly increased due to the tumor shrinkage. Moreover, the critical organs such as brainstem, spinal cord and optic chiasm would have their total doses exceeding tolerance if only one single plan was used for the whole course of treatment. This certainly increased patient's risk of developing irreversible radiation complications like central nervous system deficits, myelopathy and optic neuropathy. By restoring the target dose conformity with replannings, the doses to the OARs and thus the complication risks were significantly reduced. The sparing of the OARs also allowed safe target dose escalation with increased local disease control in NPC cases.

The results of the current study also emphasized the need of multiple replannings throughout the NPC treatment course to account for the anatomic variation that would lead to dosimetric consequences. In order to optimize the dates for replannings, the characteristic anatomic changes of various structures in NPC cases over the treatment course were quantified using the daily MVCT image

sets. It was showed that the P-NP which represented the gross tumor in nasopharyngeal region had significant volume loss over the treatment course. Nevertheless, the shrinkage was asymmetric with an unpredictable regression trend. In contrast, the parotid glands demonstrated a systematic volume reduction, and they tended to shift to the medial and superior aspects throughout the radiotherapy course. The neck volume also decreased progressively, and the loss of the subcutaneous fat led to the non-rigid backward displacement of the cervical cord during the treatment.

By analyzing the characteristic trends of organ changes in NPC cases, this study developed an optimum ART strategy specifically for NPC cases. This was done by setting thresholds that indicated significant anatomic changes thus the need of plan modification in between the treatment course. Three replans at 9^{th}, 19^{th} and 29^{th} treatment fractions were proposed, which could optimally react to the anatomic deformations and in turn cease the potential dosimetric consequences. Moreover, replanning in between the treatment course allowed safe dose escalation to the shrunk target without jeopardizing the surrounding OARs. All these should lead to an improvement in the dosimetric as well as clinical outcomes on NPC patients. The proposed ART strategy in NPC cases is clinically feasible as the process is only repeated 3 times, the increase of departmental workload is relatively less when compared to daily adaptive approach. With fixed replan schedule, the manpower allocation and machine occupancy can be prearranged. It is predicted that 80 % additional clinical resources will be needed for the implementation of the proposed ART strategy. This proposed ART strategy also provides a simple guideline for those centres

without in-room imaging modalities to adopt ART for NPC patients as clinical routine.

ART is definitely an important advancement in radiotherapy field which deserves further development. Image guidance radiation technique allows close monitoring of the organ anatomic changes. This provides opportunities to revise the treatment plan according to these changes. Nevertheless, the extra time consumed, related overheads, maintenance and manpower upon implementation should be considered. Although ART with dose correction is recently being introduced, the technical requirement of in-room imaging systems and sophisticated softwares such as deformable registration and fast reoptimization algorithms to generate and process the vast data (both image and dose) collected everyday temporarily hinder its wide application in practice. Efforts have to be put on improving the robustness and efficiency in the image acquisition and registration as well as dose calculation and accumulation processes in the coming years before ART with dose correction can be comprehensively implemented. Meanwhile, the presented optimum ART strategy for NPC cases would be a suitable alternative to effectively account for the anatomic changes throughout the radiotherapy course and clinically feasible, which should bring about improvement in dosimetric and clinical outcomes.

REFERENCES

Agha, A., Sherlock, M., Brennan, S., O'Connor, S. A., O'Sullivan, E., Rogers, B., Faul, C., Rawluk, D., Tormey, W., & Thompson, C. J. (2005). Hypothalamic-pituitary dysfunction after irradiation of nonpituitary brain tumors in adults. *J Clin Endocrinol Metab, 90*(12), 6355–6360.

Ahunbay, E. E., Peng, C., Godley, A., Schultz, C., & Li, X. A. (2009). An on-line replanning method for head and neck adaptive radiotherapy. *Med Phys, 36*(10), 4776–4790.

Ang K. K., & Garden, A. S. (2006). Nasopharynx. In K. K. Ang & A. S. Garden (Eds.), *Radiotherapy for head and neck cancers: indications and techniques* (pp. 76–87). Philadelphia: Lippincott Williams & Wilkins.

Barker, J. L., Garden, A. S., Ang, K. K., O'Daniel, J. C., Wang, H., Court, L. E., Morrison, W. H., Rosenthal, D. I., Chao, K. S. C., Tucker, S. L., Mohan, R., & Dong, L. (2004). Quantification of volumetric and geometric changes occurring during fractionated radiotherapy for head-and-neck cancer using an integrated CT/linear accelerator system. *Int J Radiat Oncol Biol Phys, 59*(4), 960–970.

Beyzadeoglu, M., Ozyigit, G., & Ebruli, C. (2010). Rabiobiology. In M. Beyzadeoglu, G. Ozyigit, & C. Ebruli (Eds.), *Basic radiation oncology* (pp. 119–124). Berlin: Springer.

Blanco, A. I., Chao, K. S. C., El Naqa, I., Franklin, G. E., Zakarian, K., Vicic, M., & Deasy, J. O. (2005). Dose-volume modeling of salivary function in patients with head-and-neck cancer receiving radiotherapy. *Int J Radiat Oncol Biol Phys, 62*(4), 1055–106

Borst, G. R., Sonke, J. J., Betgen, A., Remeijer, P., van Herk, M. & Lebesque, J. V. (2007). Kilo-voltage cone-beam computed tomography setup measurements for lung cancer patients; first clinical results and comparison with electronic portal-imaging device. *Int J Radiat Oncol Biol Phys, 68*(2), 555–561.

Broggi, S., Fiorino, C., Dell'Oca, I., Dinapoli, N., Paiusco, M., Muraglia, A., Maggiulli, E., Ricchetti, F., Valentini, V., Sanguineti, G., Cattaneo, G. M., Muzio, N. D., & Calandrino, R. (2010). A two-variable linear model of parotid shrinkage during IMRT for head and neck cancer. *Radiother Oncol, 94*(2), 206–212.

Burnet, N. G., Adams, E. J., Fairfoul, J., Tudor, G. S. J., Hoole, A. C. F., Routsis, D. S., Dean, J. C., Kirby, R. D., Cowen, M., Russell, S. G., Rimmer, Y. L., & Thomas, S. J. (2010). Practical aspects of implementation of helical tomotherapy for intensity-modulated and image-guided radiotherapy. *Clin Oncol (R Coll Radiol), 22*(4), 294–312.

Capelle, L., Mackenzie, M., Field, C., Parliament, M., Ghosh, S., & Scrimger, R. (2012). Adaptive radiotherapy using helical tomotherapy for head and neck cancer in definitive and postoperative settings: initial results. *Clin Oncol (R Coll Radiol), 24*(3), 208–215.

Castadot, P., Lee, J. A., Parraga, A., Geets, X., Macq, B., & Grégoire, V. (2008). Comparison of 12 deformable registration strategies in adaptive radiation therapy for the treatment of head and neck tumors. *Radiat Oncol, 89*(1), 1–12.

Chan, A. T. C., & Felip, E. (2009). ESMO Guidelines Working Group Nasopharyngeal cancer: ESMO clinical recommendations for diagnosis, treatment and follow-up. *Ann Oncol, 20*(S4), 123–125.

Chan, A. T. C., Teo, P. M. L., & Johnson, P. J. (2002). Nasopharyngeal carcinoma. *Ann Oncol, 13*(7), 1007–1015.

Chan, J. K. C., Pilch, B. Z., Kuo, T. T., Wenig, B. M., & Lee, A. W. M. (2005). Tumors of the nasopharynx: introduction. In L. Barnes, J. W. Eveson, P. Reichart & D. Sidransky (Eds.), *Pathology and genetics of head and neck tumours (World Health Organization Classification of Tumours)* (pp. 82–84). Lyon, France: IARC press.

Chang, E. T., & Adami, H-O. (2006). The enigmatic epidemiology of nasopharyngeal carcinoma. *Cancer Epidemiol, Biomarkers Prev, 15*(10), 1765–1777.

Chang, J. T. C., Chan, S. C., Yen, T. C., Liao, C. T., Lin, C. Y., Lin, K. J., Chen, I. H., Wang, H. M., Chang, Y. C., Chen, T. M., Kang, C. J., & Ng, S. H. (2005). Nasopharyngeal carcinoma staging by (18)F-fluorodeoxyglucose positron emission tomography. *Int J Radiat Oncol Biol Phys, 62*(2), 501–507.

Chao, K. S. C., Bhide, S., Chen, H., Asper, J., Bush, S., Franklin, G., Kavadi, V., Liengswangwong, V., Gordon, W., Raben, A., Strasser, J., Koprowski, C., Frank, S., Chronowski, G., Ahamad, A., Malyapa, R., Zhang, L., & Dong, L. (2007). Reduce in variation and improve efficiency of target volume delineation by a computer-assisted system using a deformable image registration approach. *Int J Radiat Oncol Biol Phys, 68*(5), 1512–1521.

Chao, M., Penagaricano, J., Yan, Y., Moros, E. G., Corry, P., & Ratanatharathorn, V. (2012). Voxel-based dose reconstruction for total body irradiation with helical tomotherapy. . *Int J Radiat Oncol Biol Phys, 82*(5), 1575–1583.

Cheng, J. C. H., Chao, K. S. C., & Low, D. (2001). Comparison of intensity modulated radiation therapy (IMRT) treatment techniques for nasopharyngeal carcinoma. *Int J Cancer, 96*(2), 126–131.

Cheng, S. H., Yen, K. L., Jian, J. J. M., Tsai, S. Y. C., Chu, N. M., Leu, S. Y., Chan, K. Y., Tan, T. D., Cheng, J. C., Hsieh, C. Y., & Huang, A. T. (2001). Examining prognostic factors and patterns of failure in nasopharyngeal carcinoma following concomitant radiotherapy and chemotherapy: impact on future clinical trials. *Int J Radiat Oncol Biol Phys, 50*(3), 717–726.

Chua, D. T. T., Sham, J. S. T., Wei, W. I., Ho, W. K., & Au, G. K. H. (2001). The predictive value of the 1997 American Joint Committee on Cancer stage classification in determining failure patterns in nasopharyngeal carcinoma. *Cancer, 92*(1), 2845–2855.

Chung, N. N., Ting, L. L., Hsu, W. C., Lui, L. T., & Wang, P. M. (2004). Impact of magnetic resonance imaging versus CT on nasopharyngeal carcinoma: primary tumor target delineation for radiotherapy. *Head Neck, 26*(3), 241–246.

Ciura, K., McBurney, M., Nguyen, B., Pham, M., Rebueno, N., Fuller, C. D., Guha-Thakurta, N., & Rosenthal, D. I. (2011). Effect of brain stem and dorsal vagus complex dosimetry on nausea and vomiting in head and neck intensity-modulated radiation therapy. *Med Dosim, 36*(1), 41–45.

Cooper, J. S., Fu, K., Marks, J., & Silverman, S. (1995). Late effects of radiation therapy in the head and neck region. *Int J Radiat Oncol Biol Phys, 31*(5), 1141–1164.

Daisne, J. F., Duprez, T., Weynand, B., Lonneux, M., Hamoir, M., Reychler, H., & Grégoire, V. (2004). Tumor volume in pharyngolaryngeal squamous cell carcinoma: comparison at CT, MR imaging, and FDG PET and validation with surgical specimen. *Radiology, 233*(1), 93–100.

Daly, M. E., Chen, A. M., Bucci, M. K., El-Sayed, I., Xia, P., Kaplan, M. J., & Eisele, D. W. (2007). Intensity-modulated radiation therapy for malignancies of the nasal cavity and paranasal sinuses. *Int J Radiat Oncol Biol Phys, 67*(1), 151–157.

Danesh-Meyer, H. V. (2008). Radiation-induced optic neuropathy. *J Clin Neurosci, 15*(2), 95–100.

Darzy, K. H., & Shalet, S. M. (2009). Hypopituitarism following radiotherapy. *Pituitary, 12*(1), 45–50.

Debus, J., Hug, E. B., Liebsch, N. J., O'Farrel, D., Finkelstein, D., Efird, J., & Munzenrider, J. E. (1997). Brainstem tolerance to conformal radiotherapy of skull base tumors. *Int J Radiat Oncol Biol Phys, 39*(5), 967–975.

Dickens, P., Srivastava, G., Loke, S. L., Chan, C. W., & Liu, Y. T. (1992). Epstein-Barr virus DNA in nasopharyngeal carcinomas from Chinese patients in Hong Kong. *J Clin Pathol*, *45*(5), 396–397.

Ding, G. X., Duggan, D. M., Coffey, C. W., Deeley, M., Hallahan, D. E., Cmelak, A., & Malcolm, A. (2007). A study on adaptive IMRT treatment planning using kV cone-beam CT. *Radiat Oncol, 85*(1)*,* 116–125.

Edge, S. B., Byrd, D. R., Compton, C. C., Fritz, A. G., Greene, F. L., & Trotti, A. III. (2010). *AJCC cancer staging manual* (7th ed.). pp. 41–49. New York, US: Springer.

Eisbruch, A., Kim, H. M., Terrell, J. E., Marsh, L. H., Dawson, L. A., & Ship, J. A. (2001). Xerostomia and its predictors following parotid-sparing irradiation of head and neck cancer. *Int J Radiat Oncol Biol Phys, 50*(3), 695–704.

Eisbruch, A., Ten Haken, R. K., Kim, H. M., Marsh, L. H., & Ship, J. A. (1999). Dose, volume, and function relationships in parotid salivary glands following conformal and intensity-modulated irradiation of head and neck cancer. *Int J Radiat Oncol Biol Phys, 45*(3), 577–587.

Emami, B., Sethi, A., & Petruzzelli, G. J. (2003). Influence of MRI on target volume delineation and IMRT planning in nasopharyngeal carcinoma. *Int J Radiat Oncol Biol Phys, 57*(2), 481–488.

Fang, F. M., Tsai, W. L., Go, S. F., Ho, M. W., Wu, J. M., Wang, C. J., Su, C. Y., Chen, W. C., & Huang, E. Y. (2001). Implications of quantitative tumor and nodal regression rates for nasopharyngeal carcinomas after 45Gy of radiotherapy. *Int J Radiat Oncol Biol Phys, 50*(4), 961–969.

Feldkamp, L. A., Davis, L. C., & Kress, J. W. (1984). Practical cone-beam algorithm. *J Opt Soc Am, 1*(6), 612–619.

Feng, M., & Eisbruch, A. (2007). Future issues in highly conformal radiotherapy for head and neck cancer. *J Clin Oncol, 25*(8), 1009–1013.

Fernandez, A., Brada, M., Zabuliene, L., Karavitaki, N., & Wass, J. A. H. (2009). Radiation-induced hypopituitarism. *Endocr Relat Cancer, 16*(3), 733–772.

Fleming, I. D., Cooper, J. S., Henson, D. E., Hutter, R. V. P., Kennedy, B. J., Murphy, G. P., O'Sullivan, B., Sobin, L. H., & Yarbro, J. W. (1997). *AJCC cancer staging manual* (5th ed.). pp. 31–36. Philadelphia, NY: Lippincott-Ravin.

Forrest, L. J., Mackie, T. R., Ruchala, K., Turek, M., Kapatoes, J., Jaradat, H., Hui, S., Balog, J., Vail, D. M. , & Mehta, M. P. (2004). The utility of megavoltage computed tomography images from a helical tomotherapy system for setup verification purposes. *Int J Radiat Oncol Biol Phys, 60*(5), 1639–1644.

Friborg, J., Wohlfahrt, J., Koch, A., Storm, H., Olsen, O. R., & Melbye, M. (2005). Cancer susceptibility in nasopharyngeal carcinoma families—a population-based cohort study. *Cancer Res, 65*(18), 8567–8572.

Fua, T. F., Corry, J., Milner, A. D., Cramb, J., Walsham, S. F., & Peters, L. J. (2007). Intensity-modulated radiotherapy for nasopharyngeal carcinoma: clinical correlation of dose to the pharyngo-esophageal axis and dysphagia. *Int J Radiat Oncol Biol Phys, 67*(4), 976–981.

Geets, X., Tomsej, M., Lee, J. A., Duprez, T., Coche, E., Cosnard, G., Lonneux, M., & Grégoire, V. (2007). Adaptive biological image-guided IMRT with anatomic and functional imaging in pharyngo-laryngeal tumors: Impact on target volume delineation and dose distribution using helical tomotherapy. *Radiother Oncol, 85*(1), 105–115.

Graham, S. A., Moseley, D. J., Siewerdsen, J. H., & Jaffray, D. A. (2007). Compensators for dose and scatter management in cone-beam computed tomography. *Med Phys, 34*(7), 2691–2703.

Grzadziel, A., Grosu, A. L., & Kneschaurek, P. (2006) Three-dimensional conformal versus intensity-modulated radiotherapy dose planning in stereotactic radiotherapy: application of standard quality parameters for plan evaluation. *Int J Radiat Oncol Biol Phys, 66*(4), S87–S94.

Han, C., Chen, Y. J., Liu, A., Schultheiss, T. E. & Wong, J. Y. C. (2008). Actual dose variation of parotid glands and spinal cord for nasopharyngeal cancer patients during radiotherapy. *Int J Radiat Oncol Biol Phys, 70*(4), 1256–1262.

Hansen, E. K., Bucci, M. K., Quivey, J. M., Weinberg, V., & Xia, P. (2006). Repeat CT imaging and replanning during the course of IMRT for head-and-neck cancer. *Int J Radiat Oncol Biol Phys, 64*(2), 355–362.

Hong, T. S., Tome, W. A., Chappell, R. J., Chinnaiyan, P., Mehta, M. P., & Harari, P. M. (2005). The impact of daily setup variations on head-and-neck intensity-modulated radiation therapy. *Int J Radiat Oncol Biol Phys, 61*(3), 779–788.

Hong, T. S., Tome, W.A., Chappell, R. J., & Harari, P. M. (2004). Variations in target delineation for head and neck IMRT: an international multi-institutional study. *Int J Radiat Oncol Biol Phys, 60*(3 Suppl), S157–S158.

Hong Kong Cancer Registry. (2009). *Top ten cancer in 2009*. Retrieved from http://www3.ha.org.hk/cancereg/statistics.html

Hoppe, B. S., Stegman, L. D., Zelefsky, M. J., Rosenzweig, K. E., Wolden, S. L., Patel, S. G., Shah, J. P., Kraus, D. H., Lee, N. Y. (2007). Treatment of nasal cavity and paranasal sinus cancer with modern radiotherapy techniques in the postoperative setting—The MSKCC experience. *Int J Radiat Oncol Biol Phys, 67*(3), 691–702.

Hsiung, C. Y., Ting, H. M., Huang, H. Y., Lee, C. H., Huang, E. Y., & Hsu, H. C. (2006). Parotid-sparing intensity-modulated radiotherapy (IMRT) for nasopharyngeal carcinoma: preserved parotid function after IMRT on quantitative salivary scintigraphy, and comparison with historical data after conventional radiotherapy. *Int J Radiat Oncol Biol Phys, 66*(2), 454–461.

International Commission on Radiation Units and Measurements. (1993). *ICRU Report 50: Prescribing, recording, and reporting photon beam therapy.* Bethesda, MD: ICRU Publications.

International Commission on Radiation Units and Measurements. (1999). *ICRU Report 62: Prescribing, recording, and reporting photon beam therapy (Supplement to ICRU Report 50).* Bethesda, MD: ICRU Publications.

International Commission on Radiation Units and Measurements. (2010). *ICRU Report 83: Prescribing, recording, and reporting photon beam intensity modulated radiation therapy (IMRT).* Bethesda, MD: ICRU Publications.

Jensen, A. D., Nill, S., Huber, P. E., Bendl, R., Debus, J., & Münter, M. W. (2012). A clinical concept for interfractional adaptive radiation therapy in the treatment of head and neck cancer. *Int J Radiat Oncol Biol Phys, 82*(2), 590–596.

Jeraj, R., Mackie, T. R., Balog, J., Olivera, G., Pearson, D., Kapatoes, J., Ruchala, K., & Reckwerdt, P. (2004). Radiation characteristics of helical tomotherapy. *Med Phys, 31*(2), 396–404.

Jia, W. H., Feng, B. J., Xu, Z. L., Zhang, X. S., Huang, P., Huang, L. X., Yu, X. J., Feng, Q. S., Yao, M. H., Shugart, Y. Y. & Zeng, Y. X. (2004). Familial risk and clustering of nasopharyngeal carcinoma in Guangdong, China. *Cancer, 101*(2), 363–369.

Kaiser, A., Schultheiss T. E., Wong J. Y., Smith, D. D., Han, C., Vora, N. L., Pezner, R. D., Chen, Y. J., & Radany, E. H. (2006). Pitch, roll, and yaw variations in patient positioning. *Int J Radiat Oncol Biol Phys, 66*(3), 949–955.

Kam, M. K. M., Chau, R. M. C., Suen, J., Choi, P. H. K., & Teo, P. M. L. (2003). Intensity-modulated radiotherapy in nasopharyngeal carcinoma: dosimetric advantage over conventional plans and feasibility of dose escalation. *Int J Radiat Oncol Biol Phys, 56*(1), 145–157.

Kam, M. K. M., Teo, P. M. L., Chau, R. M. C., Cheung, K. Y., Choi, P. H. K., Kwan, W. H., Leung, S. F., Zee, B., & Chan, A. T. C. (2004). Treatment of nasopharyngeal carcinoma with intensity-modulated radiotherapy: the Hong Kong experience. *Int J Radiat Oncol Biol Phys, 60*(5), 1440–1450.

Kapatoes, J. M., Olivera, G. H., Balog, J. P., Keller, H., Reckwerdt, P. J., & Mackie, T. R. (2001). On the accuracy and effectiveness of dose reconstruction for tomotherapy. *Phys Med Biol, 46*(4), 943–966.

Keime-Guibert, F., Napoltano, M., & Delattre, J. Y. (1998). Neurological complications of radiotherapy and chemotherapy. *J Neurol, 245*(11), 695–708.

Kim, K., Park, S., Cheong, K., Kang, S., Hwang, T., Lee, M., Oh, D., & Bae, H. (2009). Dosimetric changes of intensity modulated radiotherapy (IMRT) plan on the follow-up CT acquired during treatment in the patients with nasopharynx cancer. *Eur J Cancer Suppl, 7*(2), 487–488.

King, A. D., Ma, B. B., Yau, Y. Y., Zee, B., Leung, S. F., Wong, J. K. T., Kam, M. K. M., Ahuja, A. T., & Chan, A. T. C. (2008). The impact of 18F-FDG PET/CT on assessment of nasopharyngeal carcinoma at diagnosis. *Br J Radiol, 81*, 291–298.

King, A. D., Vlantis, A. C., Bhatia, K. S. S., Zee, B. C. Y., Woo, J. K. S., Tse, G. M. K., Chan, A. T. C., & Ahuja, A. T. (2011). Primary nasopharyngeal carcinoma: diagnostic accuracy of MR imaging versus that of endoscopy and endoscopic Biopsy. *Radiol, 258*(2), 531–537.

Kirkpatrick, J. P., van der Kogel, A. J. & Schultheiss, T. E. (2010). Radiation dose-volume effects in the spinal cord. *Int J Radiat Oncol Biol Phys, 76*(3 Suppl), S42–S49.

Kodaira, T., Tomita, N., Tachibana, H., Nakamura, T., Nakahara, R., Inokuchi, H., & Fuwa, N. (2009). Aichi cancer center initial experience of intensity modulated radiation therapy for nasopharyngeal cancer using helical tomotherapy. *Int J Radiat Oncol Biol Phys, 73*(4), 1129–1134.

Konings, A. W., Copes, R. P., & Vissink, A. (2005). On the mechanism of salivary gland radiosensitivity. *Int J Radiat Oncol Biol Phys, 62*(4), 1187–1194.

Kuo, Y. C., Wu, T. H., Chung, T. S., Huang, K. W., Chao, K. S. C., Su, W. C., & Chiou, J. F. (2006). Effect of regression of enlarged neck lymph nodes on radiation doses received by parotid glands during intensity-modulated radiotherapy for head and neck cancer. *Am J Clin Oncol, 29*(6), 600–605.

Kutcher, G. J. & Burman, C. (1989). Calculation of complication probability factors for non uniform normal tissue irradiation: the effective volume method. *Int J Radiat Oncol Biol Phys, 16*(6), 1623–1630.

Kwong, D. L. W., Sham, J. S. T., Leung, L. H. T., Cheng, A. C. K., Ng, W. M., Kwong, P. W. K., Lui, W. M., Yau, C. C., Wu, P. M., Wei W., & Au, G. (2006). Preliminary results of radiation dose escalation for locally advanced nasopharyngeal carcinoma. *Int J Radiat Oncol Biol Phys, 64*(2), 374–381.

Langen, K. M., Meeks, S. L., Poole, D. O., Wagner, T. H., Willoughby, T. R., Kupelian, P. A., Ruchala, K. J., Haimerl, J., & Olivera, G. H. (2005). The use of megavoltage CT (MVCT) images for dose recomputations. *Phys Med Biol, 50*(18), 4259–4276.

Lee, A. W. M., Foo, W., Law, S. C. K., Poon, Y. F., Sze, W. M., O, S. K., Tung, S. Y., & Lau, W. H. (1997). Nasopharyngeal carcinoma—presenting symptoms and duration before diagnosis. *Hong Kong Med J*, *3*(4), 355–361.

Lee, A. W. M, Sze, W. M., Au, J. S. K., Leung, S. F., Leung, T. W., Chua, D. T. T., Zee, B. C. Y., Law, S. C. K., Teo, P. M. L., Tung, S. Y., Kwong D. L. W., & Lau, W. H. (2005). Treatment results for nasopharyngeal carcinoma in the modern era: The Hong Kong experience. *Int J Radiat Oncol Biol Phys, 61*(4), 1107–1116.

Lee, C., Langen, K. M., Lu, W., Haimerl, J., Schnarr, E., Ruchala, K. J., Olivera, G. H., Meeks, S. L., Kupelian, P. A., Shellenberger, T. D., & Mañon, R. R. (2008a). Evaluation of geometric changes of parotid glands during head and neck cancer radiotherapy using daily MVCT and automatic deformable registration. *Radiother Oncol, 89*(1), 81–88.

Lee, C., Langen, K. M., Lu, W., Haimerl, J., Schnarr, E., Ruchala, K. J., Olivera, G. H., Meeks, S. L., Kupelian, P. A., Shellenberger, T. H., & Mañon, R. R. (2008b). Assessment of parotid dose changes during head and neck cancer radiotherapy using daily megavoltage computed tomography and deformable image registration. *Int J Radiat Oncol Biol Phys, 71*(5), 1563–1571.

Lee, N., Xia, P., Quivey, J. M., Sultanem, K., Poon, I., Akazawa, C., Akazawa, P., Weinberg, V., & Fu, K. K. (2002). Intensity-modulated radiotherapy in the treatment of nasopharyngeal carcinoma: an update of the UCSF experience. *Int J Radiat Oncol Biol Phys, 53*(1), 12–22.

Leong, J. L., Fong, K.W., & Low, W. K. (1999). Factors contributing to delayed diagnosis in nasopharyngeal carcinoma. *J Laryngol Otol, 113*(7), 633–636.

Li, X. A., Qi, X. S., Pitterle, M., Kalakota, K., Mueller, K., Erickson, B. A., Wang, D., Schultz, C. J., Firat, S. Y., & Wilson, J. F. (2007a). Interfractional variations in patient setup and anatomic change assessed by daily computed tomography. *Int J Radiat Oncol Biol Phys, 68*(2), 581–591.

Li, Y., Taylor, J. M., Ten Haken, R. K., & Eisbruch, A. (2007b). The impact of dose on parotid salivary recovery in head and neck cancer patients treated with radiation therapy. *Int J Radiat Oncol Biol Phys, 67*(3), 660–669.

Loo, H., Fairfoul, J., Chakrabarti, A., Dean, J. C., Benson, R. J., Jefferies, S. J, & Burnet, N. G. (2011). Tumour shrinkage and contour change during radiotherapy increase the dose to organs at risk but not the target volumes for head and neck cancer patients treated on the TomoTherapy HiArt™ system. *Clin Oncol (R Coll Radiol), 23*(1), 40–47.

Lu, W., Olivera, G. H., Chen, Q., Ruchala, K. J., Haimerl, J., Meeks, S. L., Langen, K. M., & Kupelian, P. A. (2006). Deformable registration of the planning image (kVCT) and the daily images (MVCT) for adaptive radiation therapy. *Phys Med Biol, 51*(17), 4357–4374.

Lyman, J. T. (1992). Normal tissue complication probabilities: variable dose per fraction. *Int J Radiat Oncol Biol Phys, 22*(2), 247–250.

Lyman, J. T. & Wolbarst, A. B. (1987). Optimization of radiation therapy III: a method of assessing complication probabilities from dose-volume histograms. *Int J Radiat Oncol Biol Phys, 13*(1), 103–109.

Mackie, T. R., Kapatoes, J., Ruchala, K., Lu, W., Wu, C., Olivera, G., Forrest, L., Tome, W., Welsh, J., Jeraj, R., Harari, P., Reckwerdt, P., Paliwal, B., Ritter, M., Keller, H., Fowler, J., & Mehta, M. (2003a). Image guidance for precise conformal radiotherapy. *Int J Radiat Oncol Biol Phys, 56*(1), 89–105.

Mackie, T. R., Olivera, G. H., Kapatoes, J. M., Ruchala, K. J., Balog, J. P., Tome, W. A., Hui, S., Kissick, M., Wu, C., Jeraj, R., Reckwerdt, P. J., Harari, P., Ritter, M., Forrest, L., Welsh, J., & Mehta, M. P. (2003b). Helical Tomotherapy. In J. R. Palta & T. R. Mackie (Eds.), *Intensity-Modulated Radiation Therapy—The State of the Art* (pp. 247–284). Madison, WI: Medical Physics Publishing.

Mackley, H. B., Reddy, C. A., Lee, S. Y., Harnisch, G. A., Mayberg, M. R., Hamrahian, A. H., & Suh, J. H. (2007). Intensity-modulated radiotherapy for pituitary adenomas: The preliminary report of the Cleveland Clinic experience. *Int J Radiat Oncol Biol Phys, 67*(1), 232–239.

Mail, N., Moseley, D. J., Siewerdsen, J. H., & Jaffray, D. A. (2009). The influence of bowtie filtration on cone-beam CT image quality. *Med Phys, 36* (1), 22–32.

Martel, M. K., Sandler, H. M., Cornblath, W. T., Marsh, L. H., Hazuka, M. B., Roa, W. H., Fraass, B. A., & Lichter, A. S. (1997). Dose–volume complication analysis for visual pathway structures of patients with advanced paranasal sinus tumors. *Int J Radiat Oncol Biol Phys, 38*(2), 273–284.

Martini, F. H., Ober, W. C., Garrison, C. W., Welch, K. & Hutchings, R. T. (2001). *Fundamentals of anatomy & physiology* (5th ed.). pp. 802. Upper Saddle River, N.J.: Prentice Hall.

Marucci, L., Niemierko, A., Liebsch, N. J., Aboubaker, F., Liu, M. C. C., & Munzenrider, J. E. (2004). Spinal cord tolerance to high-dose fractionated 3D conformal proton-photon irradiation as evaluated by equivalent uniform dose and dose volume histogram analysis. *Int J Radiat Oncol Biol Phys, 59*(2), 551–555.

Mayo, C., Yorke, E., & Merchant, T. E. (2010). Radiation associated brainstem injury. *Int J Radiat Oncol Biol Phys, 76*(3 Suppl), S36–S41.

Mayo, C., Martel, M. K., Marks, L. B., Flickinger, J., Nam, J. & Kirkpatrick, J. (2010). Radiation dose-volume effects of optic nerves and chiasm. *Int J Radiat Oncol Biol Phys, 76*(3 Suppl), S28–S35.

McBain, C. A., Henry, A. M., Sykes, J., Amer, A., Marchant, T., Moore, C. M., Davies, J., Stratford, J., McCarthy, C., Porritt, B., Williams, P., Khoo, V. S., & Price, P. (2006). X-ray volumetric imaging in image-guided radiotherapy: the new standard in on-treatment imaging. *Int J Radiat Oncol Biol Phys, 64*(2), 625–634.

Mechalakos, J. G., Hunt, M. A., Lee, N. Y., Hong, L. X., Ling, C. C., & Amols, H. I. (2007). Using an onboard kilovoltage imager to measure setup deviation in intensity-modulated radiation therapy for head-and-neck patients. *J Appl Clin Med Phys, 8*(4), 28–44.

Meeks, S. L., Harmon, J. F. Jr., Langen, K. M., Willoughby, T. R., Wagner, T. H., & Kupelian, P. A. (2005). Performance characterization of megavoltage computed tomography imaging on a helical tomotherapy unit. *Med Phys, 32* (8), 2673–2681.

Meyer, J. L. (2007). *IMRT, IGRT, SBRT: advances in the treatment planning and delivery of radiotherapy*. Basel, Switzerland: Karger.

Mohan, R., Zhang, X., Wang, H., Kang, Y., Wang, X., Liu, H., Ang, K. K., Kuban, D., & Dong, L. (2005). Use of deformed intensity distributions for on-line modification of image-guided IMRT to account for interfractional anatomic changes. *Int J Radiat Oncol Biol Phys, 61*(4), 1258–1266.

Monroe, A. T., Reddy, S. C., Gibbs, G. L., White, G. A., & Peddada, A. V. (2008). Factors associated with radiation-induced nausea and vomiting in head and neck cancer patients treated with intensity modulated radiation therapy. *Radiother Oncol, 87*(2), 188–194.

Morin, O., Gillis, A., Chen, J., Aubin, M., Bucci, M. K., Roach, M. 3rd., & Pouliot, J. (2006). Megavoltage cone beam CT: system description and clinical applications. *Med Dosim, 31*(1), 51–61.

Nath, S. K., Simpson, D. R., Rose, B. S., & Sandhu, A. P. (2009). Recent advances in image-guided radiotherapy for head and neck carcinoma. *J Oncol, 2009,* 752135. doi:10.1155/2009/752135

Ng, S. H., Chang, T. C., Ko, S. F., Yen, P. S., Wan, Y. L., Tang, L. M., & Tsai, M. H. (1997). Nasopharyngeal carcinoma: MRI and CT assessment. *Neuroradiology, 39*(10), 741–746.

Nieder, C., Grosu, A. L., Andratschke, N. H., & Molls, M. (2005). Proposal of human spinal cord reirradiation dose based on collection of data from 40 patients. *Int J Radiat Oncol Biol Phys, 61*(3), 851–855.

Niemierko, A. (1997). Reporting and analyzing dose distributions: a concept of equivalent uniform dose. *Med Phys, 24*(1), 103–110.

Nishimura, Y., Shibata, T., Nakamatsu, K., Kanamori, S., Koike, R., Okubo, M., Nishikawa, T., Tachibana, I., Tamura, M., & Okumura, M. (2010). A two-step intensity-modulated radiation therapy method for nasopharyngeal cancer: the Kinki University experience. *Jpn J Clin Oncol, 40*(2), 130–138.

Nithiananthan, S., Schafer, S., Uneri, A., Mirota, D. J., Stayman, J. W., Zbijewski, W., Brock, K. K., Daly, M. J., Chan, H., Irish, J. C., & Siewerdsen, J. H. (2011). Demons deformable registration of CT and cone-beam CT using an iterative intensity matching approach. *Med Phys, 38*(4), 1785–1798.

O'Daniel, J. C., Garden, A. S., Schwartz, D. L., Wang, H., Ang, K. K., Ahamad, A., Rosenthal, D. I., Morrison, W. H., Asper, J. A., Zhang, L., Tung, S. M., Mohan, R., & Dong, L. (2007). Parotid gland dose in intensity-modulated radiotherapy for head and neck cancer: is what you plan what you get? *Int J Radiat Oncol Biol Phys, 69*(4), 1290–1296.

Oelfke, U., Tucking, T., Nill, S., Seeber, A., Hesse, B., Huber, P., & Thilmann, C. (2006). Linac-integrated kV-cone beam CT: technical features and first applications. *Med Dosim, 31*(1), 62–70.

Pai, H. H., Thornton, A., Katznelson, L., Finkelstein, D. M., Adams, J. A., Fullerton, B. C., Loeffler, J. S., Leibsch, N. J., Klibanski, A., & Munzenrider, J. E. (2001). Hypothalamic/pituitary function following high-dose conformal radiotherapy to the base of skull: demonstration of a dose-effect relationship using dose-volume histogram analysis. *J Radiat Oncol Biol Phys, 49*(4), 1079–1092.

Paquin, D., Levy, D., & Xing, L. (2009). Multiscale registration of planning CT and daily cone beam CT images for adaptive radiation therapy. *Med Phys, 36*(1), 4–11.

Parkin, D. M., Whelan, S. L., Ferlay, J., Teppo, L., & Thomas, D. B. (2002). Cancer incidence in five continents Vol VIII. *Lyon: IARC Scientific Publications Number, 155*, 534–536.

Paulino, A. C., Koshy, M., Howell, R., Schuster, D., & Davis, L. W. (2005). Comparison of CT- and FDG-PET-defined gross tumor volume in intensity-modulated radiotherapy for head-and-neck cancer. *Int J Radiat Oncol Biol Phys, 61*(5), 1385–1392.

Pouliot, J., Bani-Hashemi, A., Chen, J., Svatos, M., Ghelmansarai, F., Mitschke, M., Aubinm M., Xia, P., Morin, O., Bucci, K., Roach, M., Hernandez, P., Zheng, Z., Hristov, D., & Verhey, L. (2005). Low-dose megavoltage cone-beam CT for radiation therapy. *Int J Radiat Oncol Biol Phys, 61*(2), 550–560.

Pow, E. H. N., Kwong, D. L. W., McMillan, A. S., Wong, M. C. M., Sham, J. S. T., Leung, L. H. T., & Leung, W. K. (2006). Xerostomia and quality of life after intensity-modulated radiotherapy vs. conventional radiotherapy for early-stage nasopharyngeal carcinoma: initial report on a randomized controlled clinical trial. *Int J Radiat Oncol Biol Phys, 66*(4), 981–991.

Reddy, S. P., Raslan, W. F., Gooneratne, S., Kathuria, S., & Marks, J. E. (1995). Prognostic significance of keratinization in nasopharyngeal carcinoma. *Am J Otolaryngol, 16*(2), 103–108.

Robar, J. L., Day, A., Clancey, J., Kelly, R., Yewondwossen, M., Hollenhorst, H., Rajaraman, M., & Wilke, D. (2007). Spatial and dosimetric variability of organs at risk in head-and-neck intensity-modulated radiotherapy. *Int J Radiat Oncol Biol Phys, 68*(4), 1121–1130.

Rosenthal, D. I., Chambers, M.S., Fuller, C. D., Rebueno, N. C., Garcia, J., Kies, M. S., & Garden, A. S. (2008). Beam path toxicities to non-target structures during intensity-modulated radiation therapy for head and neck cancer. *Int J Radiat Oncol Biol Phys, 72*(3), 747–755.

Ruchala, K. J., Olivera, G. H., Kapatoes, J. M., Schloesser, E. A., Reckwerdt, P. J., & Mackie, T. R. (2000). Megavoltage CT image reconstruction during tomotherapy treatments. *Phys Med Biol. 45*(12), 3545–3562.

Ryu, S., Gorty, S., Kazee, A. M., Bogart, J., Hahn, S. S., Dalal, P. S., Chung, C. C., & Sagerman, R. H. (2000). 'Full dose' reirradiation of human cervical spinal cord. *Am J Clin Oncol, 23*(1), 29–31.

Schinagl, D. A. X., Vogel, W. V., Hoffmann, A. L., van Dalen, J. A., Oyen, W. J., & Kaanders, J. H. A. M. (2007). Comparison of five segmentation tools for 18F-fluoro-deoxy-glucose-positron emission tomography-based target volume definition in head and neck cancer. *Int J Radiat Oncol Biol Phys, 69*(4), 1282–1289.

Schubert, L. K., Westerly, D. C., Tome, W. A., Mehta, M. P., Soisson, E. T., Mackie, T. R., Ritter, M. A., Khuntia, D., Harari, P. M., & Paliwal, B. R. (2009). A comprehensive assessment by tumor site of patient setup using daily MVCT imaging from more than 3800 helical tomotherapy treatments. *Int J Radiat Oncol Biol Phys, 73*(4), 1260–1269.

Schultheiss, T. E. (2008). The radiation dose-response of the human spinal cord. *Int J Radiat Oncol Biol Phys, 71*(5), 1455–1459.

Schultheiss, T. E., Kun, L. E., Ang, K. K., & Stephens, L. C. (1995). Radiation response of the central nervous system. *Int J Radiat Oncol Biol Phys, 31*(5), 1093–1112.

Schwartz, D., Ang, K., Chronowski, G., Rosenthal, D. I., Sejpal, S. V., Shah, S. J., Zhang, Y., Garcia, J., Garden, A., & Dong, L. (2009). Prospective experience with CT-guided adaptive radiotherapy for head-and-neck cancer. *Int J Radiat Oncol Biol Phys, 75* (3 Suppl), S72.

Schwartz, D. L., & Dong, L. (2011). Adaptive radiation therapy for head and neck cancer-can an old goal evolve into a new standard? *J Oncol, 2011*, 690595. doi:10.1155/2011/690595

Schwartz, D. L., Garden, A. S., Thomas, J., Chen, Y., Zhang, Y., Lewin, J., Chambers, M. S., & Dong, L. (2012). Adaptive radiotherapy for head-and-neck cancer: initial clinical outcomes from a prospective trial. *Int J Radiat Oncol Biol Phys. In press, Corrected proof.*

Shah, A. P., Langen, K. M, Ruchala, K. J., Cox, A., Kupelian, P. A., & Meeks, S. L. (2008). Patient dose from megavoltage computed tomography imaging. *Int J Radiat Oncol Biol Phys, 70*(5), 1579–1587.

Shanmugaratnam, K., & Sobin, L. H. (1991). Histological typing of tumours of the upper respiratory tract and ear. In K. Shanmugaratnam & L. H. Sobin (Eds.), *International histological classification of tumours: no 19* (pp. 32–33). Geneva: WHO.

Sheng, K., Chow, M. C., Hunter, G., Larner, J. M., & Read, P. W. (2008). Is daily computed tomography image guidance necessary for nasal cavity and nasopharyngeal radiotherapy? An investigation based on helical tomotherapy. *J Appl Clin Med Phys, 9*(1), 36–46.

Siewerdsen, J. H., Moseley, D. J., Bakhtiar, B., Richard, S., & Jaffray, D. A. (2004). The influence of antiscatter grids on soft-tissue detectability in cone-beam computed tomography with flat-panel detectors. *Med Phys, 31*(12), 3506–3520.

Spano, J–P., Busson, P., Atlan, D., Bourhis, J., Pignon, J–P., Esteban, C., & Armand, J–P. (2003). Nasopharyngeal carcinomas: an update. *Eur J Cancer, 39*(15), 2121–2135.

Stapleford, L. J., Lawson, J. D., Perkins, C., Edelman, S., Davis, L., McDonald, M. W., Waller, A., Schreibmann, E., & Fox, T. (2010). Evaluation of automatic atlas-based lymph node segmentation for head-and-neck cancer. *Int J Radiat Oncol Biol Phys, 77*(3), 959–966.

Tabuchi, K., Nakayama, M., Nishimura, B., Hayashi, K. & Hara, A. (2011). Early detection of nasopharyngeal carcinoma. *Int J Otolaryngol*, *2011*, 638058. doi:10.1155/2011/638058

Teo, P., Lee, W. Y. & Yu, P. (1996). The prognostic significance of parapharyngeal tumour involvement in nasopharyngeal carcinoma. *Radiother Oncol, 39*(3), 209–221.

Teo, P., Yu, P., Lee, W. Y., Leung, S. F., Kwan, W. H., Yu, K. H., Choi, P., & Johnson, P. J. (1996a). Significant prognosticators after primary radiotherapy in 903 nondisseminated nasopharyngeal carcinoma evaluated by computer tomography. *Int J Radiat Oncol Biol Phys, 36*(2), 291–304.

Teo, P. M. L., Kwan, W. H., Lee, W. Y., Leung, S. F., & Johnson, P. J. (1996b). Prognosticators determining survival subsequent to distant metastasis from nasopharyngeal carcinoma. *Cancer, 77*(12), 2423–2431.

Teo, P. M. L., Leung, S. F., Tung, S. Y., Zee, B., Sham, J. S. T., Lee, A. W. M., Lau, W. H., Kwan, W. H., Leung, T. W., Chua, D., Sze, W. M., Au, J. S. K., Yu, K. H., O, S. K., Kwong, D., Yau, T. K., Law, S. C. K. , Sze, W. K., Au, G., & Chan, A. T. C. (2006). Dose-response relationship of nasopharyngeal carcinoma above conventional tumoricidal level: a study by the Hong Kong Nasopharyngeal Carcinoma Study Group (HKNPCSG). *Radiother Oncol, 79*(1), 27–33.

Toogood, A. A. & Stewart, P. M. (2008). Hypopituitarism: clinical features, diagnosis, and management. *Endocrinol Metab Clin North Am, 37*(1), 235–261.

Tsuji, S. Y., Hwang, A., Weinberg, V., Yom, S. S., Quivey, J. M., & Xia, P. (2010). Dosimetric evaluation of automatic segmentation for adaptive IMRT for head-and-neck cancer. *Int J Radiat Oncol Biol Phys, 77*(3), 707–714.

Uy, N. W., Woo, S. Y., Teh, B. S., Mai, W. Y., Carpenter, L. S., Chiu, J. K., Lu, H. H., Gildenberg, P., Trask, T., Grant III, W. H., & Butler, E. B. (2002). Intensity-modulated radiation therapy (IMRT) for meningioma. *Int J Radiat Oncol Biol Phys, 53*(5), 1265–1270.

van't Riet, A., Mak, A. C., Moerland, M. A., Elders, L. H., & van der Zee, W. (1997). A conformation number to quantify the degree of conformality in brachytherapy and external beam irradiation: application to the prostate. *Int J Radiat Oncol Biol Phys, 37*(3), 731–736.

Vasquez Osorio, E. M., Hoogeman, M. S., Al-Mamgani, A., Teguh, D. N., Levendag, P. C., & Heijmen, B. J. (2008). Local anatomic changes in parotid and submandibular glands during radiotherapy for oropharynx cancer and correlation with dose, studied in detail with nonrigid registration. *Int J Radiat Oncol Biol Phys, 70*(3), 875–882.

Waldron, J., Tin, M. M., Keller, A., Lum, C., Japp, B., Sellmann, S., van Prooijen, M., Gitterman, L, Blend, R., Payne, D., Liu, F. F., Warde, P., Cummings, B., Pintilie, M., & O'Sullivan, B. (2003). Limitation of conventional two dimensional radiation therapy planning in nasopharyngeal carcinoma. *Radiother Oncol, 68*(2), 153–161.

Wang, C., Chong, F., Wu, J., Lai, M., & Cheng, J. (2007). Body weight loss associates with set-up error in nasopharyngeal cancer patients undergoing image guided radiotherapy. *Int J Radiat Oncol Biol Phys, 69*(3), S203.

Wang, H., Dong, L., O'Daniel, J., Mohan, R., Garden, A. S., Ang, K. K., Kuban, D. A., Bonnen, M., Chang J. Y., & Cheung, R. (2005). Validation of an accelerated 'demons' algorithm for deformable image registration in radiation therapy. *Phys Med Biol, 50*(12), 2887–2905.

Wang, X., Lu, J., Xiong, X., Zhu, G., Ying, H., He, S., Hu, W., & Hu, C. (2010). Anatomic and dosimetric changes during the treatment course of intensity-modulated radiotherapy for locally advanced nasophayngeal carcinoma. *Med Dosim, 35*(2), 151–157.

Wang, Z. H., Yan, C., Zhang, Z. Y., Zhang, C. P., Hu, H. S., Kirwan, J., & Mendenhall, W. M. (2009). Radiation-induced volume changes in parotid and submandibular glands in patients with head and neck cancer receiving postoperative radiotherapy: a longitudinal study. *Laryngoscope, 119*(10), 1966–1974.

Webb, S. & Nahum, A. E. (1993). A model for calculating tumour control probability in radiotherapy including the effects of inhomogeneous distributions of dose and clonogenic cell density. *Phys Med Biol, 38*(6), 653–666.

Wei, W. I., & Sham, J. S. T. (2005). Nasopharyngeal carcinoma. *Lancet, 365*(9476), 2041–2054.

Wei, W. I., Sham, J. S. T., Zong, Y. S., Choy, D., & Ng, M. H. (1991). The efficacy of fiberoptic endoscopic examination and biopsy in the detection of early nasopharyngeal carcinoma. *Cancer, 67*(12), 3127–3130.

Woodford, C., Yartsev, S., Dar, A. R., Bauman, G., & Van Dyk, J. (2007). Adaptive radiotherapy planning on decreasing gross tumor volumes as seen on megavoltage computed tomography images. *Int J Radiat Oncol Biol Phys, 69*(4), 1316–1322.

Wu, C., Jeraj, R., Olivera, G. H., & Mackie, T. R. (2002). Re-optimization in adaptive radiotherapy. *Phys Med Biol, 47*(17), 3181–3195.

Wu, Q., Chi, Y., Chen, P. Y., Krauss, D. J., Yan, D., & Martinez, A. (2009). Adaptive replanning strategies accounting for shrinkage in head and neck IMRT. *Int J Radiat Oncol Biol Phys, 75*(3), 924–932.

Xing, L., Thorndyke, B., Schreibmann, E., Yang, Y., Li, T. F., Kim, G. Y., Luxton, G., & Koong, A. (2006). Overview of image-guided radiation therapy. *Med Dosim, 31*(2), 91–112.

Yan, D., Lockman, D., Martinez, A., Wong, J., Brabbins, D., Vicini, F., Liang, J., & Kestin, L. (2005). Computed tomography guided management of interfractional patient variation. *Semin Radiat Oncol, 15*(3), 168–179.

Yan, D., Vicini, F., Wong, J., & Martinez, A. (1997). Adaptive radiation therapy. *Phys Med Biol, 42*(1), 123–132.

Yang, D., Chaudhari, S. R., Goddu, S. M., Pratt, D., Khullar, D., Deasy, J O., & El Naqa, I. (2009). Deformable registration of abdominal kilovoltage treatment planning CT and tomotherapy daily megavoltage CT for treatment adaptation. *Med Phys, 36*(2), 329–338.

Yuan, J. M., Wang, X. L., Xiang, Y. B., Gao, Y. U. T., Ross, R. K., & Yu, M. C. (2000). Preserved foods in relation to risk of nasopharyngeal carcinoma in Shanghai, China. *Int J Cancer, 85*(3), 358–363.

Zeidan, O. A., Langen, K. M., Meeks, S. L., Manon, R. R., Wagner, T. H., Willoughby, T. R., Jenkins, D. W., & Kupelian, P. A. (2007). Evaluation of image-guidance protocols in the treatment of head and neck cancers. *Int J Radiat Oncol Biol Phys, 67*(3), 670–677.

Zhang, L., Garden, A. S., Lo, J., Ang, K. K., Ahamad, A., Morrison, W. H., Rosenthal, D. I., Chambers, M. S., Zhu, X. R., Mohan, R., & Dong, L. (2006). Multiple regions-of-interest analysis of setup uncertainties for head-and-neck cancer radiotherapy. *Int J Radiat Oncol Biol Phys, 64*(5), 1559–1569.

Zhang, T., Chi, Y., Meldolesi, E., & Yan, D. (2007). Automatic delineation of on-line head-and-neck computed tomography images: toward on-line adaptive radiotherapy. *Int J Radiat Oncol Biol Phys, 68*(2), 522–530.

Zhao, L., Wan, Q., Zhou, Y., Deng, X., Xie, C., & Wu, S. (2011). The role of replanning in fractionated intensity modulated radiotherapy for nasopharyngeal carcinoma. *Radiother Oncol, 98*(1), 23–27.

Zheng, Y. M., Tuppin, P., Hubert, A., Jeannel, D., Pan, Y. J., Zeng, Y., & de The, G. (1994). Environmental and dietary risk factors for nasopharyngeal carcinoma: a case-control study in Zangwu Country, Guangxi, China. *Brit J Cancer, 69*(3), 508–514.

Zhou, X., Cui, J., Kajdacsy-Balla, A. A., Ye, H., Wang, J., & Rao, P. N. (2007). The progress on genetic analysis of nasopharyngeal carcinoma. *Comp Funct Genom, 2007*, 57513. doi:10.1155/2007/57513